ABSTRACT

LOW TEMPERATURE ADIABATIC STUDIES OF MAGNETIC PHASE BOUNDARIES IN ANTIFERROMAGNETS

by James Nathaniel McElearney

A theoretical treatment of antiferromagnetism, for arbitrary spin values, is given, based on previous extensions of the molecular field model of antiferromagnetism. Theoretical predictions involving the magnetic phase boundaries are given. A new method to predict critical fields for spin flopping, using three magnetic susceptibility measurements, is proposed and the theoretical basis for adiabatic investigations of antiferromagnetic spin flop states is given. Apparatus and methods for such experiments are described.

The results of adiabatic experiments on $CoCl_2 \cdot 6H_2O$ and $MnCl_2 \cdot 4H_2O$, whose spin flop states have been previously studied, are given, indicating the validity of the new method. Also, results are given indicating that two previously studied substances, $CoBr_2 \cdot 6H_2O$ and $FeCl_2 \cdot 4H_2O$, exhibit spin flopping in accessible experimental regions. $CoBr_2 \cdot 6H_2O$ has a critical field in the region 1.15^0K to the triple point, $2.91 \pm .01^0$K, which is well fitted by the equation $H_c = 7523 - 230.7\ T + 292.5\ T^2$. $FeCl_2 \cdot 4H_2O$ apparently spin flops below 0.68^0K above a field equal to about 5500 gauss. Finally, results are also given of investigations done on $MnBr_2 \cdot 4H_2O$, $Cs_2MnBr_4 \cdot 2H_2O$, and $NiCl_2 \cdot 6H_2O$, which indicate the lack of spin flop states in

these substances in fields below 10,000 gauss and in temperatures down to 1.0^{0}K.

LOW TEMPERATURE ADIABATIC STUDIES OF MAGNETIC PHASE BOUNDARIES IN ANTIFERROMAGNETS

By

James Nathaniel McElearney

A THESIS

Submitted to
Michigan State University
in partial fulfillment of the requirements
for the degree of

DOCTOR OF PHILOSOPHY

Department of Physics

1968

ACKNOWLEDGMENTS

The author wishes to express his appreciation and thanks to all those who have helped in this study; to Dr. H. Forstat for suggesting this study and for invaluable aid during the course of the work; to Dr. J. A. Cowen and Dr. R. D. Spence for several fruitful discussions; to Mr. Peter T. Bailey for his assistance with the experiments; to the M.S.U. Computer Center for computer time made available; and especially to the Air Force Office of Scientific Research, Office of Aerospace Research, United States Air Force for their financial support of this work.

TABLE OF CONTENTS

TABLE OF CONTENTS (Cont.)

LIST OF TABLES

LIST OF TABLES (CONT.)

LIST OF FIGURES

LIST OF FIGURES (Cont.)

INTRODUCTION

Magnetic properties of matter have interested physicists for a long time. In recent years, there has been a great deal of study done on magnetic systems in their ordered states. Many different experimental measurements supply insight into the phenomenon of magnetism.

Although there have been many experimental investigations of different magnetic systems in different substances, at present there have been few investigations involving antiferromagnetic systems in the spin flop state (although, some of those done have been thorough). The basic reason for this is that few substances exhibit the phenomenon of spin flop in regions of magnetic field and temperature accessible by common methods.

The purpose of this investigation is to develop further methods of study of spin flop states and to discover more materials exhibiting spin flop properties in accessible experimental regions. The study has been divided into three parts. The first part will develop the theoretical basis for adiabatic observations of spin flop states. The second part will describe the experimental apparatus and methods used in such a study, and finally, the third part will report results indicating the validity of the new method and will also report on the new materials which exhibit spin flop properties.

CHAPTER I

THEORETICAL BACKGROUND

I. THEORY

A. Antiferromagnetism

The concept of antiferromagnetism, interpenetrating lattices of oppositely directed magnetic moments, was first postulated by Néel[1] in 1932. Since then, many antiferromagnetic materials have been discovered and studied. There exist many excellent papers on the subject and reference 2 contains a general review of the subject.

To give a theoretical analysis of the phenomenon, one needs to describe the energy of interaction of several ions with spins. The model presently accepted as being correct was first suggested in 1928 by Heisenberg[3]. Heisenberg type exchange interactions, in the Dirac formalism[4], are equivalent to the interatomic potential

$$V_{ij} = -1/2\, J(1 + 4\, \vec{S}_i \cdot \vec{S}_j). \qquad (1.00)$$

$\vec{S}_i$ and $\vec{S}_j$ are the quantum mechanical spins of ions i and j. J is the exchange integral and is positive for ferromagnets and negative for antiferromagnets. Apart from an additive constant, then, the potential energy of atom i is given by

$$V_i = \sum_j V_{ij} = -2\, J \sum_j (\vec{S}_j \cdot \vec{S}_i). \qquad (1.01)$$

Thus, the Heisenberg model corresponds to magnetic isotropy.

Perhaps one of the most widely used approximations to equation 1.00 is that of the Ising model[5], in which it is assumed that only the components of the spins in one direction interact. That is,

$$V_i = -2J \sum_j S_{jz} S_{iz}. \qquad (1.02)$$

This model obviously corresponds to extreme magnetic anisotropy.

The most commonly used approximation is that which Néel used, the Weiss molecular field approximation[6]. In this approach, the potential energy of atom i is given as

$$V_i = \sum_j^z V_{ij} = -2J\, z\, \overline{\vec{S}_j} \cdot \vec{S}_i, \qquad (1.03)$$

where z j atoms interact with atom i with the same J and $\overline{\vec{S}_j}$ is the statistical average of $\vec{S}_j$ over the j sublattice. Since the magnetic moment of an atom may be written as $\vec{u} = -g\, \mu_B\, \vec{S}$, where g and μ_B are the usual magnetic factors, equation 1.00 becomes

$$V_i = -\vec{H}_j \cdot \vec{u}_i, \qquad (1.04)$$

where

$$\vec{H}_j = (-\,2J\, z/g^2\, \mu_B^2)\, \overline{\vec{u}_j} \qquad (1.05)$$

is the effective magnetic field (the molecular field) due to the j sublattice which is acting on atom i.

There have been many other approaches and approximations used, but for the purposes of this study, the molecular

field approach will supply the necessary insight for understanding the experimental data involved. Bitter[7], Van Vleck[8], Garrett[9], Anderson[10], Nagamiya[11], Yosida[12], Gorter and Haantjes[13], and many others have made extensions and refinements to Néel's original theory. In particular, this study will deal with a further extension of Garrett's approach which itself was an extension, to include high magnetic fields, of Van Vleck's work on the Néel model.

B. <u>Generalization of Garrett's Theory</u>

Garret's work was for a spin 1/2 substance, and his equations did not explicitly include anisotropy. This study will consider his equations for spin S and, in addition, solutions will be considered for magnetic fields applied at arbitrary angles to the preferred axis of magnetization, rather than just parallel or perpendicular to it. Also, anisotropy will be introduced to the solution through Yosida's[14] approach which was similar to Néel's calculation at absolute zero[15]. The importance of anisotropy to antiferromagnetic phenomena cannot be overemphasized, as many of the writers have pointed out. Apparently the best treatment, to date, of a molecular field theory which includes anisotropic effects is that of Gorter and Van Peski-Tinbergen[16]. However, since that approach, which was for spin 1/2 systems, involved graphical solutions, it is not the simplest to comprehend, and a generalization of Garrett's work is worthwhile.

In the Van Vleck model, the net magnetization per unit volume of an antiferromagnetic crystal is given by

$$\vec{M} = \frac{1}{2} g \mu_B N(\vec{S}_i + \vec{S}_j) = \vec{M}_i + \vec{M}_j, \qquad (1.06)$$

where g is the usual Landé factor, μ_B is the Bohr magneton, N is the number of magnetic atoms per unit volume, and $\vec{S}_i$ and $\vec{S}_j$ represent the average spins of the ions of the two sublattices. The magnitudes of $\vec{S}_i$ and $\vec{S}_j$ are given according to standard magnetic theory[17] by

$$\begin{aligned} S_i &= S\, B_S(H_i\, S\, g\, \mu_B/k\, T) \\ S_j &= S\, B_S(H_j\, S\, g\, \mu_B/k\, T), \end{aligned} \qquad (1.07)$$

where k is Boltzman's constant, T is the absolute temperature, S is the spin quantum number of the magnetic atom in the crystal, H_i and H_j are the magnitudes of the effective fields due to the j and i sublattices respectively, and B_S is the Brillouin function, given by

$$B_S(x) = \frac{2S + 1}{2S} \coth\left(\frac{2S + 1}{2S} x\right) - \frac{1}{2S} \coth\left(\frac{x}{2S}\right). \qquad (1.08)$$

For an arbitrary applied field $\vec{H}$, $\vec{H}_i$ and $\vec{H}_j$ are given by

$$\begin{aligned} \vec{H}_i &= \vec{H} + (2z\, J/g\, \mu_B)\, \vec{S}_j \\ \vec{H}_j &= \vec{H} + (2z\, J/g\, \mu_B)\, \vec{S}_i, \end{aligned} \qquad (1.09)$$

with the additional requirement for internal consistency of the model that $\vec{H}_i$ is parallel to $\vec{S}_i$ and $\vec{H}_j$ is parallel to $\vec{S}_j$.

Following Garrett's method of introducing "reduced" fields, spins and temperatures, equations 1.07 and 1.09 become

$$s_i = b_S(h_i/t)$$
$$s_j = b_S(h_j/t) \qquad (1.10)$$

$$\vec{h}_i = \vec{h} - \vec{s}_j$$
$$\vec{h}_j = \vec{h} - \vec{s}_i, \qquad (1.11)$$

where

$$b_S(x) = B_S\left(\frac{3S}{S+1}\ x\right), \qquad (1.12)$$

when the following definitions are made:

$$H_0 = (-2z\ J\ S/g\ \mu_B) \qquad (1.13)$$

$$T_n = -\ 2J\ z\ S(S+1)/3k \qquad (1.14)$$

$$\vec{h}_i = \vec{H}_i/H_0$$
$$\vec{h}_j = \vec{H}_j/H_0 \qquad (1.15)$$

$$\vec{h} = \vec{H}/H_0 \qquad (1.16)$$

$$t = T/T_n \qquad (1.17)$$

$$s_i = S_i/S$$
$$s_j = S_j/S \qquad (1.18)$$

$$\vec{m}_i = \vec{M}_i/(g\ \mu_B\ N\ S/2)$$
$$\vec{m}_j = \vec{M}_j/(g\ \mu_B\ N\ S/2) \qquad (1.19)$$

(Note now $\vec{m}_i = \vec{s}_i$ and $\vec{m}_j = \vec{s}_j$, so the reduced magnetization is $\vec{m} = \vec{m}_i + \vec{m}_j = \vec{s}_i + \vec{s}_j$.)

C. Behavior of the Sublattices in a Field

It is convenient now to define angles as in reference 2. Consider the z-x plane as in Fig. 1. Then let the preferred axis of magnetization be z and let h be applied in the z-x plane. It is shown in reference 2 that if

$$\vec{\Delta} = (\vec{s}_j/s_j) - (\vec{s}_i/s_i), \tag{1.20}$$

then $\vec{\Delta}$ is also in the z-x plane. The angle between $\vec{h}$ and the z axis is θ and the angle between $\vec{h}$ and $\vec{\Delta}$ is ψ. (ψ is not equal to θ due to the anisotropy, as will be seen shortly.)

Note that the definition of $\vec{\Delta}$ insures that the angles (denoted as ϕ in Fig. 1) between $\vec{s}_j$ or $\vec{s}_i$ and $\vec{\Delta}$ will be equal. Now, for the molecular field model, as stated in reference 2, the component of $\vec{h}$ perpendicular to $\vec{\Delta}$ causes the spin vectors of the two sublattices to cant equal angles away from $\vec{\Delta}$ toward $\vec{h}$. Furthermore, the component of $\vec{h}$ parallel to $\vec{\Delta}$ causes the magnitudes of $\vec{s}_i$ and $\vec{s}_j$ to change. It is not clear whether the authors mean the above statements to be true in general, regardless of the intensity of the applied field, or whether the statements are only true for small enough fields such that the angle of cant of the sublattices, ϕ, is small.

This description of the behavior of the sublattice vectors certainly has a better chance of matching reality

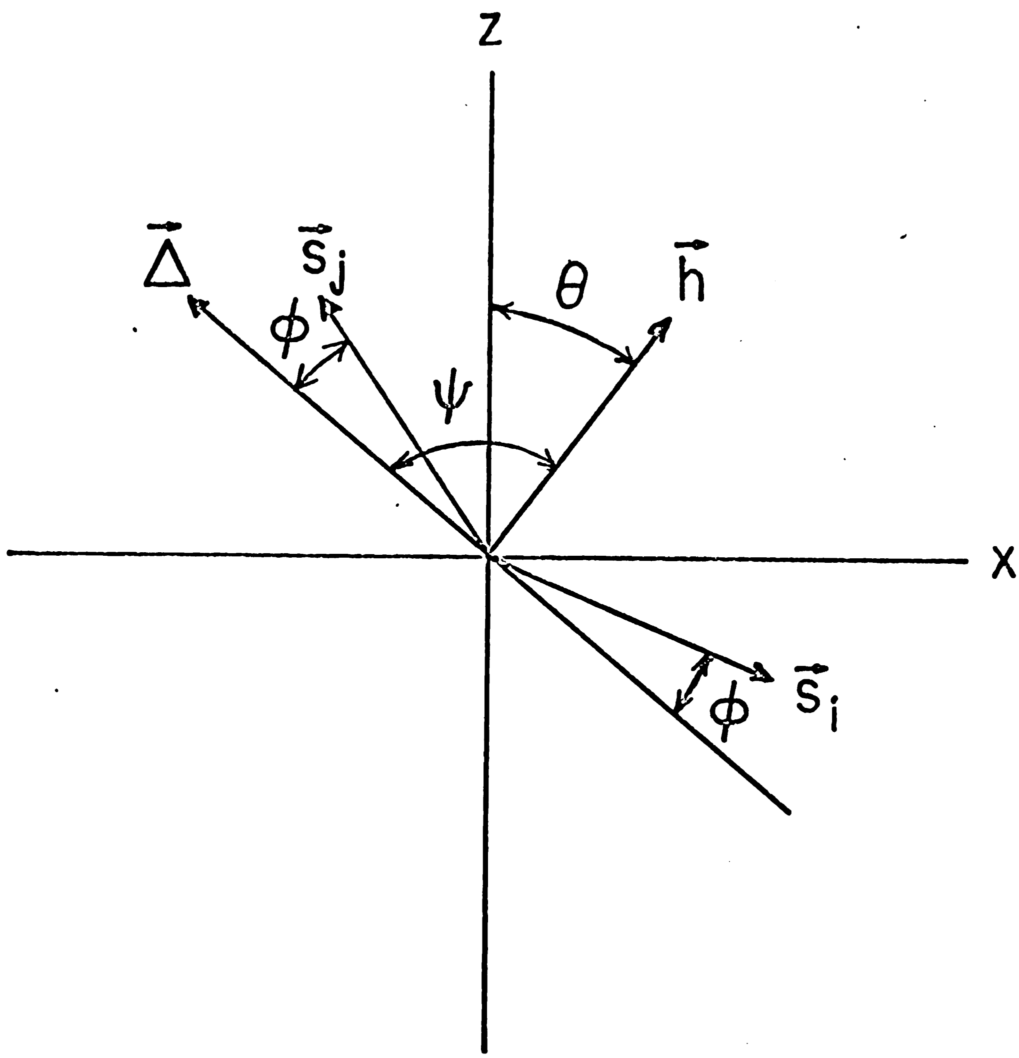

Fig. 1. Definition of angles.

than that of reference 18, in which it is stated that the components of $\vec{h}$ parallel and perpendicular to $\vec{\Delta}$ cause the parallel and perpendicular components of the magnetization to increase by $1/2\ X_{\parallel}h_{\parallel}$ and $1/2\ X_{\perp}h_{\perp}$ respectively. Were this so, then, as shown in reference 18, the following relations would hold:

$$
\begin{aligned}
s_{jz} &= (s_0+(X_{\parallel}h(\cos\psi)/2))\cos(\psi-\theta)+(X_{\perp}h\sin\psi\sin(\psi-\theta)/2) \\
s_{jx} &= -(s_0+(X_{\parallel}h(\cos\psi)/2))\sin(\psi-\theta)+(X_{\perp}h\sin\psi\cos(\psi-\theta)/2) \\
s_{iz} &= -(s_0-(X_{\parallel}h(\cos\psi)/2))\cos(\psi-\theta)+(X_{\perp}h\sin\psi\sin(\psi-\theta)/2) \\
s_{ix} &= (s_0-(X_{\parallel}h(\cos\psi)/2))\sin(\psi-\theta)+(X_{\perp}h\sin\psi\cos(\psi-\theta)/2),
\end{aligned}
\tag{1.21}
$$

where s_0 is the zero field magnetic moment of one sublattice. Then if M and M' denote the sum and difference of the magnetic moments on the i and j sublattices, the components of these vectors are:

$$
\begin{aligned}
M_z &= X_{\parallel}h\cos\psi\cos(\psi-\theta) + X_{\perp}h\sin\psi\sin(\psi-\theta) \\
M_x &= X_{\perp}h\sin\psi\cos(\psi-\theta) - X_{\parallel}h\cos\psi\sin(\psi-\theta) \\
M'_z &= 2\ s_0\cos(\psi-\theta) \\
M'_x &= 2\ s_0\sin(\psi-\theta).
\end{aligned}
\tag{1.22}
$$

But this implies $M' = 2\ s_0$ always. However, this is not possible, as is evident from consideration of the case where the applied field is perpendicular, or nearly perpendicular to the preferred axis and is large enough to almost cause saturation. M' must then obviously approach zero. The behavior of the sublattices in a high field at some angle to the easy axis seems to need clarification. For a field applied either parallel or perpendicular to the easy axis, the picture of reference 2 would seem plausible (with the necessity that the relationship between ψ and θ be modified for high fields).

Furthermore, Garrett has given the following argument to determine the effect of a perpendicular field of arbitrary value. Consider $\vec{h}$ applied perpendicular to z, as shown in Fig. 2, which represents the vector relations between $\vec{h}$, $\vec{h}_i$, $\vec{h}_j$, $\vec{s}_i$, and $\vec{s}_j$. Then the effect of the field must be to equally rotate $\vec{s}_i$ and $\vec{s}_j$ without changing their magnitudes. For, if $\vec{h}$ were to change in magnitude and if the magnitudes of $\vec{s}_i$ and $\vec{s}_j$ were to change, they would have to change proportionally to the magnitudes of h_i and h_j, as can be seen from Fig. 2. But this would imply a linear relation between s_i and h_i and also between s_j and h_j. Therefore, since the relationships of equations 1.10 are not linear, the magnitudes can not change and the only alternative is that they keep the same magnitude as in zero applied field and rotate toward the perpendicular direction when the field is applied. (This argument can not be applied in general to a field oriented at some arbitrary angle to the easy axis because of the effect of the anisotropy field.)

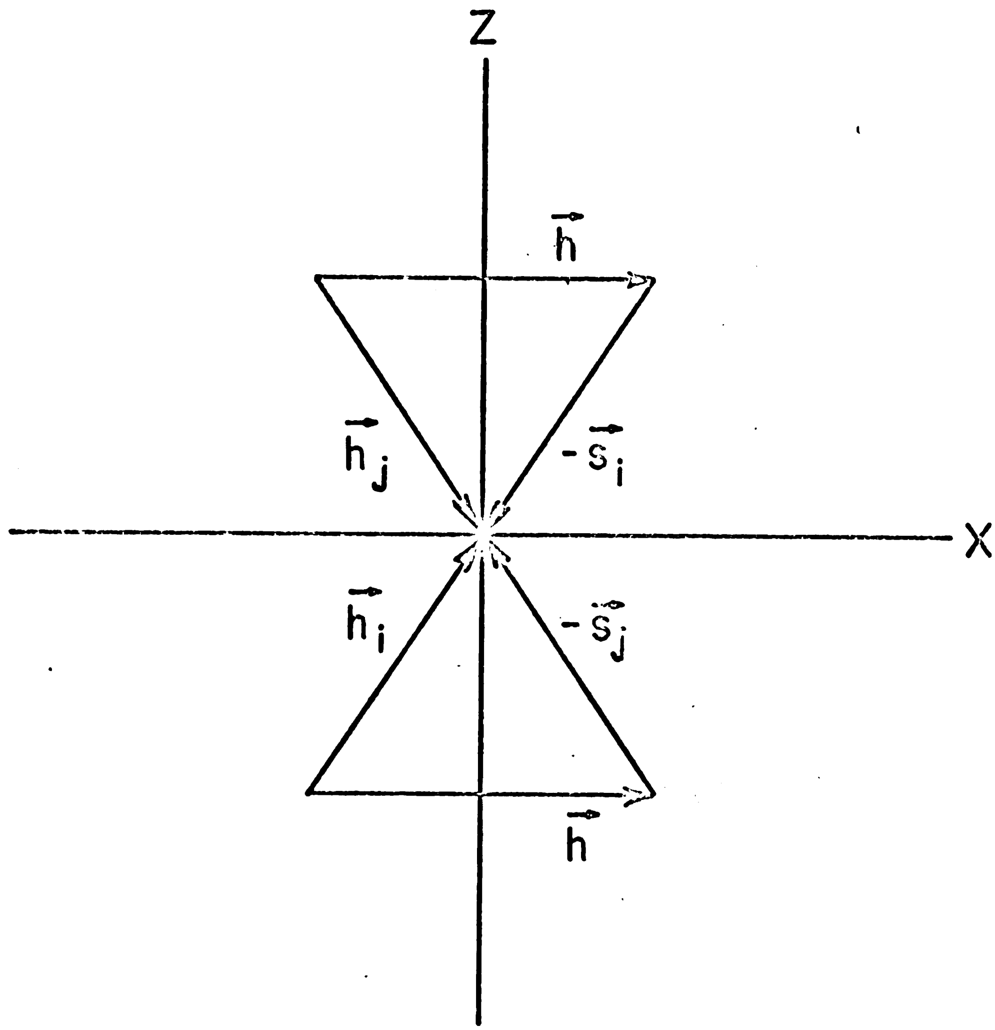

Fig. 2. Vector relations for a perpendicular field.

D. Equation for Magnetization and Entropy

Thus, adopting the viewpoint of reference 2 regarding the behavior of the sublattice vectors, with the reservation that the fields used must be small enough so as not to introduce any saturation effects, the magnitudes of $\vec{s}_i$ and $\vec{s}_j$ may be determined by merely considering the perpendicular component of the field to be zero. Then equations 1.10 become

$$\begin{aligned} s_i &= b_S((s_j - h\cos\psi)/t) \\ s_j &= b_S((h\cos\psi + s_i)/t), \end{aligned} \tag{1.23}$$

where it has been assumed that the parallel components of s_j and h point in the same direction. (Note that these equations give positive values for s_i and s_j, whereas Garrett's equations have signed values for s_i and s_j built in.)

Besides the magnetization, which may be calculated from s_i and s_j, the entropy of the system is also of interest. Garrett has given a statistical argument to determine the entropy for a spin 1/2 system in terms of the sublattice magnetizations. The general thermodynamic argument to determine the entropy of an antiferromagnet of spin j will be given here. In general,

$$s = b_j\ (h/t). \tag{1.24}$$

From the combined first and second laws of thermodynamics for a magnetic system,

$$dU = T\,dS + H\,dM, \tag{1.25}$$

where S now is entropy and U is the energy of the system (including the field energy). For $dU = 0$, $T\,dS = - H\,dM$. In reduced units,

$$t\,dS = - \frac{h\,k\,N}{2} \left(\frac{3J}{J + 1}\right) ds. \tag{1.26}$$

Thus, $$h/t = - \frac{2(J + 1)}{3JN} \frac{d(S/k)}{ds} . \tag{1.27}$$

So, $$s = B_J\left(- \frac{2(J + 1)}{3JN} \frac{d(S/k)}{ds}\right). \tag{1.28}$$

Therefore, $$B_J^{-1}(s) = - \frac{2(J + 1)}{3JN} \frac{d(S/k)}{ds} . \tag{1.29}$$

So, $$S/k = - \frac{3JN}{2(J + 1)} \int B_J^{-1}(s)\,ds. \tag{1.30}$$

Thus, for an antiferromagnet,

$$S/kN = - \frac{3J}{2(J + 1)} \left(\int B_J^{-1}(s_i)ds_i + \int B_J^{-1}(s_j)\,ds_j\right), \tag{1,31}$$

which reduces to Garrett's expression for a spin 1/2 system.

E. Introduction of Anisotropy

To introduce anisotropy into the solution, ψ is allowed to be different from θ such that the sum of the magnetic energy,

$$E_m = - \frac{1}{2}(X_\perp \sin^2 \psi + X_\parallel \cos^2 \psi)\,h^2, \tag{1.32}$$

and the anisotropy energy (assuming uniaxial anisotropy and no saturation effects),

$$E_a = a \sin^2 (\psi - \theta) \tag{1.33}$$

(where a is in reduced units and is greater than zero), takes on its minimum value. This requirement leads to the equation

$$\tan 2\psi = \frac{\sin 2\theta}{\cos 2\theta - (h/h_c)^2} , \tag{1.34}$$

where $$h_c = \sqrt{2a/(X_\perp - X_\parallel)} . \tag{1.35}$$

F. Antiferromagnetic-Paramagnetic Boundaries

1. Perpendicular Boundary

Garrett has given the following argument to determine the antiferromagnetic-paramagnetic boundary in the case of a perpendicular field. The component of magnetization in the direction of the field is $2s_0 \sin \phi$ which must equal $X_\perp h$. But $X_\perp = 1$, as will be seen later, so that

$$2s_0 \sin \phi = h \tag{1.36}$$

describes the magnetization in the perpendicular direction until the sublattice spins have been dragged into complete parallelism with the field. This occurs at $\phi = 90^0$, or $h = 2s_0$. But for a perpendicular field, equations 1.23 reduce to

$$s_0 = b_S(s_0/t) . \tag{1.37}$$

But on the boundary $h = 2s_0$, so

$$h/2 = b_S(h/2t), \tag{1.38}$$

or

$$t = h/2\ b_S^{-1}\ (h/2),$$

where b_S^{-1} refers to the inverse Brillouin function. (Note that at $t = 0$, the boundary intersects the h axis at $h = 2$.)

2. Parallel Boundary

For the parallel case ($\psi = 0$), Garrett has noted that the antiferromagnetic-paramagnetic boundary is obtained by letting s_j approach $-s_i$ as the difference of s_j and s_i remains constant. The latter condition is equivalent to $ds_i/ds_j = 1$. Application of these conditions to equations 1.23 results in the equations which define the boundary:

$$s_i = b_S\left(\frac{-s_i - h}{t}\right) \tag{1.39}$$

and

$$t = b_S'\left(\frac{h + s_i}{t}\right), \tag{1.40}$$

where b_S' is the derivative of the Brillouin function with respect to its argument. So, denoting the inverse of b_S' by $b_S'^{-1}$, 1.40 becomes

$$b_S'^{-1}(t) = \frac{h + s_i}{t}, \tag{1.41}$$

and therefore, using 1.41 in 1.39,

$$-s_i = b_S(b_S'^{-1}\ (t)). \tag{1.42}$$

Also, 1.39 is equivalent to

$$b_S^{-1}(-s_i) = \frac{h + s_i}{t} \ . \tag{1.43}$$

Solving 1.43 for h,

$$h = t\ b_S^{-1}(-s_i) - s_i . \tag{1.44}$$

Therefore, using 1.42 in 1.43,

$$h = t\ b_S'^{-1}\ (t) + b_S(b_S'^{-1}\ (t)) \tag{1.45}$$

defines the paramagnetic boundary for a field applied in the parallel direction. For $S = 1/2$ this reduces to the equation which Garrett derived:

$$h = t \tanh^{-1} \sqrt{1 - t} + \sqrt{1 - t} \ . \tag{1.46}$$

For S not equal to $1/2$, equation 1.45 cannot be solved in closed form and numerical solutions are necessary. Computer programs were written to solve the boundary equations for fields applied both parallel or perpendicular to the easy axis, (see Appendix IA) and the results for two values of S are shown plotted in Fig. 3. Ziman[19], using the higher order Bethe-Peierls-Weiss method has found that the critical curve, for the parallel case, drops continuously from $h = 1$ at $t = 0$ to $h = 0$ at $t = 1$, so that the peculiar maximum in the parallel critical curve near $t = 0.2$ for the molecular field model, as shown in Fig. 3, probably does not exist in an exact solution.

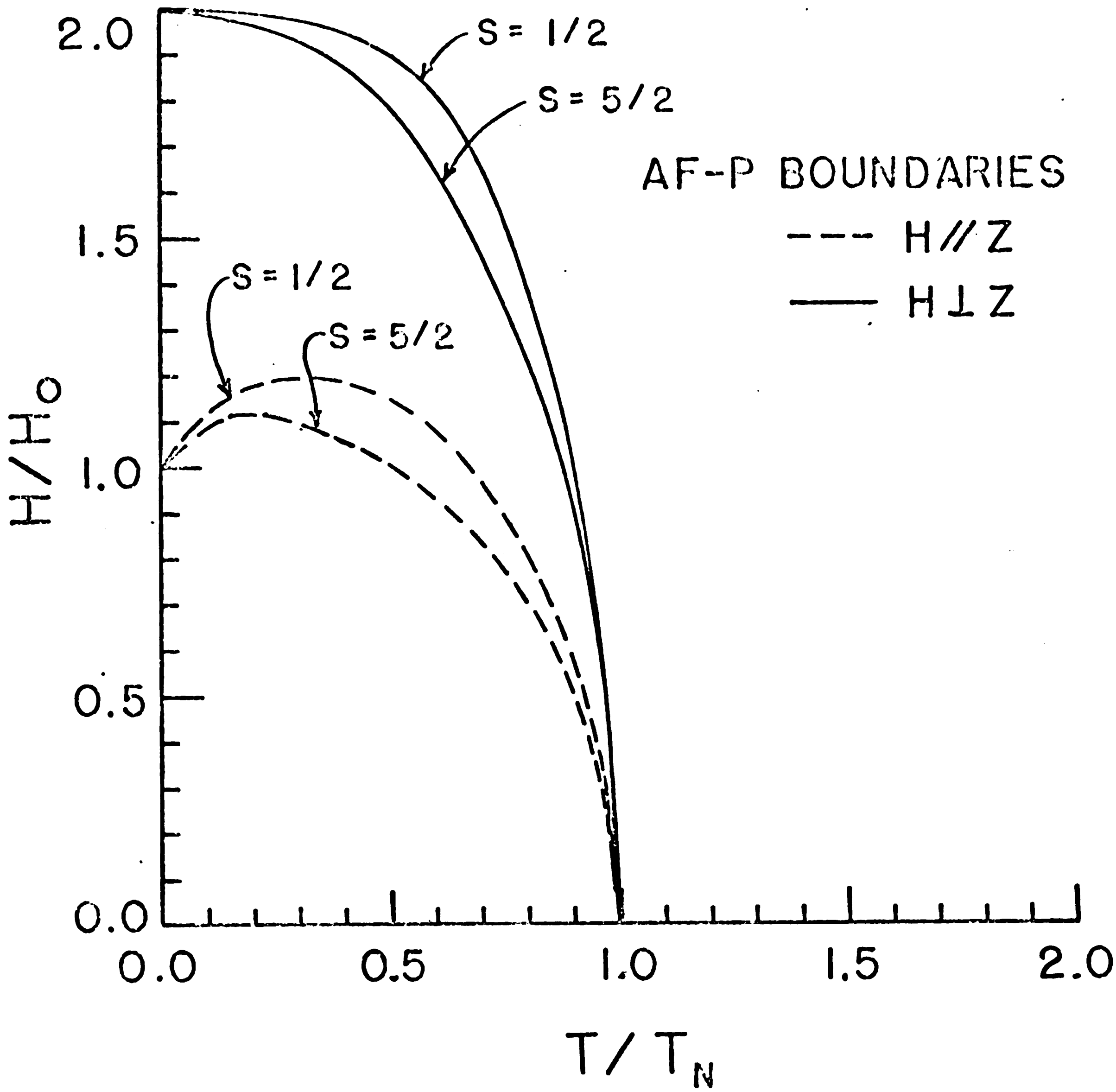

Fig. 3. Parallel and perpendicular antiferromagnetic-paramagnetic boundaries.

G. Susceptibilities

1. Perpendicular Case

As will be seen shortly, the magnetic susceptibilities of antiferromagnets are related to some of the phenomena connected with antiferromagnetism, so it is worthwhile to calculate theoretical expressions for them. The susceptibility for a perpendicular field is most easily calculated by noting that the torque on a sublattice spin, due to the field acting on it, must be zero. That is,

$$|\vec{s}_i \times \vec{h}_i| = 0, \tag{1.47}$$

or,

$$|\vec{s}_i \times (\vec{h} - \vec{s}_j)| = 0 \tag{1.47'}$$

(having neglected anisotropy). For $\vec{h}$ perpendicular to $\vec{\Delta}$, $s_i = s_j = s_0$, and the angle between $\vec{s}_i$ or $\vec{s}_j$ and $\vec{\Delta}$ is ϕ. So

$$s_i\, h \cos\phi - s_i\, s_j \sin 2\phi = 0 \tag{1.48}$$

or,

$$h = 2\, s_0 \sin\phi. \tag{1.49}$$

But the right hand side of this equation is the magnetization in the perpendicular direction which must equal $X_\perp\, h$. Therefore,

$$X_\perp = 1. \tag{1.50}$$

2. Parallel Case

For a parallel field, the susceptibility may be calculated from equations 1.23, since $X_\parallel = m/h = (s_j - s_i)/h$. Following

Van Vleck's argument, the Brillouin function is expanded about s_0/t as a Taylor's series in its argument. Considering only the first two terms,

$$b_S(\frac{h}{t}) = b_s(\frac{s_0}{t}) + (\frac{h - s_0}{t}) \; b_S'(\frac{s_0}{t}) \; , \tag{1.51}$$

Since

$$m = s_j - s_i = b_S(\frac{h_j}{t}) - b_S(\frac{h_i}{t}), \tag{1.52}$$

using 1.51 in 1.52,

$$s_j - s_i = \frac{h_j - h_i}{t} \; b_S'(\frac{s_0}{t})$$

$$= \frac{2h + s_i - s_j}{t} \; b_S'(\frac{s_0}{t}) \; . \tag{1.53}$$

Solving 1.53 for $s_j - s_i$:

$$s_j - s_i = \frac{2h \; b_S'(s_0/t)}{t + b_S'(s_0/t)} \; . \tag{1.54}$$

Therefore,

$$X_{\parallel} = \frac{2 \; b_S'(s_0/t)}{t + b_S'(s_0/t)} \; . \tag{1.55}$$

3. <u>Paramagnetic Case</u>

In order to calculate the paramagnetic susceptibility (t greater than 1), it is necessary to assume t large enough so that the argument of the Brillouin function is small enough so that the function may be expanded. For small y,

$$B_S(y) = (\frac{S + 1}{3S}) \; y, \tag{1.56}$$

or $$b_S(y) = y. \tag{1.57}$$

Then, since in the paramagnetic state the sublattice vectors are in the same direction as the field, equations 1.10 become

$$s_i = \frac{h - s_j}{t} \tag{1.58}$$

and $$s_j = \frac{h - s_i}{t} . \tag{1.59}$$

So, $$m = s_i + s_j = \frac{2h - (s_j + s_i)}{t} . \tag{1.60}$$

Or, $$s_i + s_j = \frac{2h}{1 + t} , \tag{1.61}$$

and therefore, $$X_{para} = \frac{2}{1 + t} \tag{1.62}$$

for t large. Note that the derivation of this expression does not guarantee its validity for t only slightly greater than 1, although it may actually be valid.

$X_{\parallel}$ and $X_{\perp}$, along with X_{para}, are shown in Fig. 4 for two values of S. Two points are to be noted. First that $X_{\perp}$ is greater than $X_{\parallel}$, and second that $X_{\parallel}$ decreases to 0 at $t = 0$.

4. Arbitrary Orientation Case

If a field is applied at an arbitrary angle from the easy axis, the susceptibility in that direction is calculated as follows. For a relatively small field, the parallel and perpendicular components of the induced magnetization

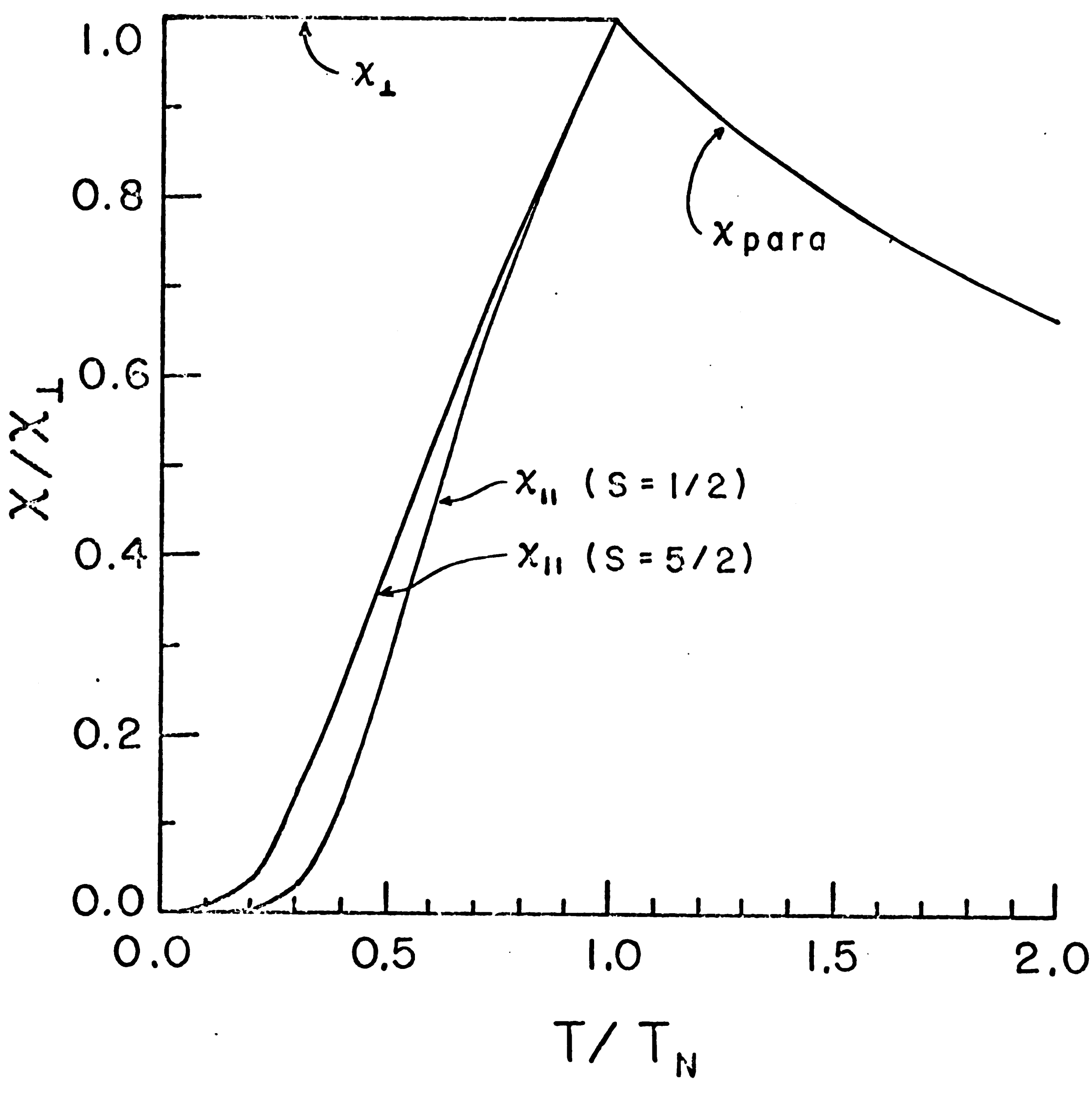

Fig. 4. Parallel, perpendicular and paramagnetic susceptibilities.

are:

$$m_{\parallel} = X_{\parallel}\ h_{\parallel} \tag{1.63}$$

and

$$m_{\perp} = X_{\perp}\ h_{\perp}\ , \tag{1.64}$$

where $h_{\parallel} = h \cos \psi$ and $h_{\perp} = h \sin \psi$. The component of the induced magnetization in the direction of the field is given by the sum of the projections, in the direction of the field, of the above magnetization components:

$$X_{\parallel}\ h_{\parallel} \cos \psi + X_{\perp}\ h_{\perp} \sin \psi \tag{1.65}$$

or,

$$X_{\parallel}\ h \cos^2 \psi + X_{\perp}\ h \sin^2 \psi . \tag{1.66}$$

So,

$$X = X_{\parallel} \cos^2 \psi + X_{\perp} \sin^2 \psi . \tag{1.67}$$

H. Spin Flop

1. The Phenomenon of Spin Flop

An immediate consequence of the difference between $X_{\parallel}$ and $X_{\perp}$ is the phenomenon of spin flop. This involves a 90^0 rotation of the direction of magnetization when $\vec{h}$ is applied along the easy axis. That this is possible is seen upon comparison of the free energy in the case that $\vec{h}$ is parallel to the easy axis and $\vec{\Delta}$ is also parallel to it to the free energy in the case that $\vec{h}$ is parallel to the easy axis and $\vec{\Delta}$ is perpendicular to it. The free energy of the first case is $-\frac{1}{2} X_{\parallel}\ h^2$, and for the second case it is $a - \frac{1}{2} X_{\perp}\ h^2$, where a is the anisotropy constant of equation 1.33. Thus there is a field such that

$$-\frac{1}{2}\chi_{\parallel}\, h_c^2 = a - \frac{1}{2}\chi_{\perp}\, h_c^2 \ . \tag{1.68}$$

Or,

$$h_c = \sqrt{\frac{2a}{\chi_{\perp} - \chi_{\parallel}}} \ . \tag{1.69}$$

This is the same as equation 1.35. As can be seen from equation 1.34, for $\theta = 0$ and h greater than h_c, $\psi = 90^0$. That is to say, Δ's direction flops at $h = h_c$. This phenomenon was first predicted by Néel[15] in 1936 and was first observed in 1951 by Gorter et. al.[20] in a crystal of $CuCl_2 \cdot 2H_2O$.

2. Prediction of the Critical Field

It is worth noting at this point that h_c may be predicted from three susceptibility measurements. If χ is measured along $\vec{h}$ at an angle θ from the easy axis, and if the near zero field values of $\chi_{\perp}$ and $\chi_{\parallel}$ are obtained, then the following two equations, previously derived, can be used to predict h_c:

$$\begin{aligned} \chi &= \chi_{\parallel} \cos^2 \psi + \chi_{\perp} \sin^2 \psi \\ \tan 2\psi &= \frac{\sin 2\theta}{\cos 2\theta - (h/h_c)^2} \ . \end{aligned} \tag{1.70}$$

This possibility does not seem to have been previously considered. (Indeed, approximations are involved in the above equations, but an order of magnitude prediction is certainly a realistic possibility.)

3. Equations for the Critical Field

Upon substitution of the previously derived values of $X_{\parallel}$ and $X_{\perp}$ in equation 1.69, the following equation may be written:

$$h_c^2 = \frac{2a}{1 - \dfrac{2}{1 + \dfrac{t}{b_S'(s_0/t)}}} \tag{1.71}$$

To evaluate this equation, one needs to know a as a function of temperature and spin. Yosida[14] has made a calculation, based on statistical mechanics, of the temperature variation of a for S greater than $\frac{1}{2}$, based on the assumption that the ionic energy causes the anisotropy of the entire crystal (versus the Zeeman energy and the exchange energy of neighboring magnetic ions). His result for the anisotropy constant is

$$a = A\, S^2 \left(\frac{S+1}{S} - 3B_S(x)\, \frac{1}{2S} \coth\left(\frac{x}{2S}\right)\right) \tag{1.72}$$

where

$$x = -2J\, z\, S\, S_0/kT.$$

At $T = 0$ this becomes $AS(S - \frac{1}{2})$. So,

$$\frac{h_c(t)}{h_c(0)} = \left[\frac{S\left(\dfrac{S+1}{S} - 3b_S\left(\dfrac{s_0}{t}\right) \dfrac{1}{2S} \coth\left(\dfrac{3}{S+1}\, \dfrac{s_0}{2t}\right)\right)}{\left(S - \frac{1}{2}\right)\left(1 - \dfrac{2}{1 + \dfrac{t}{b_S'(s_0/t)}}\right)}\right]^{1/2} \tag{1.73}$$

This function has been calculated numerically on the computer and the results are shown in Fig. 5 for several values of S.

For the case $S = \frac{1}{2}$, the expression giving a in equation 1.72 identically vanishes. Yosida[12] has made a calculation of the anisotropy constant for this case under the assumption that the anisotropy energy arises from the crystalline electric field at a magnetic ion site and from an anisotropic coupling of two spins (such as dipole-dipole interaction). In this case the anisotropy constant shows the same temperature variation as s_0^2. Thus,

$$\frac{h_c(t)}{h_c(0)} = \left[\frac{s_0^2}{1 - \cfrac{2}{1 + \cfrac{t}{b_S'(s_0/t)}}}\right]^{1/2} . \qquad (1.74)$$

This equation is also shown in Fig. 5.

II. Applications of the Theory

A. Observation of Spin Flop Boundaries

1. Variation of Temperature in an Isentropic Magnetization

On the basis of the preceding theory, it is obvious that the phenomenon of spin flop may easily be observed by adiabatic means. Whether the system is in the normal antiferromagnetic state, or whether it is in the spin-flop state may be determined by observation of the quantity dT/dH. Now,

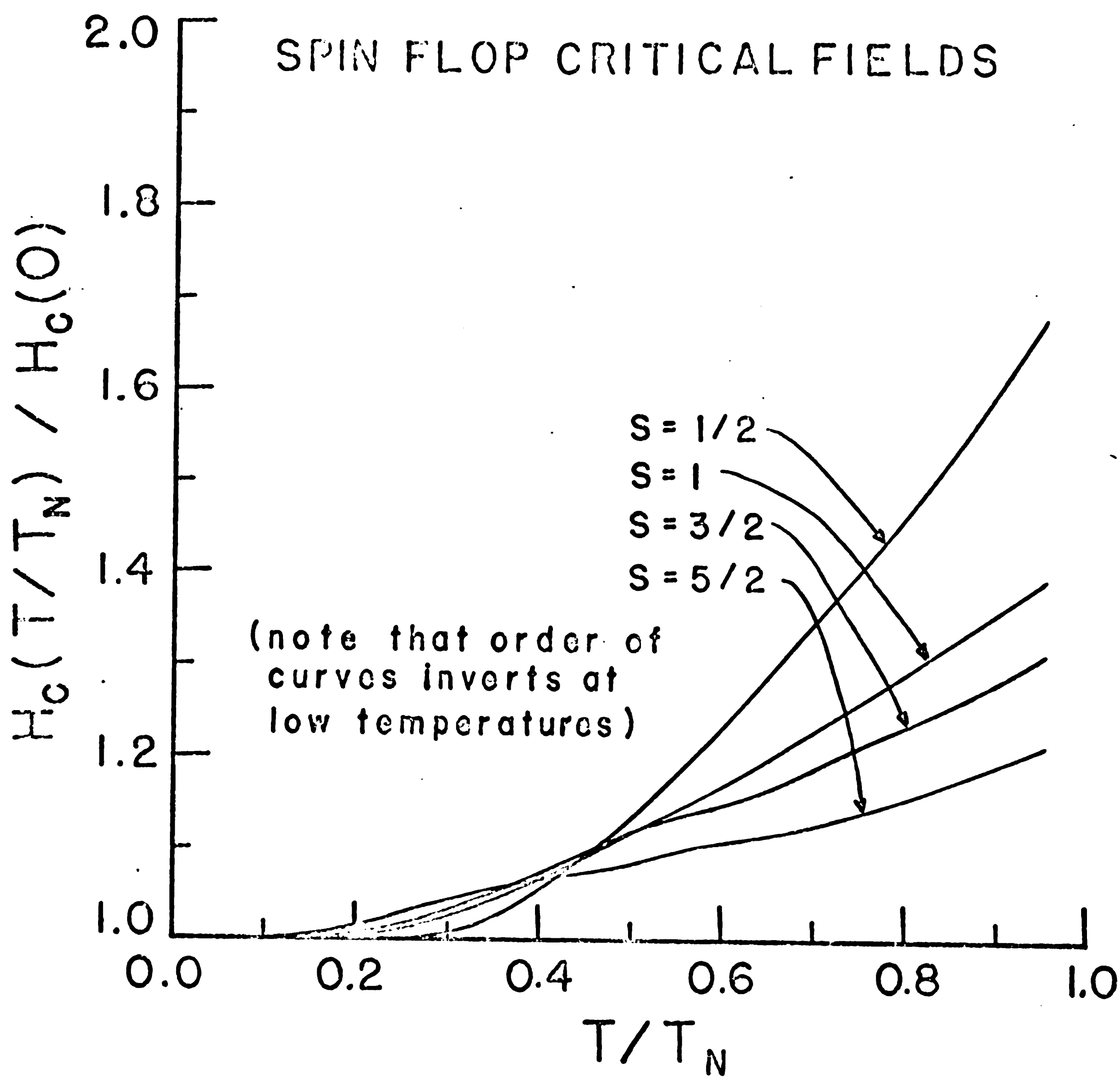

Fig. 5. Normalized spin flop critical fields.

$$\frac{dT}{dH} = \left(\frac{\partial T}{\partial H}\right)_S = - \frac{\left(\frac{\partial S}{\partial H}\right)_T}{\left(\frac{\partial S}{\partial T}\right)_H} \, , \tag{1.75}$$

where S now is entropy, H is field, and T is temperature. But

$$T \left(\frac{\partial S}{\partial T}\right)_H = C_H(T,H) \, , \tag{1.76}$$

where C_H is the constant field specific heat, and by a Maxwell relation:

$$\left(\frac{\partial S}{\partial H}\right)_T = \left(\frac{\partial M}{\partial T}\right)_H \, . \tag{1.77}$$

So,
$$\frac{dT}{dH} = \frac{-T}{C_H} \left(\frac{\partial M}{\partial T}\right)_H \, , \tag{1.78}$$

or,
$$\frac{dT}{dH} = - \frac{TH}{C_H} \left(\frac{\partial \chi}{\partial T}\right)_H \tag{1.79}$$

Thus if the system is in a state such that $X = X_{\parallel}$, then dT/dH is negative, since $dX_{\parallel}/dT$ is positive. If the system is such that $X = X_{\perp}$, then dT/dH is zero, since $dX_{\perp}/dT$ is zero. So, if the field is aligned along the easy axis and increased adiabatically, the temperature of the sample should decrease until the spins flop. Thereafter, there should be no magnetocaloric effect.

On the basis of the molecular field model Garret has computed the values of h and t along several isentropes for a spin 1/2 system and it is seen that the isentropes indeed have negative slopes in the h-t plane. Isentropes could be calculated for a spin S system using the generalized Garrett equations previously derived above, but their general features should not be expected to vary much from the spin 1/2 system.

2. Variation of Temperature in an Isentropic Rotation

In addition, equation 1.67 may be combined with equation 1.79, for the case when the field is at an arbitrary angle θ from the easy axis. Then,

$$\frac{dT}{dH} = -\frac{TH}{C_H}\cos^2\psi\left(\frac{\partial\chi_\parallel}{\partial T}\right)_H, \tag{1.80}$$

where ψ is given by equation 1.34. In terms of θ,

$$\frac{dT}{dH} = -\frac{TH}{C_H}\frac{1}{2}\left(1 + \frac{\cos 2\theta - (H/H_c)}{(1 - 2(H/H_c)\cos 2\theta + (H/H_c)^2)^{1/2}}\right)\left(\frac{\partial\chi_\parallel}{\partial T}\right)_H . \tag{1.81}$$

Then, if $\left(\frac{\partial\chi_\parallel}{\partial T}\right)_H$ is relatively constant between T_0 and T_H, and if C_H is also relatively constant, equation 1.81 may be integrated from $(T_0, 0)$ to (T_H, H). Then,

$$T_h = T_0 \exp\left[c\int_0^h h'\left(1 + \frac{\cos 2\theta - h'}{(1 - 2h'\cos 2\theta + h'^2)^{1/2}}\right) dh'\right], \tag{1.82}$$

where $c = -\left(\frac{\partial\chi_\parallel}{\partial T}\right)_H H_c^2/2C_H$, and $h = H/H_c$.

(For the type of substances used in this study, c turns out to be of the order 1/10 to 1.)

$(T_h/T_0)^{1/c}$ has been calculated from 1.82 and is shown in Fig. 6. T_h/T_0 has

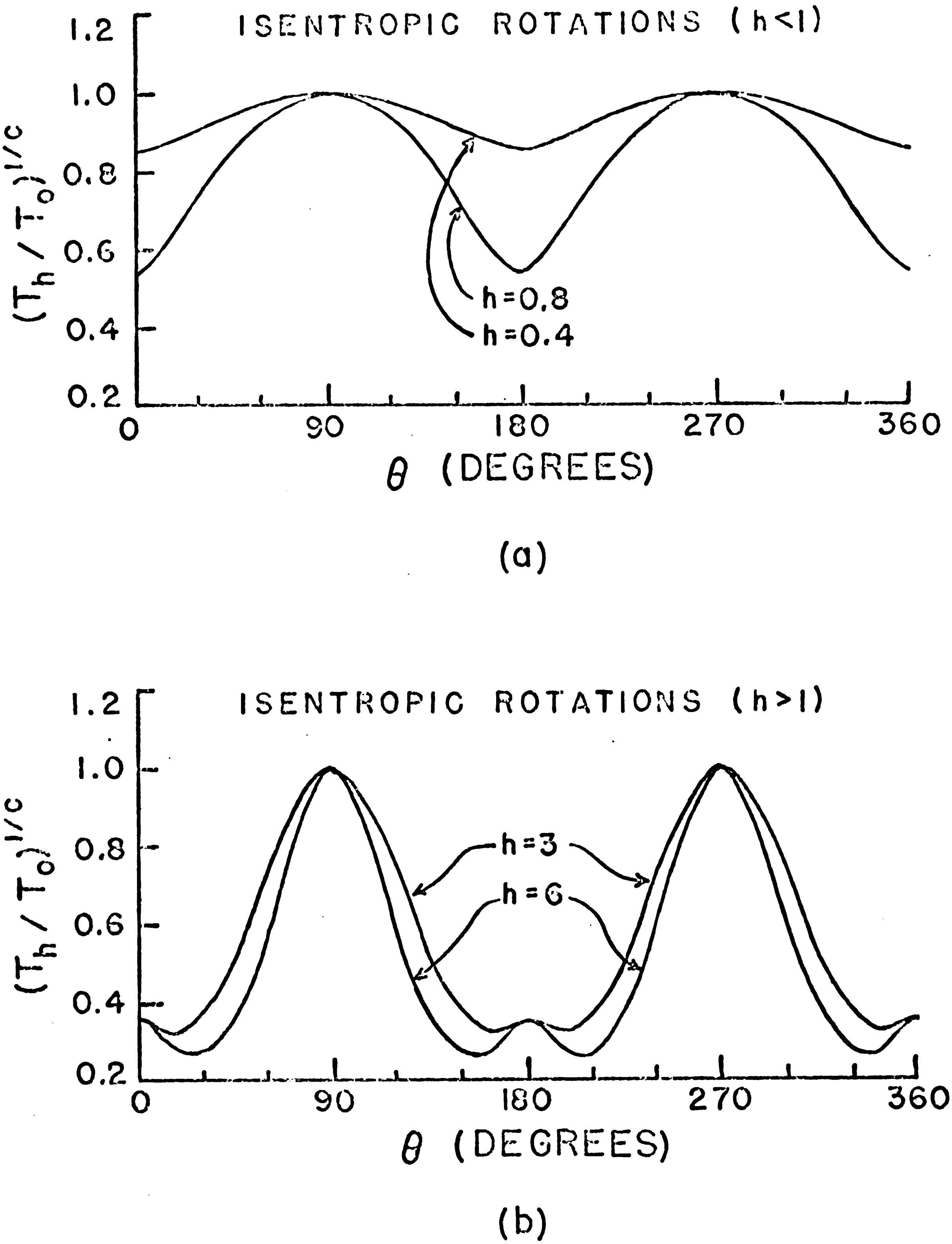

Fig. 6. Predicted temperature variation in an isentropic rotation.

been plotted against θ for several values of h. As can be seen in Fig. 6a, for h less than 1, the sample takes on its minimum temperature at $\theta = 0$. This fact can be used to align a magnetic field along the easy axis in an isentropic situation.

Furthermore, note should be taken of the fact that for h greater than 1, the minimum in temperature (as a function of angle in an isentropic rotation of the field) becomes a maximum, as seen in Fig. 6b. This may be used as confirmation of spin-flopping, although caution must be used, since the model is basically a two dimensional model, and the same results are not to be expected if the spins flop out of the plane of rotation of the field. Also, since, in fact, there also exists anisotropy in the paramagnetic state, if there is a change of principal axes between the antiferromagnetic and paramagnetic states, a temperature minimum becoming a temperature maximum may only indicate an antiferromagnetic-paramagnetic transition.

As an aside, note that although basically a two dimensional model has been used, Nagamiya[21] has done calculations for fields in different planes of a three dimensional system, and has found that spin-flop can exist in one crystal plane for values of h within a critical hyperbola region.

B. Observation of Paramagnetic Boundaries

Finally, as noted by Garrett, the transition from the antiferromagnetic state to the paramagnetic state is a second order transition. Thus, the point of the transition may easily be determined adiabatically by finding the temperature at which there is a discontinuity in the slope of the specific heat as a function of temperature in a constant field.

CHAPTER II

EXPERIMENTAL METHODS

I. Experimental Apparatus

The experimental data were taken, using two distinct types of calorimeters. With the exception of minor modifications, the main experimental apparatus has been described elsewhere[22], but for the sake of completeness it will be briefly redescribed below. A secondary triple-can calorimeter system, with modifications to cut down heat leaks, was used on a set of zero field specific heat runs and has also been previously described[23]. Only the modifications to it will be noted here.

A. Triple-Can Calorimeter Modifications

To reduce the heat leaks to the inner sample can of the triple-can system, the leads which previously came down this can's pumping line were brought in from the liquid helium bath through an epoxy seal similar to those of Wheatley[24]. A small tube was also attached to the end of the inner can's pumping line such that the line terminated in a T-joint, the pumping being through the sides of the T. Also, only the outer and middle cans were used on the runs. Prior to the above modifications, there were appreciable heat leaks to the sample at $1.2^{o}K$; these were eliminated for all practical purposes.

B. Main Dewar and Calorimeter

The main experimental apparatus consisted of the narrow-tailed pyrex helium dewar shown in Fig. 7 and the calorimeter shown in Figs. 8 and 9. The dewar is of common style, designed for insertion between the poles of a magnet, and was made to order by H. S. Martin & Son, Evanston, Illinois. The calorimeter was designed so that hopefully, temperatures below $1.2^{o}K$ could be reached. This was the lowest temperature that could be attained with the standard medium sized pump, which was available, pumping on a large volume of liquid helium through a large line. By pumping on a smaller volume of liquid helium which was surrounded by liquid helium, although still isolated from it, lower temperatures could be attained. This calorimeter was somewhat successful in this aspect, in that the temperature of the helium can normally could be reduced to $1^{o}K$. Note also should be made of the attempts to cut heat leaks to the inner can: 1) an extra shield was placed inside the top of the outer can to cut down radiation from the outer can evacuation line; 2) to reduce radiation into the inner can, right angle bends were put in its pumping line inside the top of the outer can flange; 3) the inner can evacuation lines (and the electrical leads in one of those lines) were partially surrounded by the inside helium bath; 4) the leads were wrapped around and varnished to the bottom of the helium can for good thermal contact; 5) a brass radiation shield to

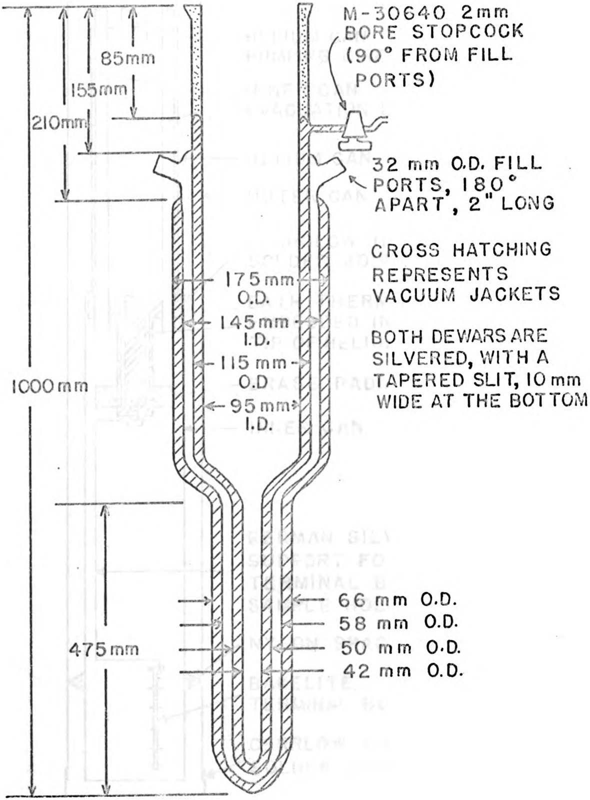

Fig. 7. Pyrex helium dewar.

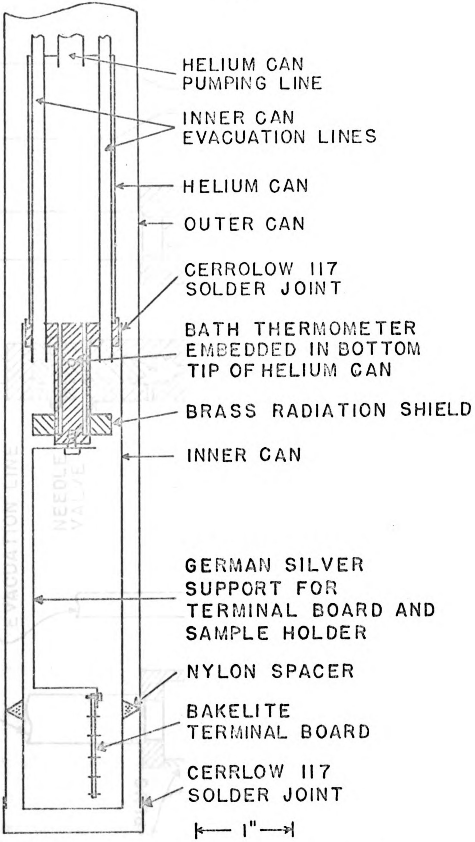

Fig. 8. Cross section of body of calorimeter.

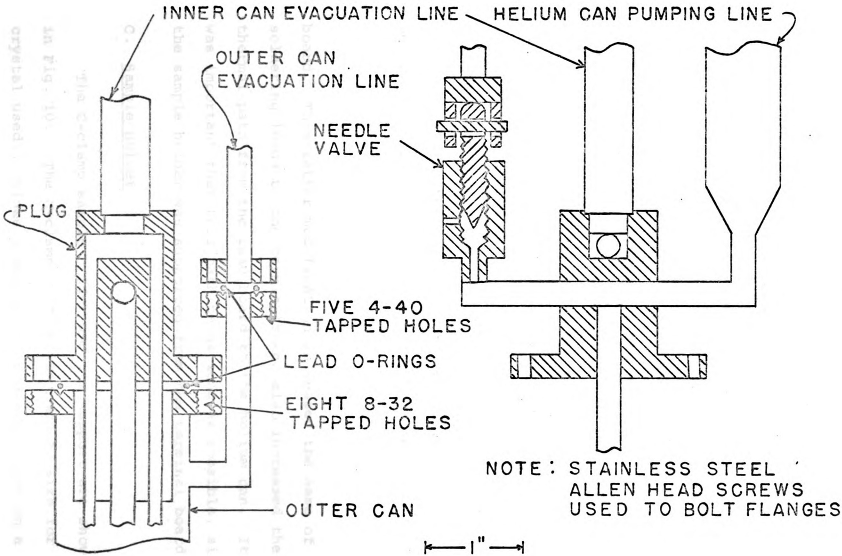

Fig. 9. Front and side cross sections of top of calorimeter.

block any radiation that did get down the inner can evacuation line was placed directly below the ends of the line; 6) copper, which has a higher thermal conductivity than brass, was used in most of the calorimeter below the outer can flange; 7) German silver, which has a low thermal conductivity and is non-magnetic, was used in the pumping lines which essentially support the outer can and its flange to the upper flange, and the inner can and the helium can to the outer can flange; 8) the bottom of the outside can was made removable to allow insertion of a nylon spacer which insured no direct physical thermal contact of the inner and outer cans.

The calorimeter differs from its previous description only in the brass radiation shield (which replaced an epoxy terminal ring-radiation shield) and the German silver extension strip which now supports a bakelite terminal board. This latter modification increased the ease of soldering leads to the terminals and also increased the thermal path from the lead board to the helium can. It was important that this path be as long as possible, since the sample holder was supported from the terminal board.

C. Sample Holder

The C-clamp sample holder and its support are shown in Fig. 10. (The C-clamp section was made to size for each crystal used.) Since a magnetic field experiment on a single crystal depends on the relative orientation of the

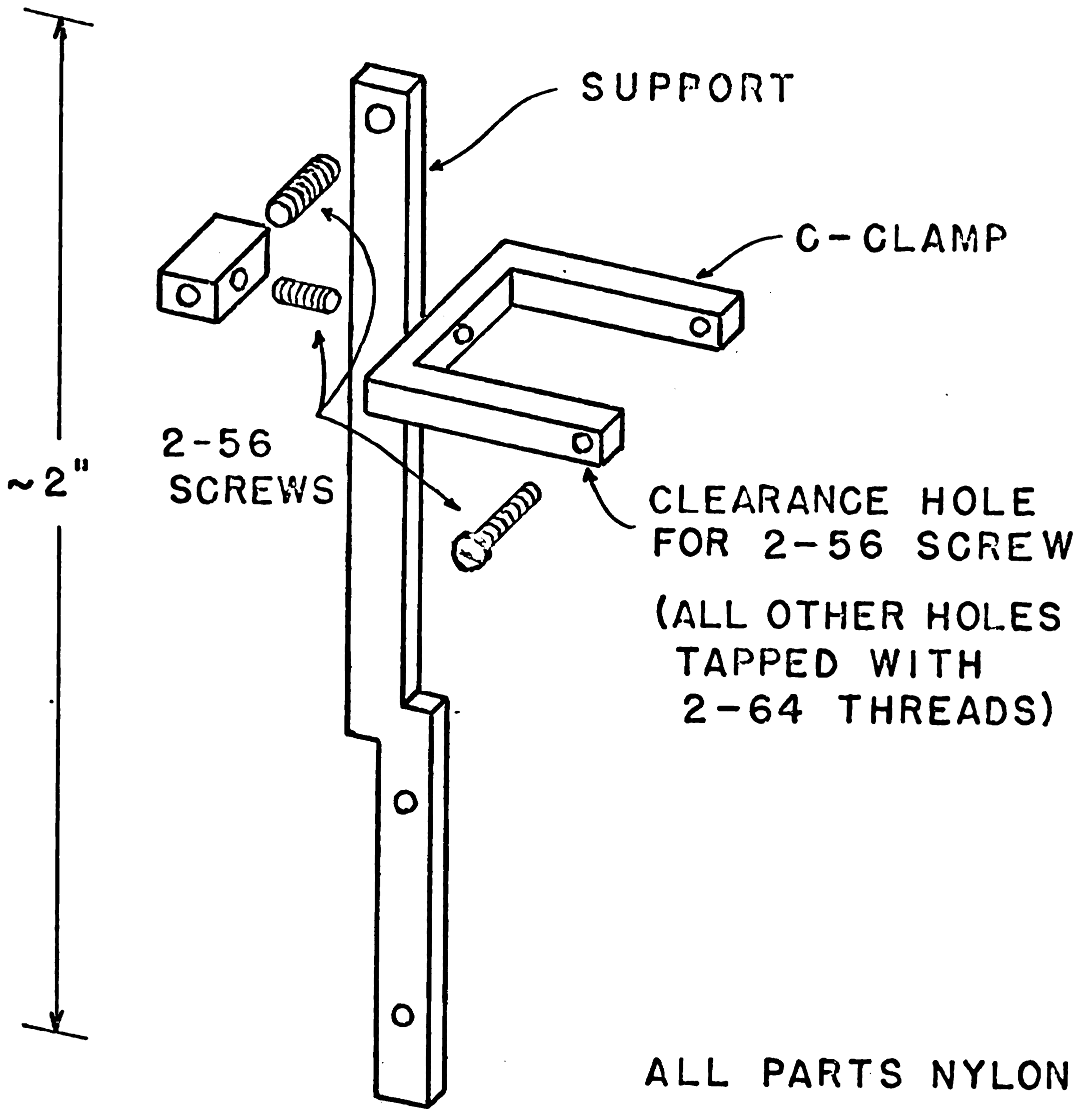

Fig. 10. C-clamp sample holder.

crystal and the field, it was important that the crystal be immobile. An early experiment showed that when a single crystal was supported by nylon threads and a field rotated about it, there was enough torque on the crystal to break the threads and free the crystal.

So, a more solid support was needed. However, since adiabatic experiments were to be done, a support with low thermal conductivity was needed. In addition, it was highly desirable that the support have some internal degrees of freedom so that a crystal's orientation might be changed. Other workers have used pyrex glass[25] and carbon[26], but it was felt that nylon had advantages over both of these, since it can be tapped to take a screw and since its thermal conductivity is lower than most other materials[27]. It should be noted that the threads tapped in the holder were for the next size smaller screw than was actually used in the holes. This procedure insured that the holder would maintain its position, once set.

It must be noted that the holder was not completely satisfactory, since a certain amount of heat leak still existed. How much these heat leaks actually affected the measurements depended on the heat capacity of the sample. The larger the heat capacity, the less a given heat leak affected its temperature. So, the holder provided only an apparent adiabatic situation and was not satisfactory in a region where the sample's specific heat was small.

D. Pumps

Five pumps were used in the experiments. The medium size, high capacity pump used to pump on the liquid helium was a Kinney KDH-130. The high vacuum system used to evacuate the inner and outer cans consisted of a Welch DuoSeal pump used as a forepump for a water cooled diffusion pump which, in turn, was used as a forepump of another water cooled diffusion pump. Pressures as low as 10^{-6}mm Hg were possible with this system. These pumping systems are shown schematically in Fig. 11. Another Welch DuoSeal pump was used to maintain a good vacuum on one side of the U-tube manometer system.

E. Pressure Gauges

Pressures in the high vacuum system could be read by means of an NRC thermocouple-ion gauge meter. Pressures in the liquid helium pumping system could be read on any of three gauges which could be connected to the system: a mercury filled U-tube manometer, an oil filled U-tube manometer, or a McLeod type gauge. Above 2.5 cm Hg of pressure, pressure was measured by measuring the difference in height of the mercury levels in the two arms of the mercury U-tube manometer. Below 2.5 cm Hg , the Todd McLeod type gauge was used. (It is important that no condensable vapors, e.g., air moisture, be allowed into a McLeod gauge system. Therefore, dry nitrogen gas was used to pressurize the gauge for each reading, and as there could

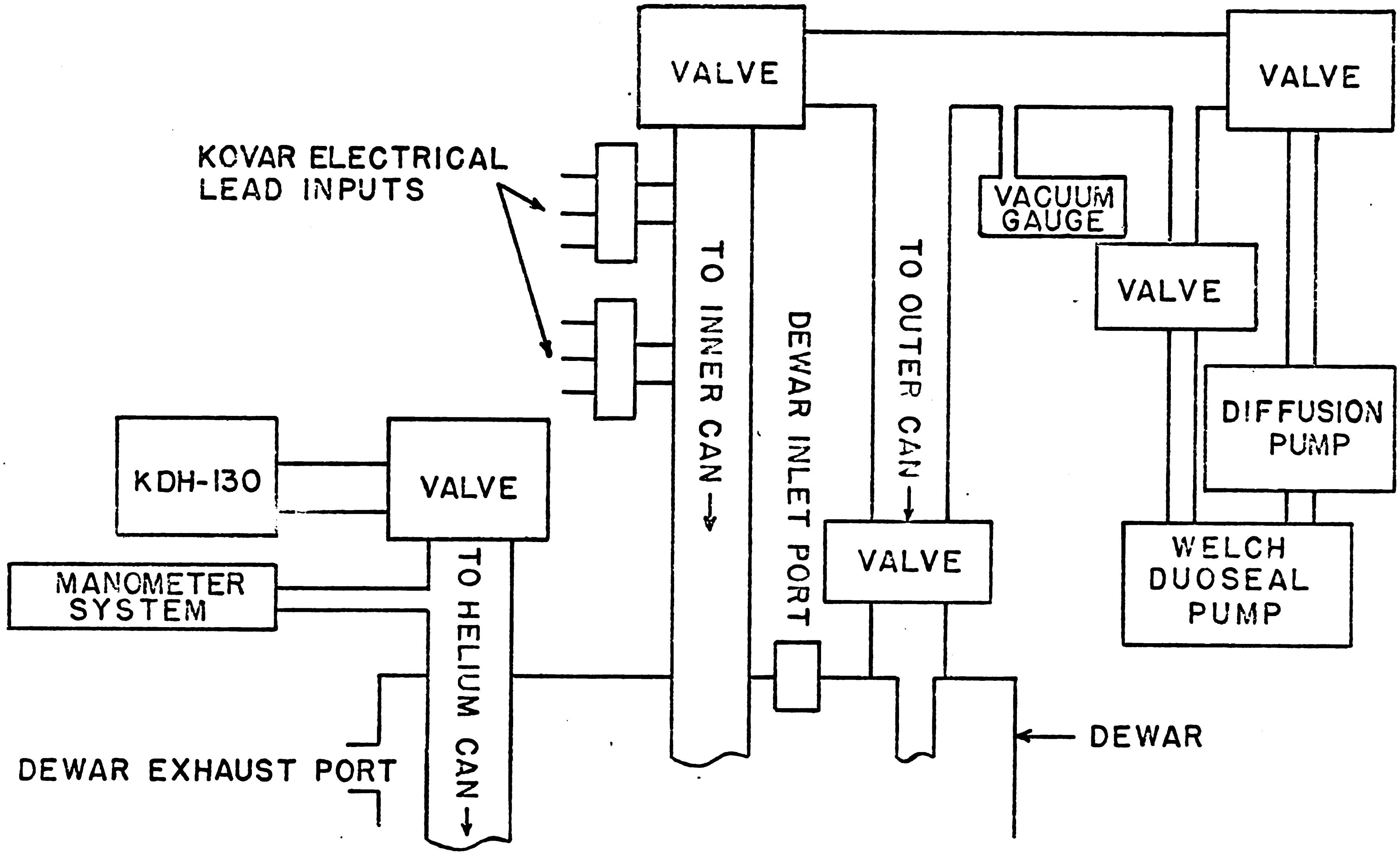

Fig. 11. Schematic diagram of pumping systems.

be a small amount of leakage of air into the system when it was shut down, the gauge was completely pumped out prior to its usage.)

The oil filled U-tube manometer was used below 4.0 cm. Hg for a qualitative observation of decrease in pressure (temperature) during the thermometer calibration part of a run. A Duragauge gauge (30 in. of vacuum to 15 # of pressure) connected to the pumping system at all times could be used as a crude qualitative measure of vacuum also.

F. Thermometers and Current Supplies

To measure temperatures, 1/10th watt 56 ohm Allen Bradley carbon resistors were used. Two six inch 31 mil manganin wires were soldered to each lead of a resistor, close to its body. Soldering was done at as low a temperature as possible while the resistor was being air cooled in order to lessen damage to the resistor. Current was passed through the resistor through two of the leads and the voltage across the resistor was measured potentiometrically through the other two leads. A one micro-ampere current was supplied by two 28 volt Mallory mercury batteries in series with three precision wirewound resistors totalling 56 megohms and a variable 20 megohm carbon potentiometer. The variable resistor was set to give the required current by potentiometrically checking the voltage across a 100K ohm precision resistor which was also in series with the batteries. To insure a stable temperature environment, all the above resistors and batteries were encased in a 1/2-inch thick wooden box, as it was determined that fluctuating room temperatures significantly affected the current output (this probably was due to variations in the carbon resistor or the batteries). Two of these current supplies were used: one to supply the sample thermometer, and another to supply the helium bath thermometer.

G. Measuring Electronics

A Leeds and Northrup K-3 potentiometer with a galvanometer system consisting of a Leeds and Northrup 9835-B microvolt amplifier used in conjunction with a Leeds and Northrup two-pen Speedomax G recorder (with a 5 millivolt range card) was used to either measure the resistance of the sample thermometer (the potentiometer balanced), or observe its change in time (the potentiometer unbalanced). The amplifier was attached to the potentiometer so as to give maximum sensitivity to the system. (The sensitivity of the system could be changed by means of the amplifier's range selector.)

A similar system (with only a one-pen recorder) was used to observe fluctuations in the temperature of the bath. This latter system was also used to measure the voltage across a 400 ohm heater on the sample. (A heater consisted of one foot of 14 mil Evanohm wire* with four leads similar

---

*Available from Wilber B. Driver Co., Newark, N.J.

to those attached to the thermometer.) (In this case the other pen of the two-pen recorder was used in the galvanometer system.) When a heater voltage was being measured, the current through the heater was monitored by using the one-pen recorder to read the voltage across a precision resistor in series with the heater. (The heater current supply consisted of three five-cell 6.6 volt Edison batteries in series with a variable resistor used to adjust the current output.)

The heater was switched on and off by a relay attached to an electronic timer which could be preset to run for a given length of time, once started. The relay connected an external resistor (of the same value resistance as the heater) in place of the heater in the heater circuit when the timer was off so as to minimize any pulses from the current monitoring recorder.

All the measuring circuits are box-diagramed in Fig. 12.

H. Magnet

The magnet used in the experiments was constructed from a yoke and poles made to order to accommodate 36 copper strip coils 21 inches in diameter. The poles were made from 10-10 cold rolled steel and were 6.75 inches in diameter. The pole gap was 2.75 inches. Current for the magnet was obtained from two D.C. generators placed in series with the coils. The current output of the generators

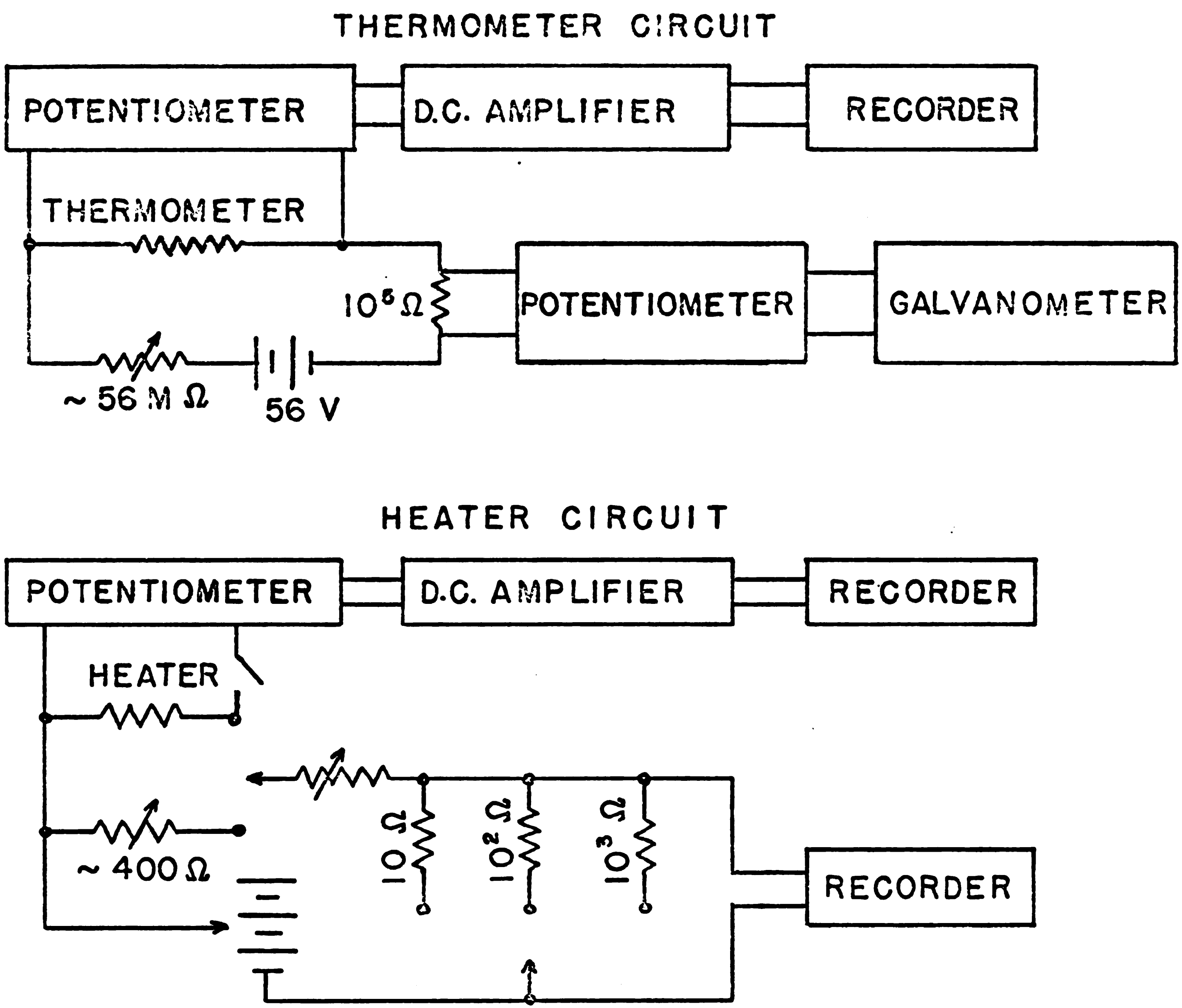

Fig. 12. Diagram of electrical measuring circuits.

was controlled by a variable rheostat in the field circuit of the generators, and a 50 ampere Simpson meter was used with a 50 mv shunt to measure the current in the coils. A Rawson-Lush rotating coil gaussmeter was used with a type 501 Rawson-Lush indicator to measure the field between the pole faces. The field was observed to be uniform, within the reading sensitivity of the indicator (about 20 gauss), over about five cubic inches in the center of the gap. The magnet was placed on a frame with a rotating base. A Selsyn motor was attached to the magnet frame and the motor's shaft was attached to the non-rotating center section of the base. This motor was connected in parallel to a similar motor attached to a two foot diameter dial. The latter motor's shaft had a pointer attached to it. This arrangement allowed easy angular adjustment of the magnet (a lever arm was attached to the magnet frame to ease its rotation). The magnet was air cooled by two fans placed beneath it.

II. Experimental Procedures

A. Sample Preparation and Precooling

An experiment actually begins with the growing of the sample to be used. Single crystals of one to two cc in size, of the types of materials used in this study, are often difficult to grow and much patience is required. Once an adequate size single crystal was available, it was refrigerated to prevent its losing or gaining water. When it was to be used in an experiment, the external angles between its faces were measured with a protractor-goniometer, and by comparison of these angles with those given in the literature, the crystallographic axes were determined. The sample was then weighed, a heater was wound around the crystal, and a carbon thermometer was tied to the crystal with a cotton thread. Usually the sample, the heater and the thermometer were then coated with G. E. 1202 varnish to insure good thermal contact. (Since the varnish reacted with $FeCl_2 \cdot 4H_2O$, Krylon clear plastic spray was used on the fourth sample of that substance, instead.)

The sample was then placed in the C-clamp portion of the nylon holder, and the clamp then tightened. Care was taken so that major edges and faces of the crystal remained visible. The entire holder was then screwed tight to the bakelite terminal board and the leads from the sample heater and thermometer were then soldered to their terminals. Then, it having been previously decided which crystallographic plane was to be parallel to the rotation plane of the magnet, the holder was adjusted so that the appropriate edges or faces of the crystal were horizontal or vertical. This was done carefully by eyesight, and, depending on the orientation desired and the sizes of the faces and edges used for the orientation, the amount of misorientation was estimated to be from two to five degrees.

The inside can was then slipped up under the helium can and soldered closed with Cerrolow Alloy 117*. The outside can was then slipped up onto its flange (with five-ampere Buss fuse wire O-rings in place on the O-ring grooves) and tightened down. The nylon spacer was slipped up between the inner and outer cans from the bottom of the outer can, after which the bottom was soldered in place with the Cerrolow alloy. The calorimeter being completely assembled, it was put inside the dewar and all flanges were sealed tight and electrical connections were checked for continuity.

The inner and outer can evacuation line valves were closed, the helium can pumping valve closed, the needle valve opened, and the dewar evacuated with the high capacity pump. Liquid nitrogen was then put into the dewar's nitrogen jacket; when the jacket was filled to the top, the pump was closed off and helium gas at atmospheric pressure was admitted to the inside of the dewar.

B. Helium Transfer and Calibration

The above procedure was generally accomplished in two to three hours so that there would be little damage to the crystal from exposure to air at room temperature. Several hours later, when it was certain the crystal was cold enough to be pumped on without damage, the air which had been trapped in the inner and outer cans was pumped off with the Welch pump of the high vacuum system. When the pressure

*Available from Cerro Sales Corporation, New York.

was below 50 microns Hg, the diffusion pumps were cut into the pumping system and were allowed to pump until the pressure was about 10^{-4} mm Hg. The high vacuum system was then closed off and helium gas at atmospheric pressure was admitted to the inner and outer cans. This procedure insured complete pre-cooling of the sample overnight.

Early the next morning, a thermometer calibration point at liquid nitrogen temperatures was taken by recording the thermometer's resistance, atmospheric pressure and room temperature. The helium exchange gas pressure was then reduced with the Welch pump to about 1000 microns Hg; with this pressure inside the cans and with the needle valve closed, liquid helium was transferred from a storage dewar into the experimental dewar. Both the bath and sample thermometer resistances were monitored on the two-pen recorder during the transfer. The transfer was done slowly enough to insure the sample's complete cooling to liquid helium temperatures before the end of the transfer. This procedure usually resulted in a five to seven liter transfer.

After the transfer, liquid helium was admitted into the helium can by opening the needle valve. The outer can valve was opened to the high vacuum system, the helium can pumping valve was opened, and the dewar vent valve was opened. When both the bath and sample thermometers had come to equilibrium, and when the pressure in the outer can was less than about $8 \cdot 10^{-5}$ mm Hg, another thermometer calibration point was taken by recording the resistance of the sample thermometer, room temperature, atmospheric pressure, and the approximate height of liquid above the sample. The needle valve was then closed, the dewar vent valve connected to a helium recovery system, and the high capacity pump needle valve opened to pump on the helium in the helium can. Approximately every 0.2-0.3^{0}K the pumping was slowed down to allow both bath and sample thermometers to come to equilibrium. Equilibrium of the bath was attained by adjusting the needle valve to keep the resistance of the bath thermometer (observed on the recorder) constant. When both thermometers were stable, the sample thermometer's resistance and atmospheric pressure were recorded, and the pump valve was again opened until the next calibration point was reached. Each calibration point generally took from ten to thirty minutes, and the entire calibration procedure lasted about three hours.

When the calibration was finished, the outer can valve was closed, and the inner can was evacuated. The sample was considered to be isolated when the pressure in the inner can was less than about $5 \cdot 10^{-5}$ mm Hg; the outer can valve could then be reopened.

C. Specific Heat Measurements

For a specific heat experiment, the potentiometer system which was being used to observe the bath thermometer was then set to observe the voltage across the sample heater, and the variable resistance in the heater circuit was set to give a heater current of about 0.1 ma. The potentiometer observing the sample thermometer was set off balance so that the recorder pen was near the left side of the chart, and the potentiometer reading (converted to resistance) was recorded. The automatic timer was started, the sample was heated, and the effect on the sample's temperature was observed on the chart recorder. The heat input was adjusted so that in 20-30 seconds there would be 10-20 divisions change in the position of the pen observing the sample. Since there are always some heat leaks present in a calorimeter, the sample's temperature was seldom constant when the heater was off. Depending on its temperature and the temperature of the bath, the sample was normally either warming or cooling. Heat was introduced to the sample only after there was a relatively constant rate of change of temperature for about a minute. When the recorder pen was at the right side of the chart, the potentiometer was adjusted so the pen moved back to the left side and the above procedure was repeated. (Each time the timer was on, the length of time it was on, the amount of current being used, and the voltage across the heater were recorded.)

D. Magnetic Field Experiments

Four different types of magnetic field experiments were done in this study: 1) adiabatic rotation of the magnetic field about the sample, 2) adiabatic magnetization of the sample, 3) discontinuous heat input to the sample (specific heat measurements), and 4) continuous constant power input to the sample. Generally a rotation was done immediately after isolating the sample and turning on the field.

By adiabatically rotating the field, the preferred axis of magnetization could be determined by looking for the magnet position in which the temperature of the sample was a minimum. For this positioning to be unambiguous, there could only be two minima 180^0 apart, thus insuring the sample to be in the AF state at the position of the minima. (If the field were higher than some critical value, the sample would be in some other state in the easy direction, and other minima would appear.) Generally, in order to be able to see a temperature difference upon rotation, the field had to be several kilogauss.

Although most rotation data points were taken five or ten degrees apart, the position of the easy axis was always determined to within one degree by careful observation of the temperature change on a slow continuous rotation. For each point taken in an adiabatic rotation, the magnet position was read from the Selsyn dial and the sample's temperature was determined by making a null measurement with the potentiometer of the voltage across the sample thermometer, thus determining its resistance.

After the direction of the easy axis was determined, isentropes could be measured along either the easy or hard axis (the hard axis being 90^0 away from the easy direction). Points on a given isentrope were obtained by potentiometrically measuring the sample's temperature for different values of field (the value of the field being determined from the current in the magnet).

After the initial isentrope was obtained, higher temperature isentropes could be obtained by warming up the sample through its heater and then measuring the temperature at different fields again. Since the nylon holder permitted a heat leak, any measured isentrope actually consists of parts of many close-lying isentropes. So, although the isentropes are not quantitatively correct in every detail, their shapes should be qualitatively correct.

Isentropes along the easy axis direction were used to observe first-order phase boundaries. In this case there was sometimes a change in sign of the slope of the isentrope at the boundary in the H-T diagram and the point of change could easily be followed in the H-T plane by observing only a small part of the isentrope near the change. Points were obtained by slowly varying the field and recording resistance and field values as near as possible to the point of change. In order to get a good average, since the measurements were quasi-static, several points were generally taken, both with the field being raised and with it being lowered. (If there was no point of change, a complete isentrope was taken with static measurements.)

To observe a second-order transition boundary, a constant field specific heat experiment was done until the boundary was crossed (easily seen by the sudden increase in the amount of temperature change for a given heat input). Then the field was set to a new value, the inner and outer can valves shut, the high vacuum pumping system closed off, and about .05-.2 mm Hg of helium gas admitted to the pumping line outside the inner can valve. The valve was slowly opened and the sample would cool back to the temperature of the helium bath. The amount of exchange gas determined the speed of cooling. The inside can was evacuated with the high vacuum system as soon as it was evident that the sample had cooled enough so that it was sure to be in the ordered state again. Then specific heat measurements were done again.

In some cases, for instance, when the heat leak was very large, the second-order transition point was observed by looking for a change in the slope of a continuous heating track on the recorder. (The point of slope change was also looked for in the specific heat measurements.) In these measurements , the potentiometer reading (converted to resistance) was recorded whenever the recorder pen was moved to the left side of the chart.

E. Shut-Down

At the end of a run, all pumps were opened wide, the diffusion pump heaters turned off, and liquid nitrogen maintained in the dewar jacket until about twelve hours before the calorimeter was to be removed from the dewar. The pumps were shut off and dry nitrogen gas was admitted to the dewar about four hours before removal of the calorimeter. Through these procedures, the sample was still cold when it was removed, so that damage to the crystal (from sitting in air at room temperature) was minimized. The sample was returned to the refrigerator after it was removed from the calorimeter.

III. Reduction of Experimental Data

Except for preliminary reduction of data from the recorder chart, all data reduction and calculations were done on the M.S.U. CDC 3600 computer. Appendix I contains a listing of the programs used plus a listing of a typical input deck.

A. Conversion of Pressures to Temperatures

Most of the data reduction is involved with determining the temperature of the sample. The pressure readings taken for each run, for the calibration of the thermometer, were first changed into pressures at $0^{o}C$. Then hydrostatic corrections were made for the pressure of the amount of liquid helium above the sample, since the vapor pressure measurements correspond to the temperature at the surface of the liquid. A correction was added to the $0^{o}C$ corrected manometer reading, equal to the height of the helium times the density of helium at its estimated temperature divided by the density of mercury at $0^{o}C$. (For the main calorimeter, the height of the helium could not be seen after the initial point, since the helium was isolated inside the cans, so the height was guessed to be six or seven cm.) Since a temperature gradient cannot exist in liquid helium below the lambda point ($2.17^{o}K$), hydrostatic corrections were not made below this temperature. Also, below a pressure of 2.5 cm Hg, no pressure corrections to $0^{o}C$ were made, since those readings were taken on the McLeod gauge which is relatively insensitive to temperature changes.

The corrected pressure readings were translated to temperatures using "The 1958 He^4 Scale of Temperatures"[28]. The nitrogen temperature calibration point, taken before the helium transfer, was translated to a temperature from the equation[29]

$$T = \frac{255.821}{6.49594 - \log_{10} P} + 6.6 \ ,$$

where P is the $0^{o}C$ corrected manometer reading in mm.

B. Temperature Calibration Equation

An equation was then fitted to these resistance-thermometer calibration points for interpolation (or extrapolation) of temperatures from thermometer resistances. The standard equation that has been used[30] is

$$\sqrt{\log R/T} = a + b \log R,$$

where R is resistance and T is temperature. However, it has been observed that when the calibration points are least-square fitted with the above equation, there are systematic deviations of the points from this curve for the thermometers used in this study. To take advantage of this fact, the relative deviations are then least-square fitted to a polynomial in log(resistance). (Normally, a fourth degree polynomial was used, although, in order to reduce extrapolation errors, a third degree fit could be used if there was to be any extrapolation from the equation.) Thus, given a thermometer resistance, the corresponding temperature could generally be calculated from the following equation:

$$T = \log R \left[\frac{a + b \log R}{1 - \sum_{0}^{4} C_n (\log R)^n} \right]^{-2} .$$

This type of fit usually resulted in no more than 0.1-0.2% deviations of the measured points from the fitted curve. If there was to be much extrapolation above the helium calibration region, the unmodified two parameter equation was used for the fit, since a separate experiment in which a carbon resistance thermometer was calibrated against a germanium resistance thermometer showed there to be less extrapolation error in this case. Similarly, if there was much extrapolation below the lowest calibration point, the straight line fit was assumed to induce less error. (Another possiblity of a calibration equation is $1/T$ = a polynomial in log R. The fits resulting from this equation were never as good as those from the modified straight line fit, so it was never used.)

C. Determination of Thermometer Resistances

If a potentiometer null reading was taken, the thermometer resistance was merely determined by dividing the reading by the current in the thermometer. For the cases, as in specific heat measurements, where null measurements were not made, but the distance of the recorder pen from the null position was known, a "voltage calibration" had to be made in order to relate the resistance of the thermometer and the potentiometer setting when the pen was at a given distance from the potentiometer null position. The relationship used was (see Appendix II):

$$R_T = \frac{R_0 - [C_1 - C_2R - 2C_3R^2 - 3C_4R^3]D}{1 + [C_2 + 2C_3R + 3C_4R^2]D} ,$$

where R_T = the actual thermometer resistance, D = the number of divisions on the chart the recorder pen was to the right of the null position; R initially was set equal to R_0, the potentiometer setting divided by the thermometer current, and the C's are constants determined from the fit to the voltage calibration points. The calculation was reiterated then, using $R = R_T$ of the previous calculation until two successive iterations differed by less than 0.1%. The C's in the above equation were the coefficients obtained from fitting the voltage calibration points taken off the chart to a third degree polynomial. A voltage calibration point was automatically obtained each time the recorder pen was made to move across the chart by changing the potentiometer setting. R_0L was the potentiometer setting when the pen was at the left of the change and R_0R the setting when it was at the right (both readings were converted to resistance). DL and DR were the number of divisions to the right of the null position when the pen was at the left and right sides of the change respectively. (See Fig. 13.) The abscissa and ordinate used in the fit were $(R_0L + R_0R)/2$ and $(R_0L - R_0R)/(DL - DR)$ respectively. (Generally, the change was made across the null position so that $(R_0L + R_0R)/2$ approximated R_T.)

During the runs on sample four of $FeCl_2 \cdot 4H_2O$, in which the thermometer resistance was very large, it was discovered that there was considerable non-linearity across the chart page. Some of the observed voltage calibration points, plotted against the average number of divisions from the null position at which each point was taken are shown in Fig. 14. A graph of voltage calibration points plotted against thermometer resistance, for different distances from the null position, derived from the previous plot, is shown in Fig. 15. Using this last graph, it was possible to estimate R_T, for the pen sitting D divisions right of the null position and a converted potentiometer setting of R_0, using the crude equation

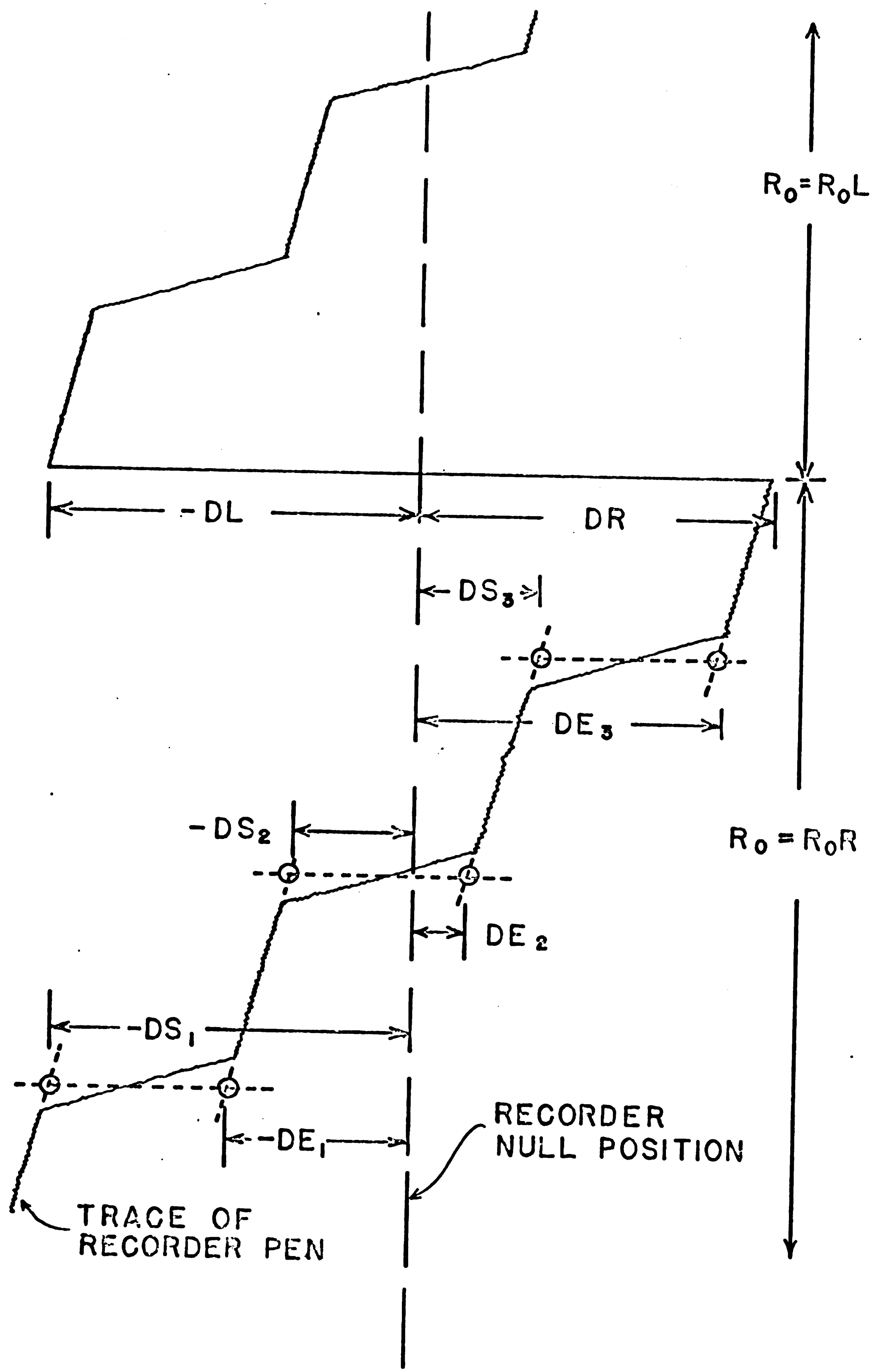

Fig. 13. Example of preliminary reduction of chart data.

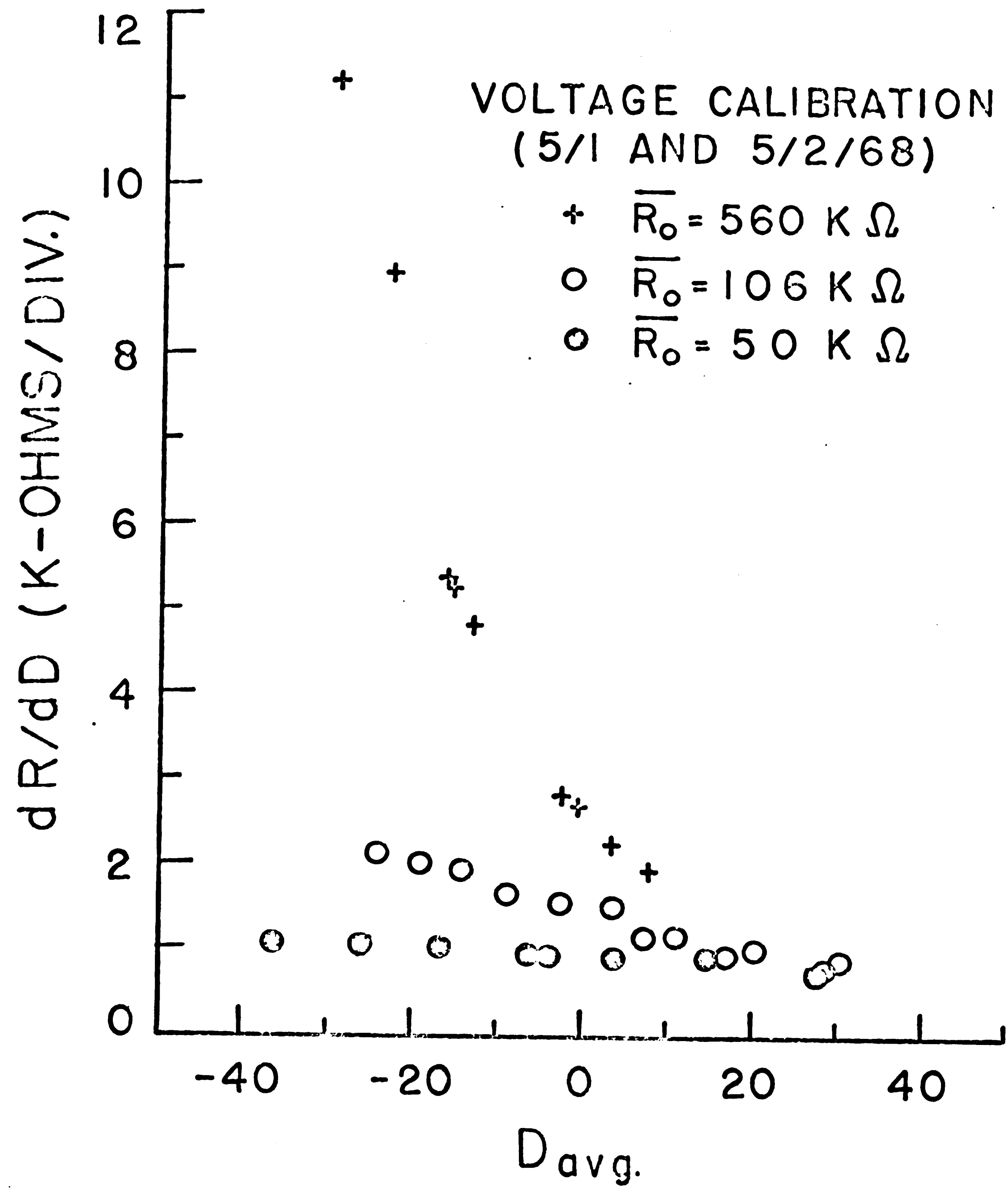

Fig. 14. Voltage calibration points from $FeCl_2 \cdot 4H_2O$ (sample 4) runs.

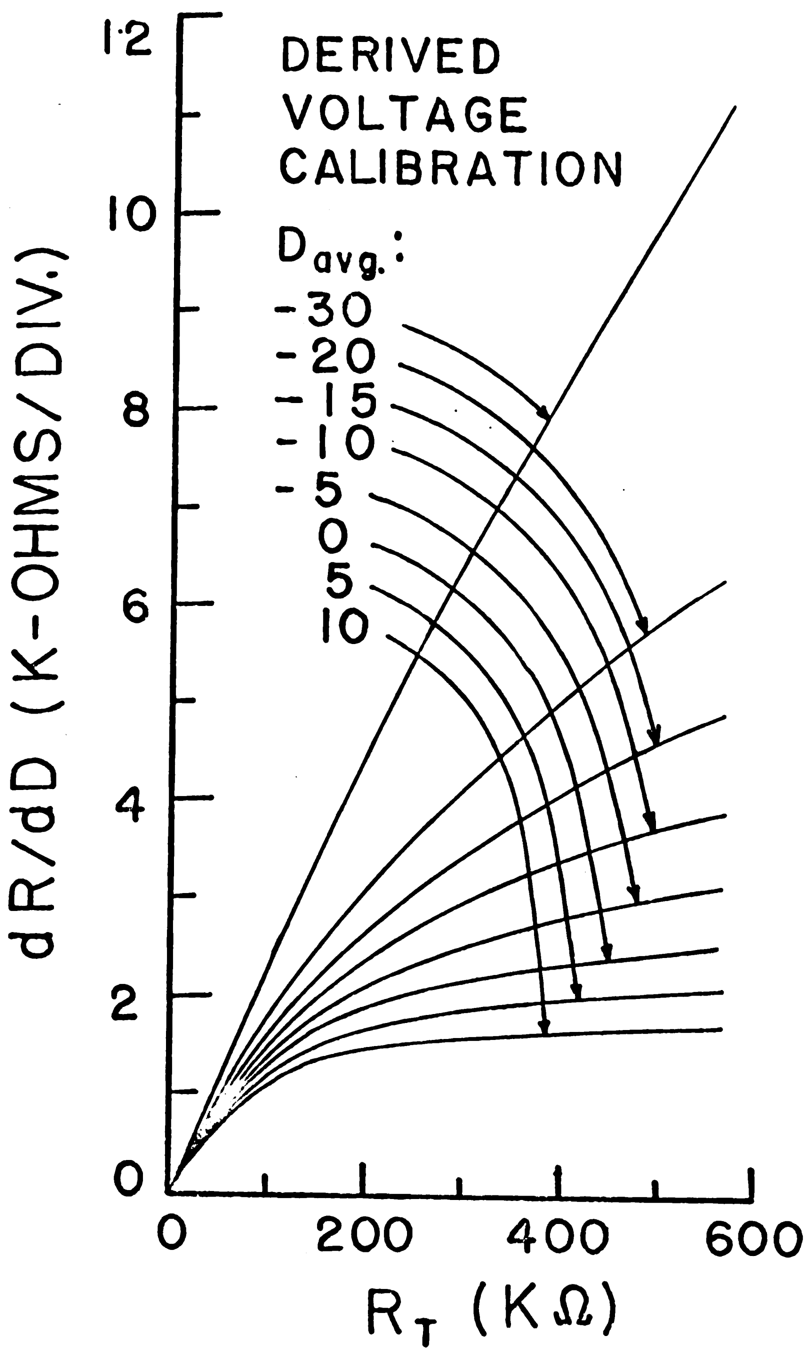

Fig. 15. Voltage calibration derived from Fig. 14.

$$R_T = R_0 - \left(\frac{dR}{dD}\right)_{D,R_0} D,$$

where the quantity in parentheses is the appropriate number estimated from the second graph.

D. Specific Heat Calculations

The variable quantities in a specific heat measurement were the heat input to the sample and the temperature change of the sample produced by that heat input. The quantity of heat was equal to the (voltage across the heater) x (the current through the heater) x (the length of time the heater was on). The effect of heat leaks on the sample was subtracted out by the graphical method indicated in Fig. 13. The method minimizes any effect from a change in the rate of the heat leaks and approximates the ideal situation where the heat input is instantaneous to the sample. (For a small heat input, there should be little effect to the heat leak rates.) Thermometer resistances were calculated for the positions DS and DE with a converted potentiometer setting of R_0 and were then transformed into temperatures. The difference of the temperatures was used to calculate the specific heat and their average was considered to be the temperature of the sample.

E. Calculation of Magnetic Field

In order to obtain slightly better values for the magnetic field as a function of the magnet current, an eighth degree polynomial in the current was fitted to about 50 current-field calibration points. Any necessary interpolation was then made from the fitted curve. The calibration curve of the magnet is shown in Fig. 16.

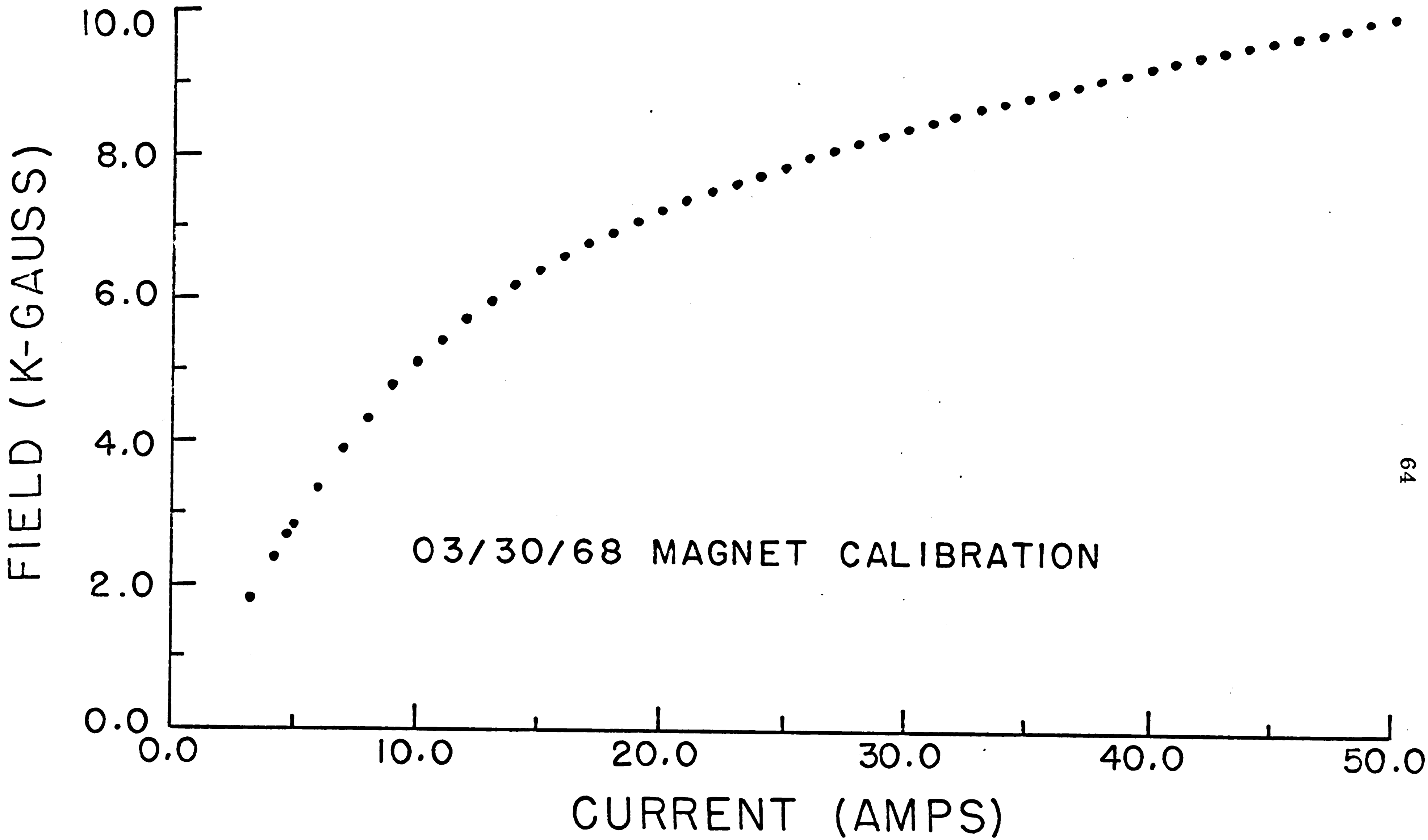

Fig. 16. Magnet calibration curve.

CHAPTER III

RESULTS AND CONCLUSIONS

I. Results

A. Results of Experiments on Samples with Known Spin Flop Phases

Since the adiabatic method used to observe the spin flop state of an antiferromagnet was new, observations were made on two materials whose spin flop states have been previously studied. The studies on $CoCl_2 \cdot 6H_2O$[31,32] and $MnCl_2 \cdot 4H_2O$[33,34] have indicated that both substances exhibit spin flop properties near 1^oK below 10,000 gauss. Thus, since these regions of field and temperature were attainable with the present equipment, these substances offered a good test for the adiabatic method of observing the spin flop state.

A nearly single crystal of $CoCl_2 \cdot 6H_2O$, weighing about 0.8 grams, was grown from an aqueous solution at room temperature. $CoCl_2 \cdot 6H_2O$ is monoclinic with the angle $\beta = 122^o19'$. The habit has been described by Groth[35] and the crystal was oriented on the basis of that description. As noted by Schmidt and Friedberg[32], large single crystals of $CoCl_2 \cdot 6H_2O$ are difficult to grow. Since the faces of the crystal used in this study exhibited some irregularities, more than likely it was not completely single.

Experimental measurements were made in three different crystallographic planes: the BC plane, the AB plane and the AC plane. Isentropic field rotations were made in each of these planes at two different fields, one below and one above the critical field for spin-flopping. (The previous measurements on $CoCl_2 \cdot 6H_2O$ have indicated a critical field of 7200 gauss at 1^0K which rises to a value of 7825 gauss at 2.06^0K.) The results are shown in Figs. 17, 18, and 19, and the data are listed in Tables 1, 2, and 3 of Appendix III. (It should be noted that in most of the isentropic rotations in this study, there were imperfect adiabatic conditions, so that at the end of a complete rotation, a sample's temperature may have been different from its temperature at the beginning of the rotation.)

Note should be made of the peculiar shift of the maximum in the two BC rotations, for which there is no explanation at present. Also, a third BC rotation, which is not shown, was done in a higher field of 8830 gauss. The results of this rotation reproduced, almost point for point, the results of the low field rotation of Fig. 17a. Although it is doubtful, there is a slight possibility there was a misreading of the field in one of these rotations. Thus, further investigation into the behavior of the magnetization in the BC plane is indicated.

Since in two of the isentropic rotations, in fields below the reported critical field (Figs. 17a and 19a), the temperature is a minimum in the C direction; this direction

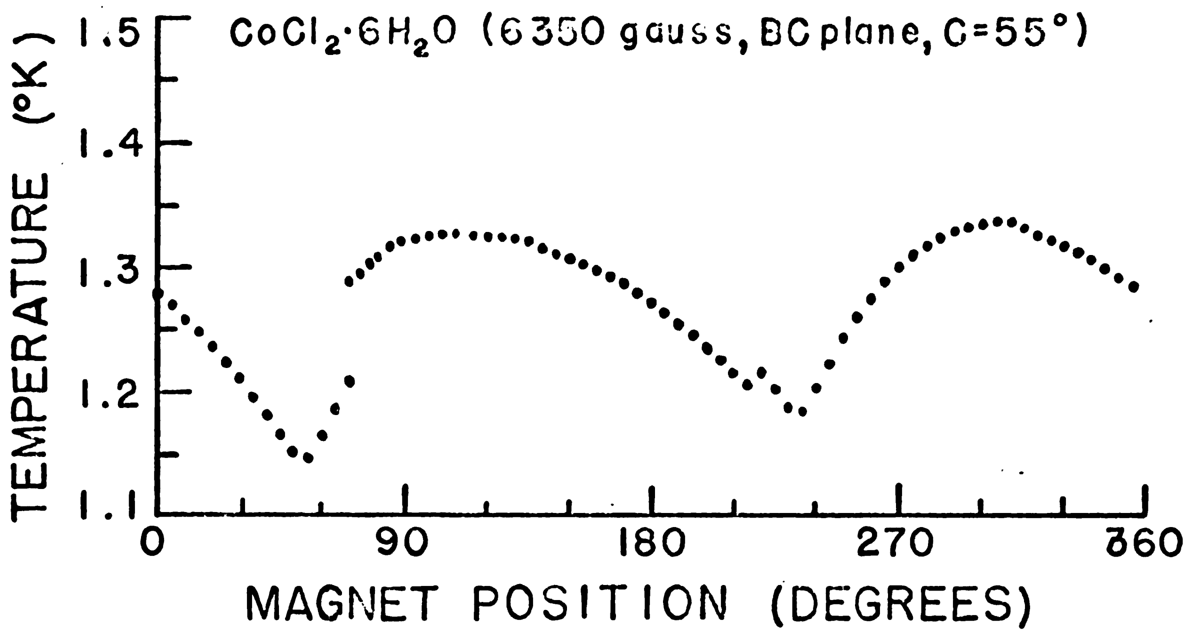

(a)

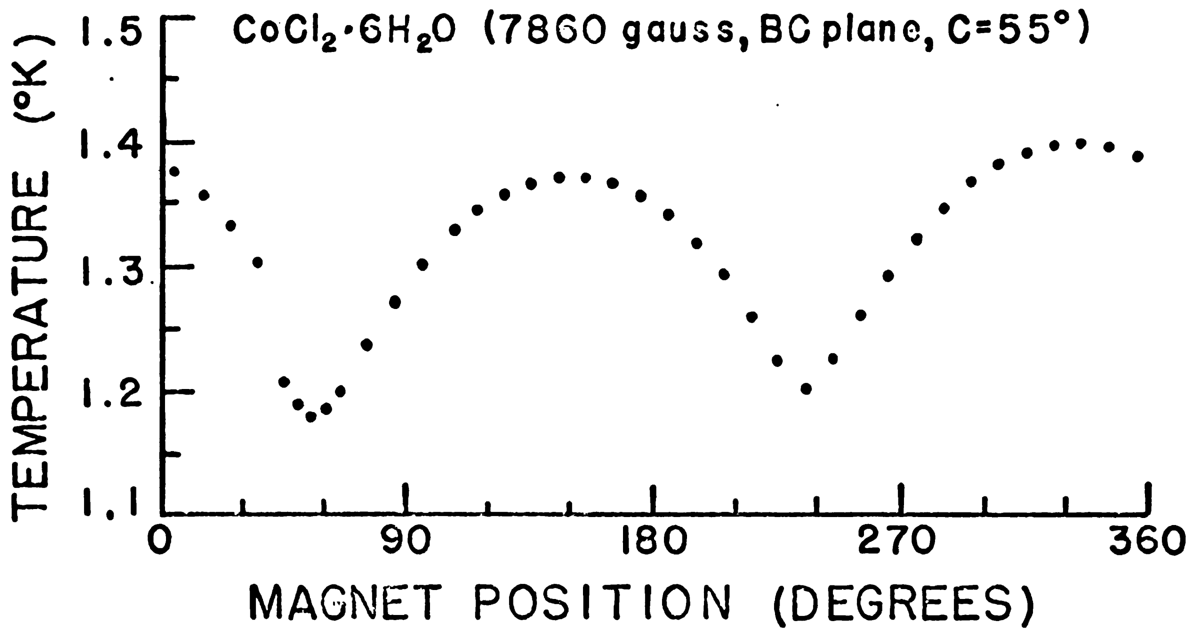

(b)

Fig. 17. $CoCl_2 \cdot 6H_2O$ BC plane isentropic rotations.

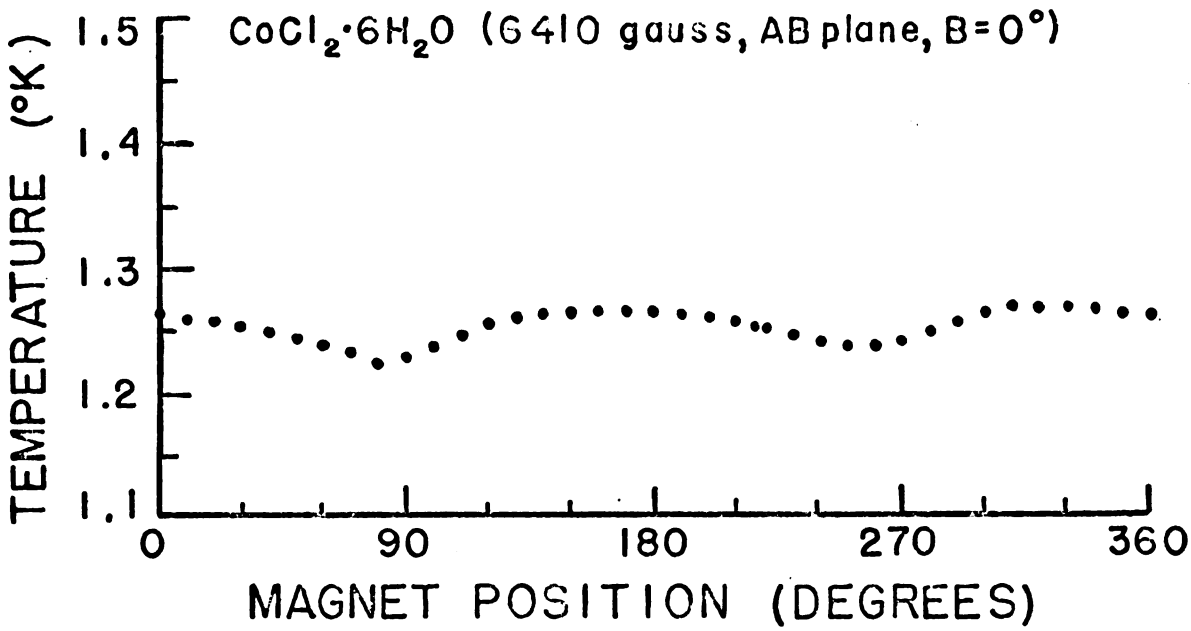

(a)

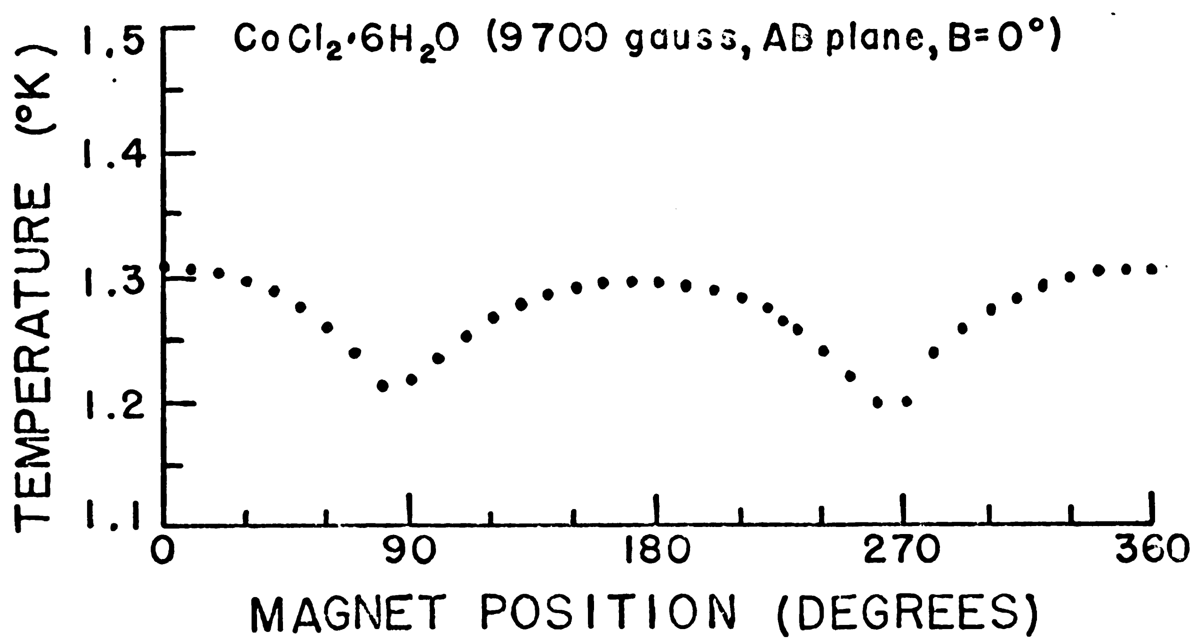

(b)

Fig. 18. $CoCl_2 \cdot 6H_2O$ AB plane isentropic rotations.

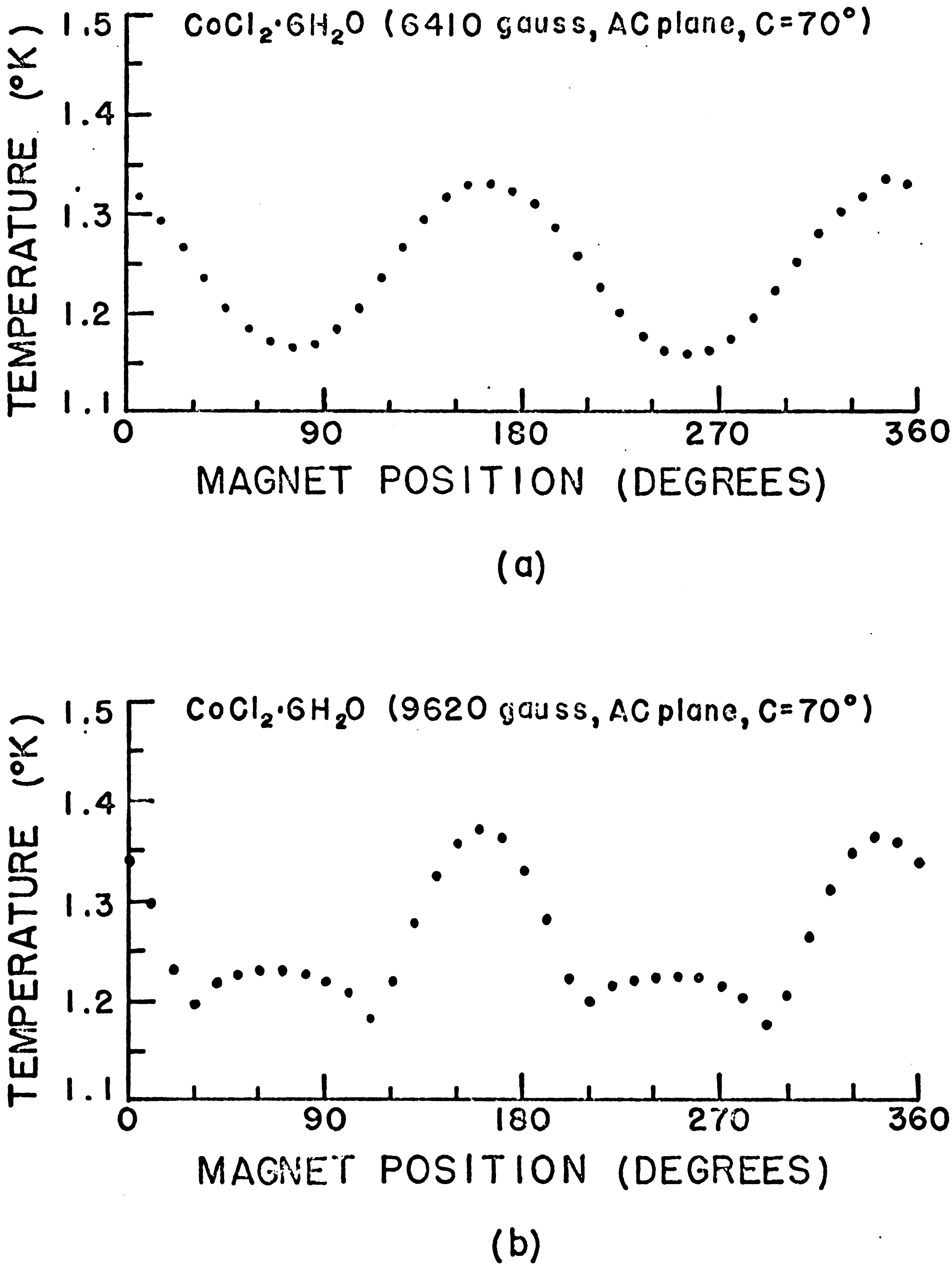

Fig. 19. $CoCl_2 \cdot 6H_2O$ AC plane isentropic rotations.

is, on the basis of the discussion of isentropic rotations in Chapter I and the predicted behavior shown in Fig. 6a, the preferred axis of magnetization. This is consistent with the susceptibility results of Haseda[36], which gave the same indication.

The AB rotations (Fig. 18) show nothing remarkable, although it is worth noting that it can be seen from these rotations, that since the temperature is a minimum in the A direction, after the C axis, the A axis (or perhaps the A' axis) is the next most preferred axis of magnetization. Thus if the spins flop, they should flop to the A (or maybe A') direction, and an AC plane isentropic rotation, above the critical field, would be expected to produce results as predicted in Fig. 6b.

The results of the AC plane high field rotation, shown in Fig. 19b, do indeed qualitatively correspond to Fig. 6b, and that $CoCl_2 \cdot 6H_2O$ undergoes spin flop (the spins flopping to the A' direction) is partially indicated by these results.

More conclusive evidence that $CoCl_2 \cdot 6H_2O$ enters a spin flop phase between 7200 and 7800 gauss in the temperature region 1.2-1.7^0K is given by the results of the isentropic magnetizations along the C axis. The isentrope points thus obtained are listed in Table 4 of Appendix III and Fig. 20 shows smooth curves which have been drawn through the individual data points. As can be seen, there is cooling upon magnetization initially, which disappears when the spins flop.

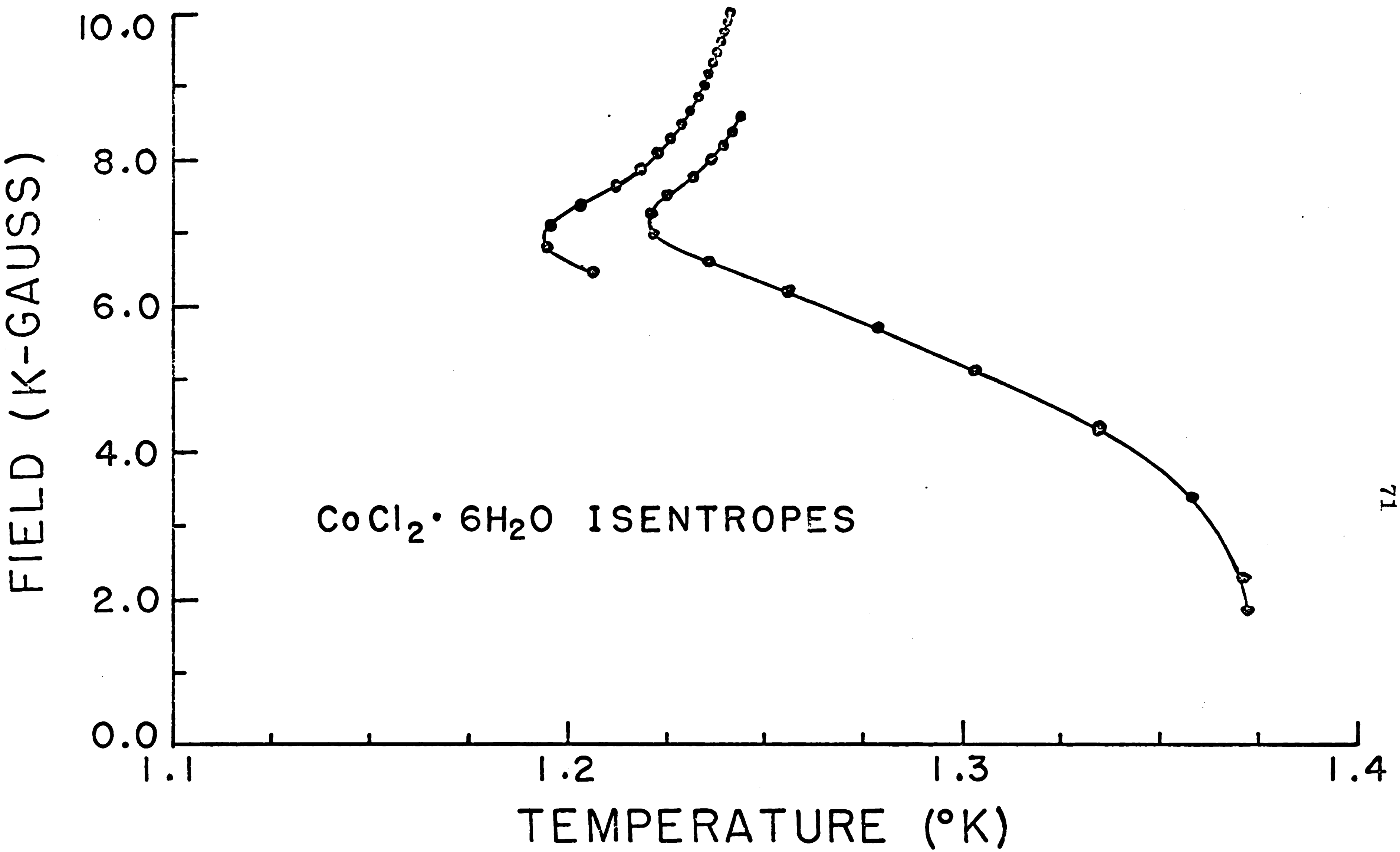

Fig. 20. $CoCl_2 \cdot 6H_2O$ isentropes.

Note should be taken of the change in sign of the isentropes' slopes near 7200 gauss. This fact, as mentioned in Chapter II, allowed determination of the point of the phase change without measuring a complete isentrope. The points thus obtained are listed in Table 5 of Appendix III and are shown in Fig. 21, along with a smooth line representing the phase boundary results of Van der Lugt and Poulis. (The results of Schmidt and Friedberg coincide closely to those results and therefore are not shown.) No points were taken above about 1.76^0K, since the change in sign of the isentropes' slopes disappeared above that temperature. However, it is clear that the points obtained coincide very well with the previously published results.

(To further verify that there is no magnetocaloric effect when the spins are perpendicular to the field, an isentropic magnetization along the B axis was done when the crystal was in the AB plane of rotation orientation. When the field was changed from about 6400 gauss to near 10,000 gauss, there was less than 5 millidegrees fluctuation in the sample's temperature, thus confirming the predictions of the theory.)

Also, an isentropic rotation was done in the paramagnetic state in the BC plane. The data is given in Table 6 of Appendix III and is shown in Fig. 22. It is seen that in this plane, from observation of the temperature variation in the rotation, the anisotropy is considerably smaller in the paramagnetic state than in the ordered state. Also

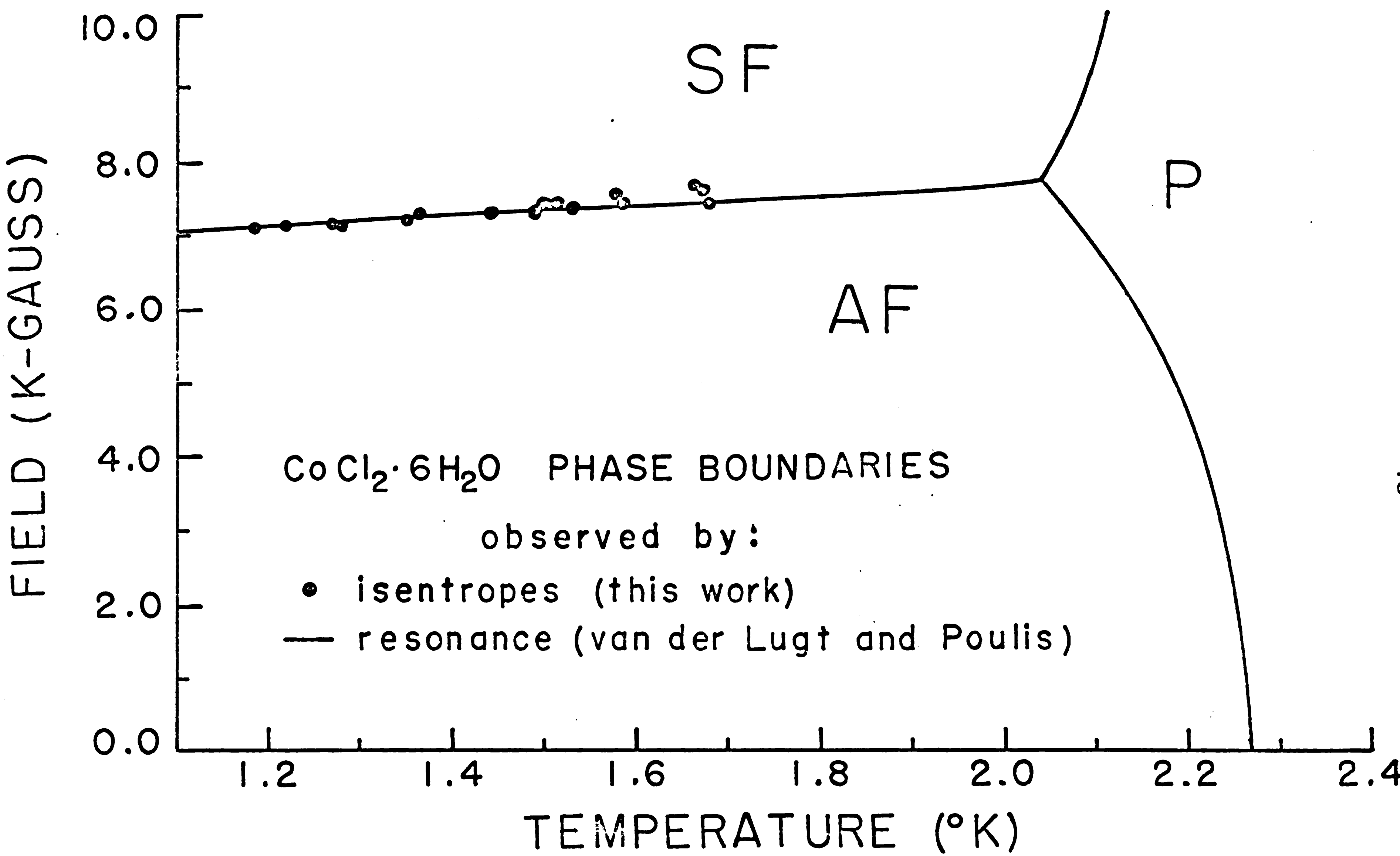

Fig. 21. $CoCl_2 \cdot 6H_2O$ phase boundaries.

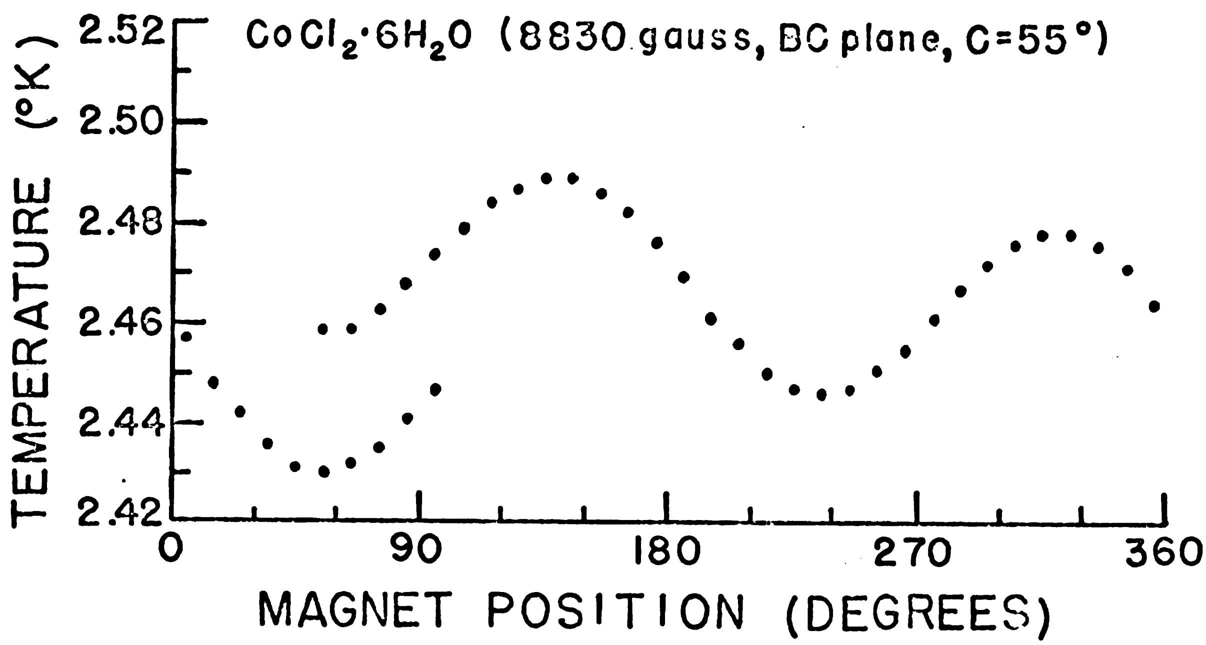

Fig. 22. $CoCl_2 \cdot 6H_2O$ BC plane paramagnetic isentropic rotation.

it is seen that there is no change of principal magnetic axes between the ordered and unordered state, at least as far as the B and C axes are concerned.

Two points that may merit further investigation are the following. First, the magnitude of the field used in the high field AC rotation, relative to the critical field, should not have been expected to produce the relatively large change in the behavior of the sample when the field was near the C axis, as seen in Fig. 19. Secondly, the observed change in sign of the isentrope slopes was not predicted by the simple molecular field theory, and is not yet understood.

For the measurements on $MnCl_2 \cdot 4H_2O$, two different portions of single crystals, borrowed from R. D. Spence, were used in separate experiments. The first crystal weighed about 1.0 grams and the second about 1.7 grams. The morphological description given by Groth[35] was used as the basis of the orientation of each crystal. Like $CoCl_2 \cdot 6H_2O$, $MnCl_2 \cdot 4H_2O$ is monoclinic with $\beta = 99.74^0$.

The previous measurements have indicated that the preferred axis in $MnCl_2 \cdot 4H_2O$ is the C axis and that a transition to the spin flop phase takes place in a field near 8000 gauss near 1^0K. Thus, measurements were made only in the AC and BC planes for $MnCl_2 \cdot 4H_2O$. The results of two isentropic rotations (below and above the critical field) in each of these two planes, using the first crystal, are shown in Figs. 23 and 24, and the data are listed in Tables 7 and 8 of Appendix III.

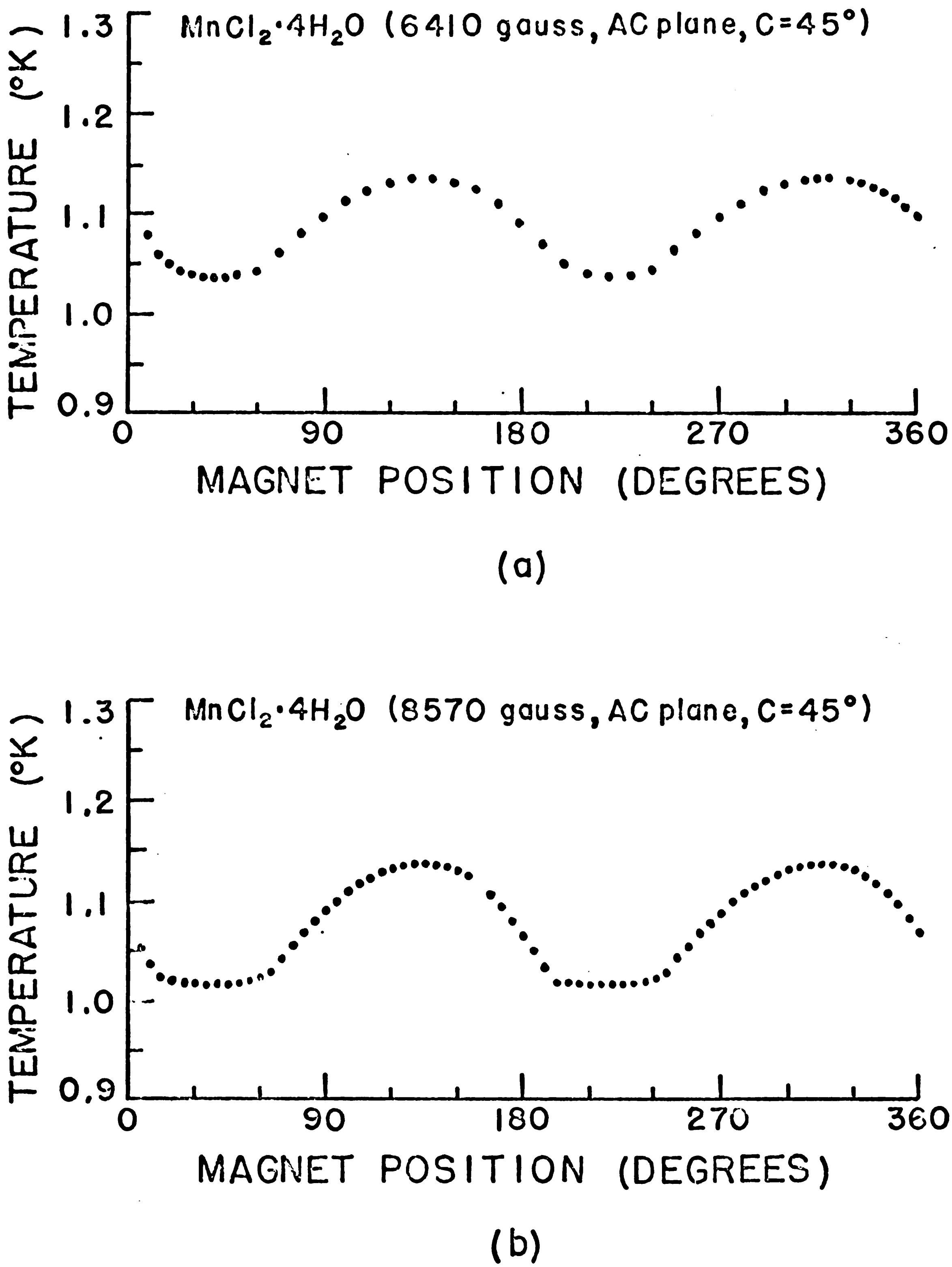

Fig. 23. $MnCl_2 \cdot 4H_2O$ AC plane isentropic rotations.

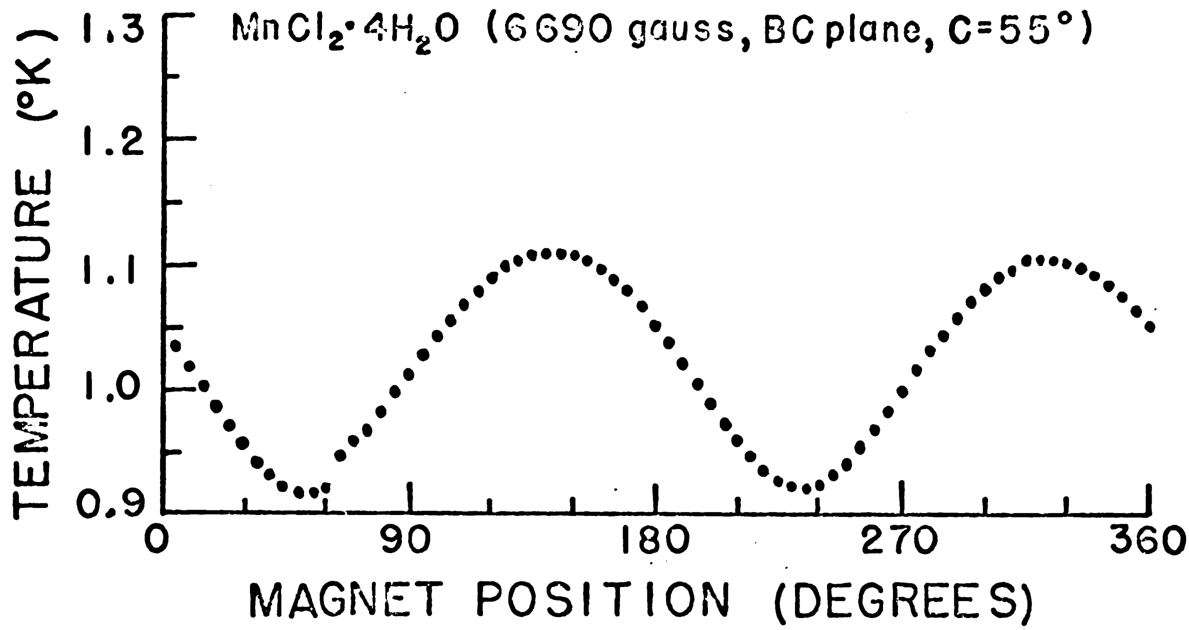

(a)

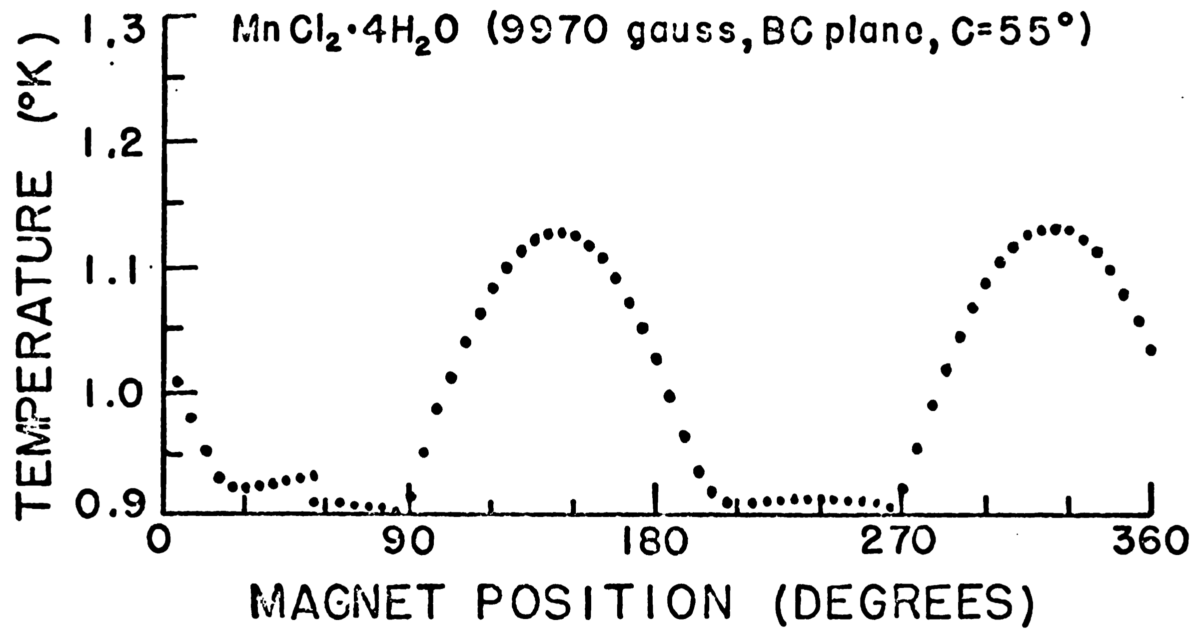

(b)

Fig. 24. $MnCl_2 \cdot 4H_2O$ BC plane isentropic rotations.

As in $CoCl_2 \cdot 6H_2O$, the results of the rotations below the critical field indicate that the C axis is the preferred axis of magnetization. Other than the flatness near the C axis in the high field rotation (Fig. 23b), nothing remarkable is seen in the AC plane rotations. However, in the BC rotation above the critical field, shown in Fig. 24b, the behavior is again similar to that of Fig. 6b. Thus there is partial indication that $MnCl_2 \cdot 4H_2O$ undergoes a spin flop transition and that the spins flop to the B axis. Rives[34], in one of his experiments, with the field initially aligned along the C axis, experienced a 90^0 rotation of his crystal, about the A' axis, upon a quick demagnetization. This is consistent with the conclusion that the spins flop to the B axis.

Further evidence of the spin flop phase in $MnCl_2 \cdot 4H_2O$ is given by the C axis isentropic magnetization results. The data points are given in Table 9 of Appendix III and smooth curves drawn through the points are shown in Fig. 25. Also shown in Fig. 25 as a dashed line is the spin flop-antiferromagnetic boundary obtained by Rives.[34] (Rives results are about 100-200 gauss higher than the results of Gijsman, <u>et. al.</u>[33], which are not shown.) From the measured isentropes, it is seen that the initial cooling upon magnetization disappears in the spin flop phase.

Also shown in Fig. 25 are several points obtained from the maxima of specific heat measurements made in this study (these points are listed in Table 10 of Appendix III).

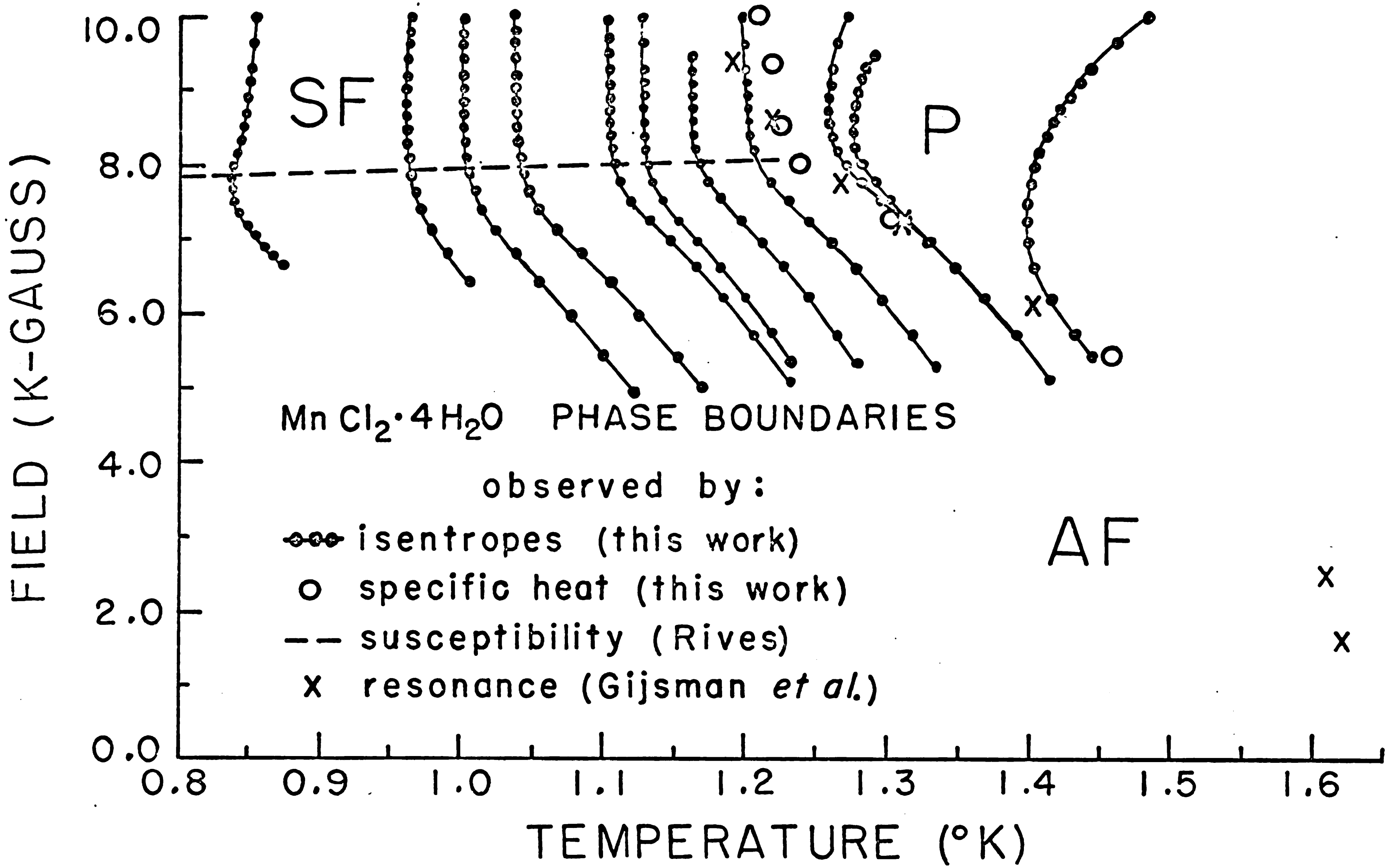

Fig. 25. $MnCl_2 \cdot 4H_2O$ phase boundaries and isentropes.

It is seen that there is close agreement between the specific heat and nuclear resonance paramagnetic boundary results of Gijsman _et. al_.[33] which are shown in Fig. 25 also. (Note, however, that Rives' paramagnetic boundary results, which are not shown, are considerably higher in temperature than the boundary points shown in Fig. 25.)

The lowest temperature isentrope was obtained from the first crystal when it was in the BC plane orientation, while the others were obtained from the second crystal. (The second crystal was oriented in the AC plane. For this crystal, isentropic rotations in this plane gave results similar to those obtained for the first crystal.) Although there is a change in sign of the slope of the isentrope from the first crystal, similar to the $CoCl_2 \cdot 6H_2O$ results, there is none for the second crystal results and the isentropes behave as predicted by the theory. Unfortunately, the gradual decrease of the magnetization cooling effect near the spin flop boundary makes it nearly impossible to define a single point as a phase change point. However, the results, at least, do show the existence of the spin flop state, with a critical field in the vicinity of the results of the previous studies.

Also worthy of note are the measured isentropes which start in the antiferromagnetic state and cross over into the paramagnetic state. It is seen that adiabatic magnetization in the paramagnetic state, near the antiferromagnetic boundary produces cooling. Although this is unusual, such an effect has been observed before by Friedberg and Schelleng[37] in $MnBr_2 \cdot 4H_2O$. In contrast with those observations, though, these antiferromagnetic-paramagnetic isentropes apparently do not cross the phase boundary tangentially. It is possible that this is due to imperfect adiabatic conditions, although further measurements are needed for a better determination of the true isentropes.

B. Materials Discovered to Exhibit Spin Flop

Since the above results on $CoCl_2 \cdot 6H_2O$ and $MnCl_2 \cdot 4H_2O$ showed the practicality of the adiabatic method of observing the spin flop state in antiferromagnets, a search was begun to discover substances with previously unobserved spin flop states. From these investigations, it has been found that two previously studied substances, $CoBr_2 \cdot 6H_2O$ and $FeCl_2 \cdot 4H_2O$, undergo spin flopping in accessible field and temperature regions.

Previous specific heat[38] and susceptibility[39] measurements had been made on $CoBr_2 \cdot 6H_2O$, indicating it is antiferromagnetic below about 3.2^0K. Although it is isomorphic to $CoCl_2 \cdot 6H_2O$, $CoBr_2 \cdot 6H_2O$ is a more desirable substance to study than $CoCl_2 \cdot 6H_2O$, since it easily grows in long, large single crystals, while single crystals of $CoCl_2 \cdot 6H_2O$ are grown with difficulty.

About a cubic centimeter portion of a single crystal of $CoBr_2 \cdot 6H_2O$ grown from an aqueous solution at room temperature was used in the measurements. Since the previous susceptibility results indicated the C axis to be the preferred axis of magnetization, measurements were made in the BC and AC crystallographic planes. Groth's morphology of $CoCl_2 \cdot 6H_2O$ was used as a basis for orienting the crystal. The AC plane orientation was an easier orientation to make than the BC orientation, and it is believed, for this reason, that there was less mis-alignment of the crystal in the AC orientation than in the BC orientation.

Isentropic field rotations at two different fields were made in each of these planes. The results are listed in Table 11 of Appendix III and are shown in Figs. 26 and 27. As in $CoCl_2 \cdot 6H_2O$ and $MnCl_2 \cdot 4H_2O$, the results show that the C axis is the preferred axis. It is interesting to note the similarity of the shift of the maximum in the BC rotations to that observed in $CoCl_2 \cdot 6H_2O$. This provides further evidence of the reality of that shift.

The results of the 8830 gauss AC plane rotation (Fig. 27b) are similar to the higher field rotation in $CoCl_2 \cdot 6H_2O$ and the predictions shown in Fig. 6b. Thus there is partial evidence, from the rotation data, that $CoBr_2 \cdot 6H_2O$ undergoes spin flop below 8830 gauss near 1.3^oK, with the spins flopping to the A' direction.

As further evidence of the existence of the spin flop state in $CoBr_2 \cdot 6H_2O$, the isentropes obtained in isentropic magnetization along the C axis are shown as smooth lines through the data points in Fig. 28 (the data points are

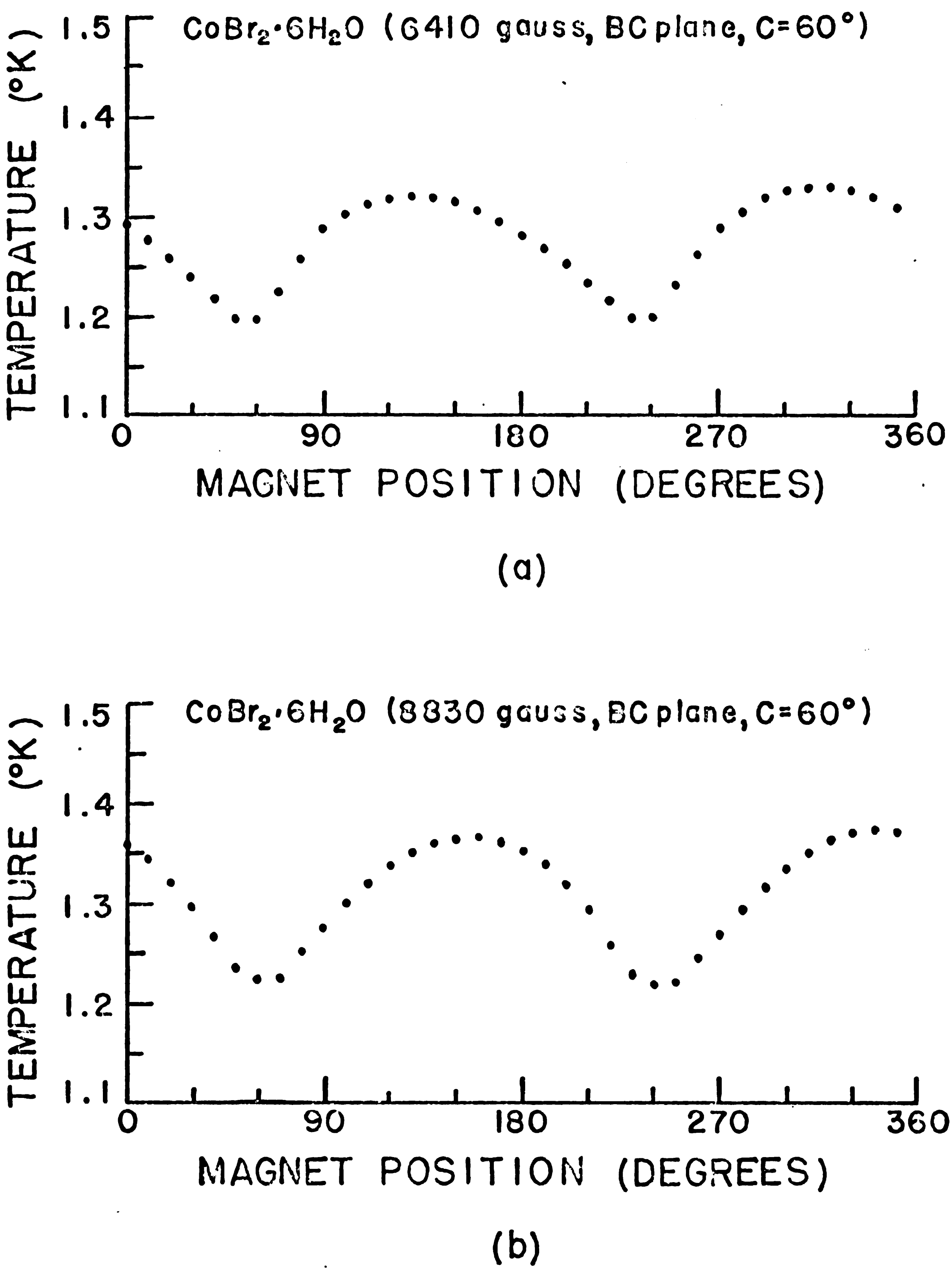

Fig. 26. $CoBr_2 \cdot 6H_2O$ BC plane isentropic rotations.

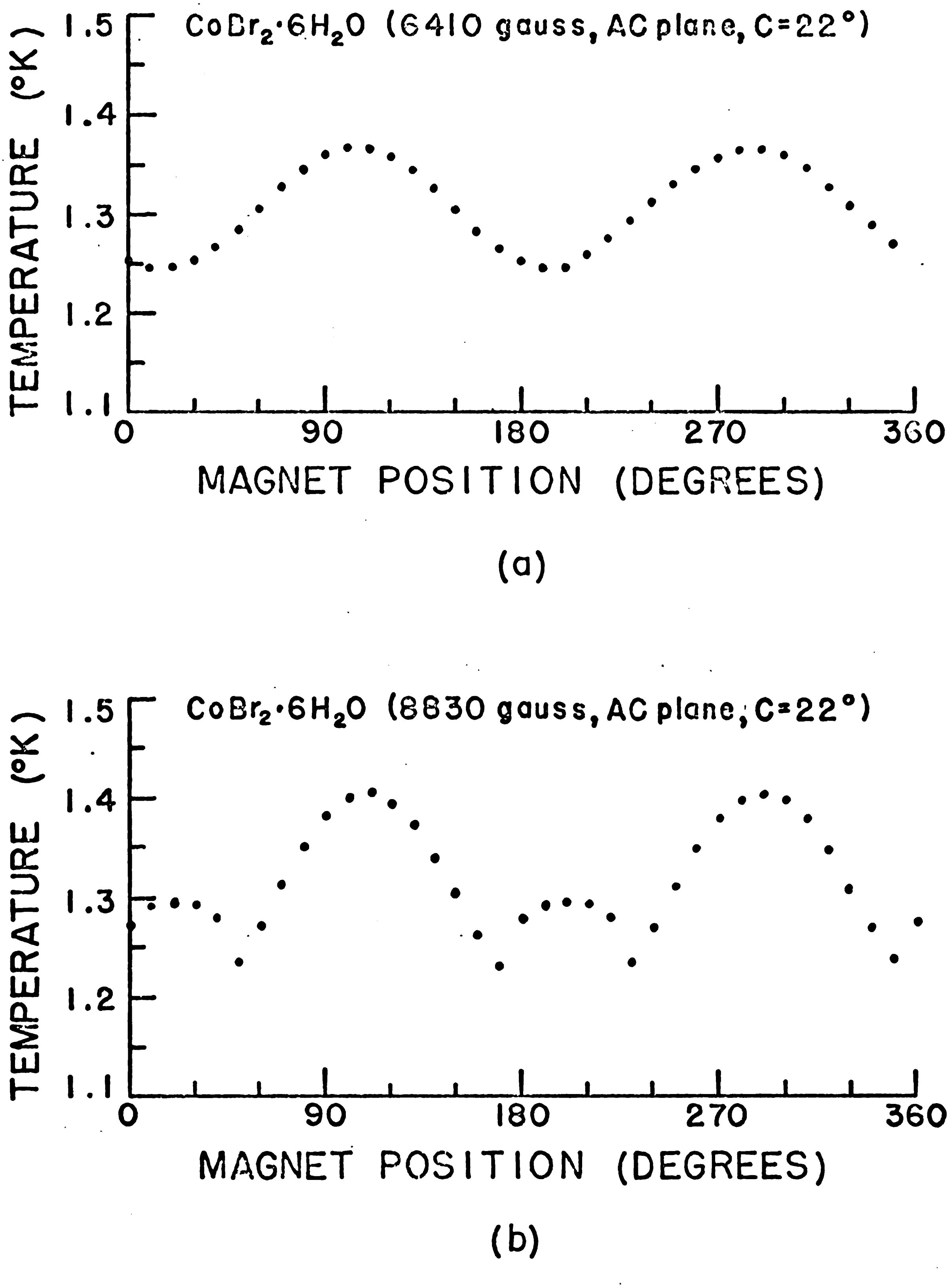

Fig. 27. $CoBr_2 \cdot 6H_2O$ AC plane isentropic rotations.

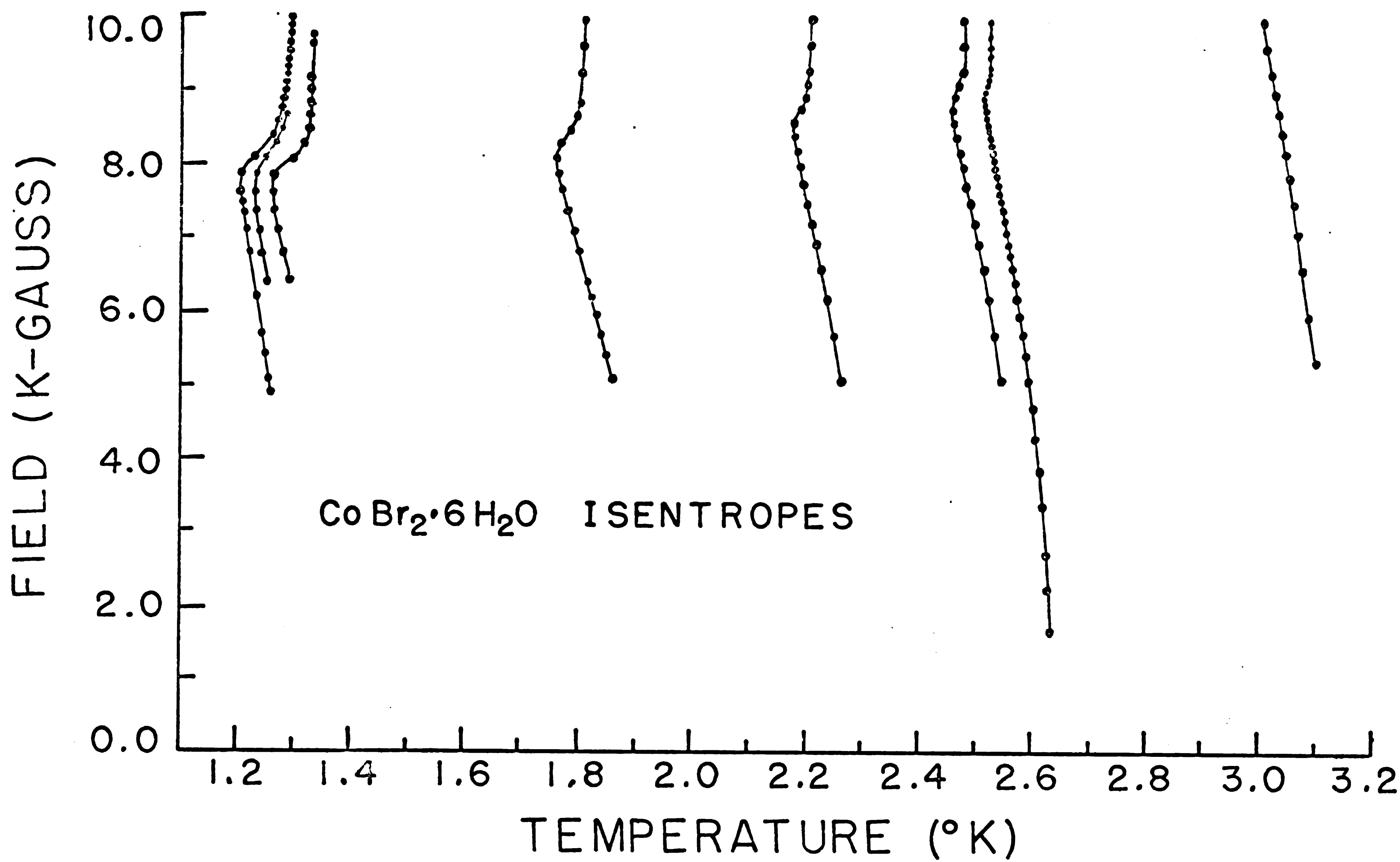

Fig. 28. $CoBr_2 \cdot 6H_2O$ isentropes.

listed in Table 12 of Appendix III). Similar to the $CoCl_2 \cdot 6H_2O$ results, there is initial cooling upon magnetization in the antiferromagnetic state which disappears when the spin flop state is entered. The change in sign of the slopes of the isentropes, seen in $CoCl_2 \cdot 6H_2O$, also exists in $CoBr_2 \cdot 6H_2O$.

Measurements of this point of change were made both when the crystal was in the AC plane orientation and when it was in the BC plane orientation. The BC plane results gave a slightly higher critical field than the AC plane measurements; this would correspond to a poorer alignment in the BC plane than in the AC plane as hypothesized.

Measurements of the paramagnetic boundary, using constant field specific heat measurements, were also made, both above and below the critical field. These results, along with the spin flop boundary results, are shown in the phase diagram shown in Fig. 29. All the data points are listed in Tables 13 and 14 of Appendix III.

The value of the triple point is ($2.91 \pm .01^0$K, 9320 ± 40 gauss). A second degree polynomial was used to fit the observed spin flop boundary. The result of the fit was

$$H_C = 7523 - 230.7\ T + 292.5\ T^2\ , \qquad (3.00)$$

where H_C is the critical field at temperature T. Thus on the basis of the observed data, a critical field of about 7250 gauss is expected at 0^0K. Note that the spin

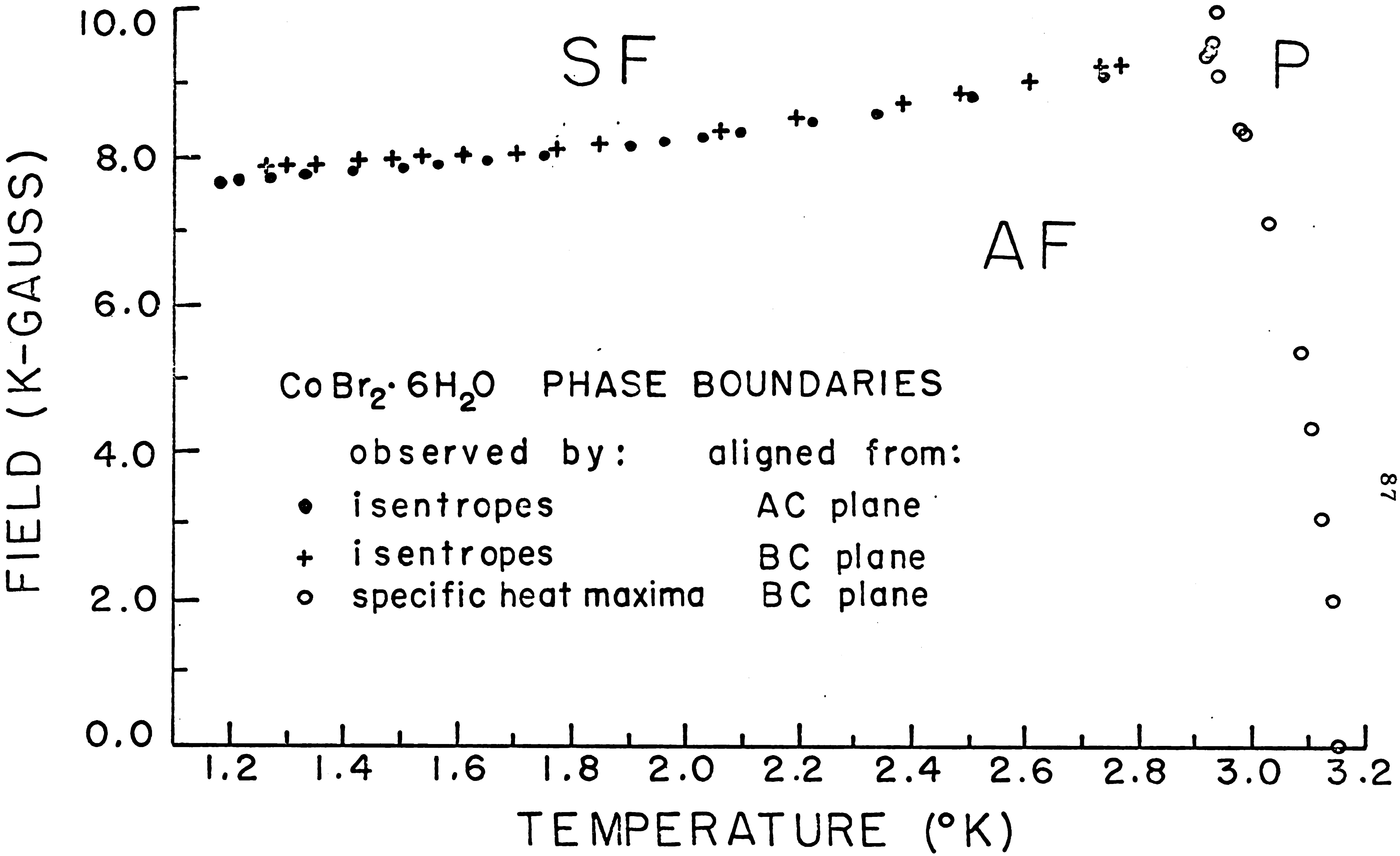

Fig. 29. $CoBr_2 \cdot 6H_2O$ phase boundaries.

flop boundary results do not quantitatively agree with the predictions of Yosida's theory for a spin 1/2 system, which is assumed for $CoBr_2 \cdot 6H_2O$. The spin flop boundary rises more slowly than the prediction. However, note that the antiferromagnetic-paramagnetic boundary corresponds to the predictions of the theory quite well with an H_0 of 18,000 gauss.

It is also worth noting that the antiferromagnetic-paramagnetic boundary apparently intersects the temperature axis perpendicularly. This is what was predicted from the results of the simple molecular field theory shown in Fig. 3a. (It should be noted that the zero field Néel temperature measured in this study, 3.152^{0}K, differs from the result of the previous specific heat study, 3.07^{0}K. At present, there is no explanation for this.) Again, as in $MnCl_2 \cdot 4H_2O$, it is also interesting to note the behavior of the isentrope measured in the paramagnetic state.

Previous specific heat[40,41], susceptibility[42] and NMR[43] studies on $FeCl_2 \cdot 4H_2O$ indicated it is in an ordered state below about 1.1^{0}K. This temperature is near the lowest temperature attainable in the apparatus used in this study, but since cooling takes place upon magnetization of an antiferromagnet, and since spin flopping was observed near 5400 gauss at 0.4^{0}K in the NMR studies[44], a search for the spin flop state in $FeCl_2 \cdot 4H_2O$ was made.

The samples which had been used in the resonance experiments were borrowed from R. D. Spence and were used in some initial measurements. However, it subsequently was discovered that the McLeod pressure gauge of the temperature measuring system was giving spurious measurements. Since there also was some question about the orientations of Spence's crystals (they had been ground into cylinders), it was decided to use the initial results only as qualitative indications of the behavior of $FeCl_2 \cdot 4H_2O$.

A new single crystal of $FeCl_2 \cdot 4H_2O$ was grown from an aqueous solution in a desiccator so that more precise measurements could be made. It weighed about 1.3 grams and was stored in a refrigerator until its use, since, as noted by Schriempf and Friedberg[42], $FeCl_2 \cdot 4H_2O$ tends to lose or gain water when exposed to air at room temperature. Also, before its use, it was spray coated with Krylon clear plastic spray to further protect it from contamination.

Like the crystals previously studied, $FeCl_2 \cdot 4H_2O$ forms monoclinic crystals with $\beta = 112^0$. The growth habit described by Groth[35], was used as a basis for orientation of the crystal. The susceptibility results indicated that the B axis is the preferred axis of magnetization, so experiments were done in the AB and BC crystallographic planes. It is felt that, since the BC plane is prominent on the crystal, that the BC plane orientation was more precise.

The results of high field isentropic rotations in these planes are shown in Fig. 30, and the data is listed in Table 15 of Appendix III. The earlier data gave the same qualitative results. In addition, the earlier data showed

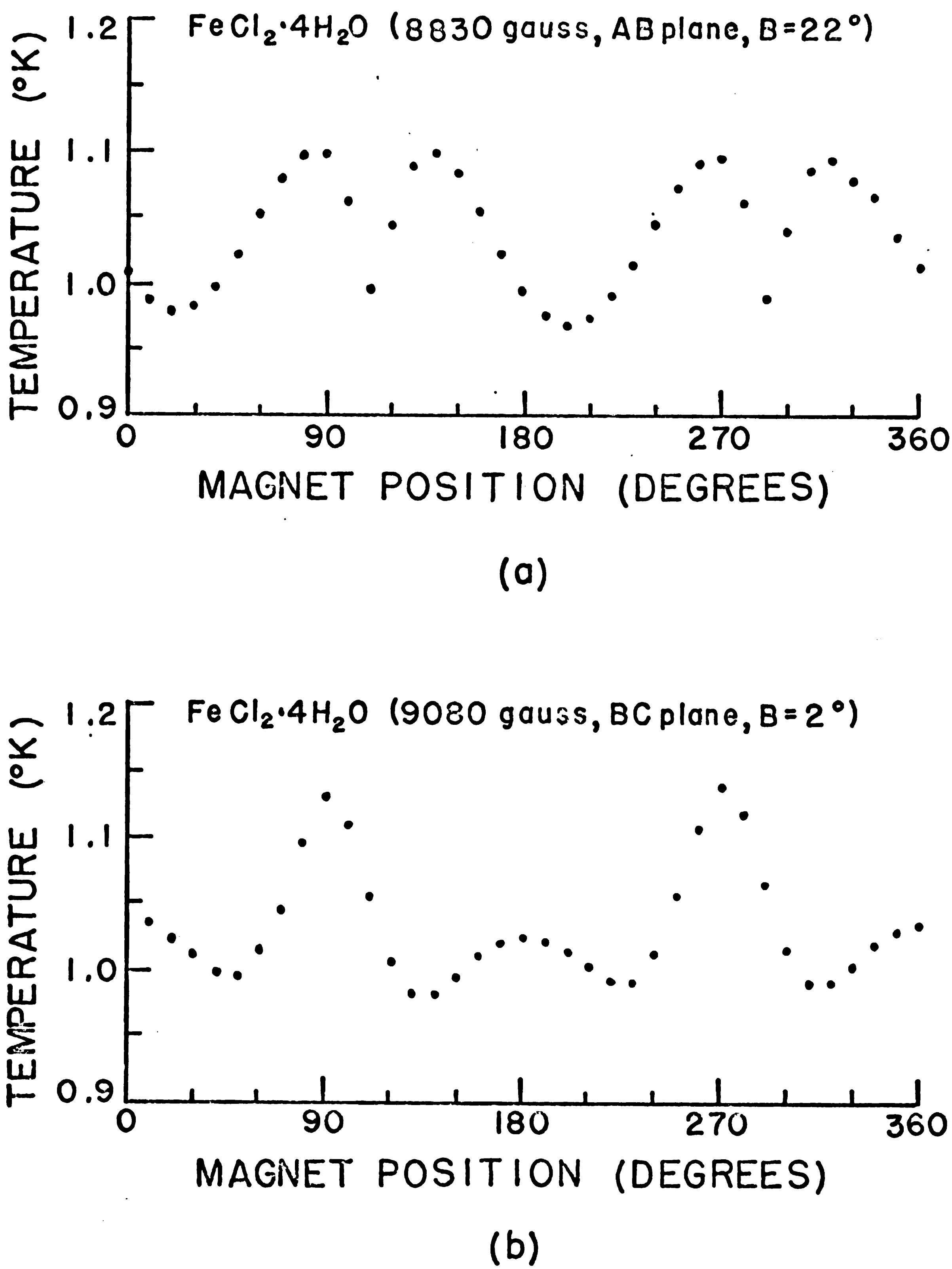

Fig. 30. $FeCl_2 \cdot 4H_2O$ AB and BC plane isentropic rotations.

that the rise in temperature near the B axis for the BC rotation disappears at lower fields and also that the dip in temperature near the A axis in the AB rotation disappears at lower fields. Also, the earlier data included AC plane isentropic rotations which gave results similar to the AB plane behavior discussed here. Furthermore, the earlier results also included a high field (about 8000 gauss) BC plane rotation at higher temperatures (about 1.5-1.6^{0}K). The results of that rotation were similar to the low field rotations done in previous crystals. However, in direct contrast to the $FeCl_2 \cdot 4H_2O$ low field BC plane rotations at lower temperature, mentioned above, the temperature was a maximum with the field along the B axis and a minimum when the field was along the C axis. These qualitative results seem to imply a change in the principal magnetic axes between about 1.1^{0}K and 1.5^{0}K.

Although the BC plane results, to some extent, correspond to what would be seen in a spin flopping material, the AB plane results definitely do not correspond with the results seen in the other crystals studied.

In addition, when the crystal was in the AB plane orientation, with the field directed along the B axis, isentropic magnetizations produced cooling to a point and then warming. This also does not strictly correspond with the spin flop results previously seen (although the initial measurements were reported[45] as being partially similar to the $MnCl_2 \cdot 4H_2O$ results.)

For the above reasons, it was deemed worthwhile to measure the antiferromagnetic-paramagnetic boundary to determine in which phase the isentropic magnetizations had been taken. The results of these measurements indicated the previously measured isentropes were probably antiferromagnetic-paramagnetic or paramagnetic isentropes similar to the ones previously seen in other crystals. In one experiment, the turning point of the paramagnetic isentropes from cooling to warming was followed to near 1.3^0K. (Such a large region of negatively sloped paramagnetic isentropes is probably due, to some extent, to the large anisotropies seen in the susceptibilities.)

After the BC plane orientation had been made, it was discovered that a region of temperature (near 0.75^0K) could be reached upon isentropic magnetization where the isentropes behaved similar to those in the spin flop state of $MnCl_2 \cdot 4H_2O$. Unfortunately, the interval between 0.75^0K and the first calibration point of the thermometer, 1.0^0K, is relatively large, so there may be as much as 0.05^0K error in the absolute temperatures measured, due to extrapolation of the thermometer calibration. However, the observations made are certainly at least, qualitatively correct.

Several times when temperatures near 0.75^0K were reached upon isentropic magnetization, the field was held constant at different values and the heat leaking in to the sample was allowed to warm it. In this manner, second order phase transitions were easily seen as discontinuous changes in the rate of rise of temperature of the sample.

The measured isentropes (with smooth lines drawn through the points obtained) and all the second order phase transition points are shown in Fig. 31. All the data points are listed in Tables 16 and 17 of Appendix III.

Several points may be made from these results. First, from observation of the lowest temperature isentrope, it seems that $FeCl_2 \cdot 4H_2O$ goes into a definite spin flop state above about 7000 gauss near 0.68^0K. Second, the paramagnetic boundary points indicate that, if there is a spin flop state, the triple point is about 5500 gauss near 0.76^0K. Third, since this field is near the one reported by Spence, it is possible that the critical field is actually near 5400-5500 gauss in the entire region 0.4-0.75^0K. Fourth, if that is so, it would seem, on observation of Fig. 31, that one conclusion is that the inflection point of the antiferromagnetic-spin flop isentropes may be the point of spin flop. (If this method of determining the spin flop point were then applied to the $MnCl_2 \cdot 4H_2O$ results, the critical field observed would turn out to be slightly lower than the previously published results.) Fifth, the nearly constant temperature of the paramagnetic boundary above the critical point is highly unusual. Sixth, these results, coupled with the four-sublattice models that have been previously hypothesized[42,46] for $FeCl_2 \cdot 4H_2O$ and the unusual NMR results between 0.7 and 1.1^0K, indicate that further isentropic measurements, perhaps using a He^3 refrigerator,

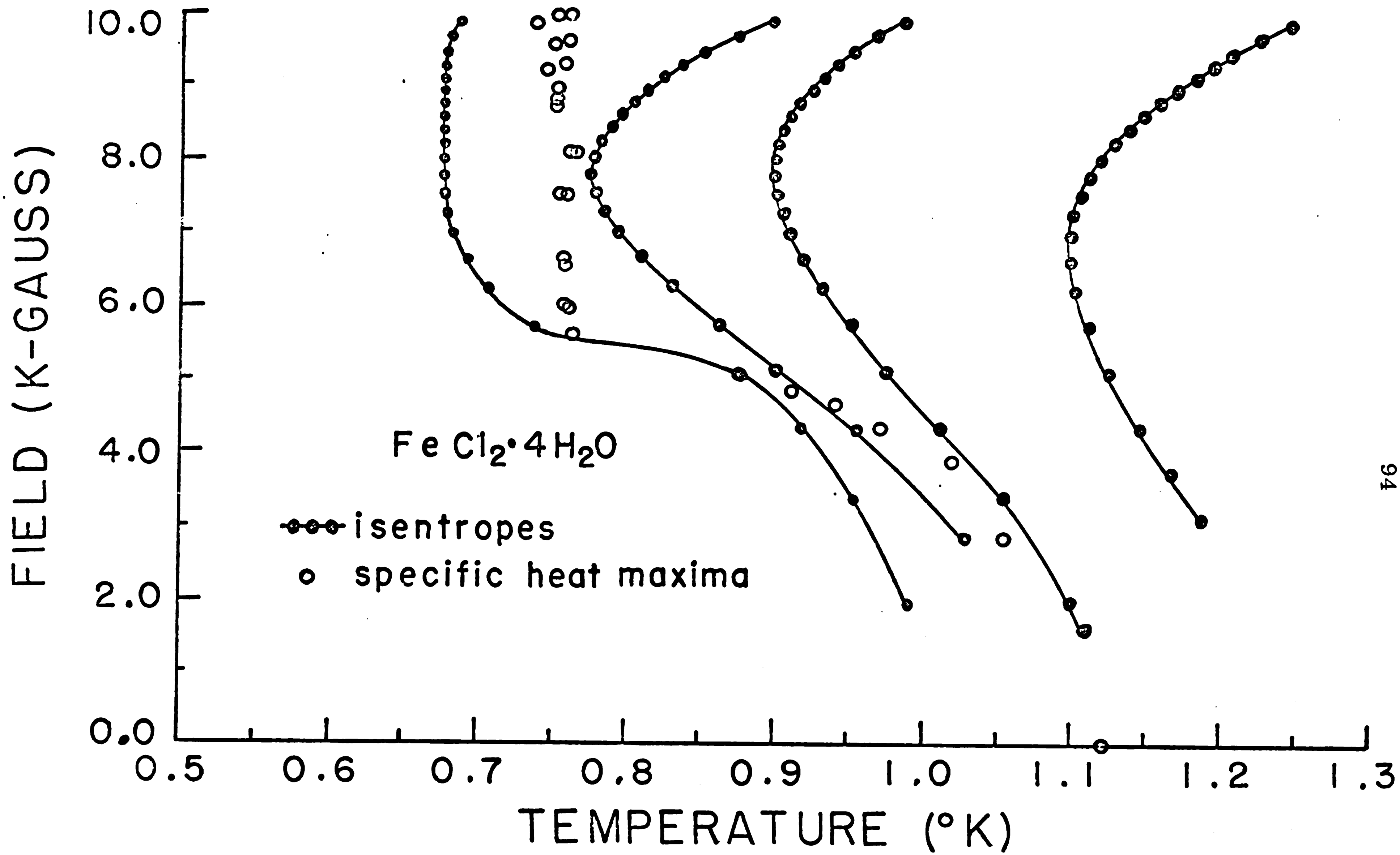

Fig. 31. $FeCl_2 \cdot 4H_2O$ phase boundary and isentropes.

in the region 0.7-1.1^{0}K from 0-7000 gauss would be interesting. Seventh, and finally, it should be noted that the zero field Néel temperature determined here (1.116^{0}K) is slightly higher than that reported previously (1.097^{0}K), and that, in either case, the antiferromagnetic-paramagnetic phase boundary would not seem to intersect the temperature axis quite perpendicularly, in contrast to what was seen in the other crystals studied (although finer measurements are needed to verify this fact).

C. Materials Investigated Which Did Not Exhibit Spin Flop

In the search for substances exhibiting spin flop states, experimental observations were made on three other hydrated salts: $MnBr_2 \cdot 4H_2O$, $Cs_2MnBr_4 \cdot 2H_2O$, and $NiCl_2 \cdot 6H_2O$. None of these exhibited spin flop in the region 0-10,000 gauss between 1^{0}K and 4^{0}K.

The first of the above three salts, $MnBr_2 \cdot 4H_2O$, has been previously studied by means of susceptibility[32,33], specific heat[37,47,48], proton resonance[33], optical absorption[49], and antiferromagnetic resonance[50] experiments. The latter two experiments have inferred spin flopping near 9000 gauss near 1.2-1.4^{0}K, while the others have shown no such results.

A single crystal of $MnBr_2 \cdot 4H_2O$, weighing about 2 grams was grown from an aqueous solution at room temperature. $MnBr_2 \cdot 4H_2O$ crystals are monoclinic with β = 99.6^0. Under the assumption that the lattice structure is similar to the isomorphic crystal, $MnCl_2 \cdot 4H_2O$, the crystal was aligned with the AC crystallographic plane as the plane of rotation of the field. (The susceptibility measurements have indicated the C axis to be the easy axis.) The field was precisely aligned along the C axis by observation of the temperature variation in an isentropic rotation (no data points were taken). Isentropic magnetizations were then done at several temperature regions. The isentrope results are shown in Fig. 32 with smooth curves drawn between the points measured and the data is given in Table 18 of Appendix III. As can be seen, from the continuous cooling effect of magnetization, there is no evidence of spin flop in the regions observed.

Although a previous investigation[22] of the paramagnetic phase boundary in $Cs_2MnCl_4 \cdot 2H_2O$, which is a triclinic crystal, failed to exhibit any spin flop characteristics, a single crystal of the isomorphic compound $Cs_2MnBr_4 \cdot 2H_2O$ was grown so that a search could be made for the spin flop state in it. A solution of CsBr and $MnBr_2 \cdot 4H_2O$ in water at room temperature was used to grow the crystal. A specific heat study of this substance indicated it to be in a magnetically ordered state below 2.82^0K.

The bromide was assumed to have the same preferred axis as the chloride ($[\bar{1}\ \bar{1}\ \bar{1}]$ direction) so it was oriented with the $[0\ \bar{1}\ 1]$ direction parallel to the axis of rotation of the field. Isentropic magnetizations were done with the field aligned parallel and perpendicular to the

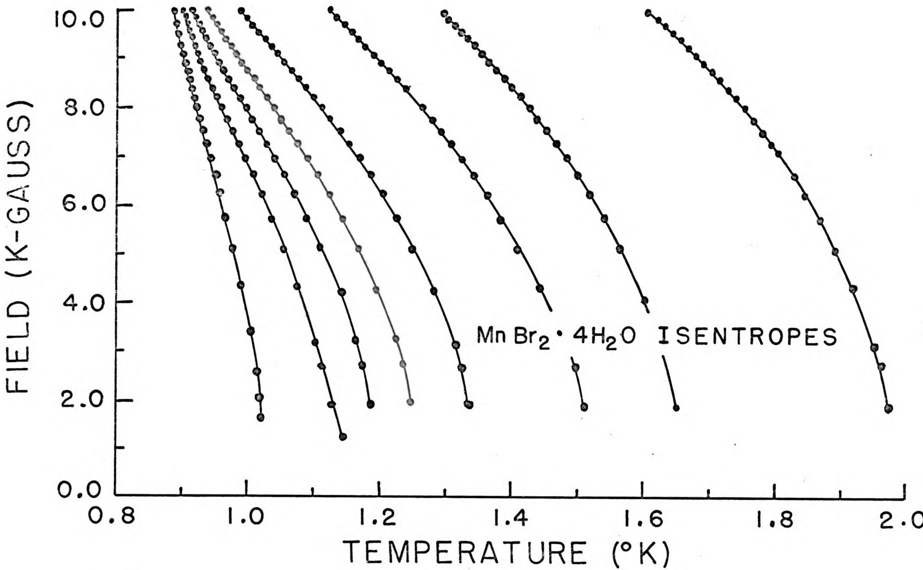

Fig. 32. $MnBr_2 \cdot 4H_2O$ isentropes.

apparent preferred axis, determined from an isentropic rotation. The isentropes are shown in Fig. 33, along with several paramagnetic boundary points measured from constant field specific heat measurements. (The data points are given in Tables 19 and 20 of Appendix III.) As can be seen from the expanded portion of the data shown in Fig. 34, there is no indication of spin flopping from the behavior of the parallel isentropes. However, it should be noted that the perpendicular isentropes are not temperature independent, as would be expected. Thus, it might be concluded that the magnetization direction in $Cs_2MnBr_4 \cdot 2H_2O$ (and probably $Cs_2MnCl_4 \cdot 2H_2O$, also) is not in the plane perpendicular to the [0 $\bar{1}$ 1] direction. (In fact, resonance experiments on the chloride[51] do indicate the magnetization direction to be out of that plane.) Thus a better alignment might be necessary, before any conclusions are drawn concerning spin flopping either in the bromide or the chloride.

Previous specific heat[52] and magnetic susceptibility[53] experiments indicated that the salt $NiCl_2 \cdot 6H_2O$, which is isomorphic to $CoCl_2 \cdot 6H_2O$, becomes antiferromagnetic below 5.34^0K. For this reason, an investigation was undertaken to search for spin flopping in $NiCl_2 \cdot 6H_2O$.

A single crystal of $NiCl_2 \cdot 6H_2O$, weighing about one gram, was borrowed from R. D. spence. The crystal is monoclinic with $\beta = 122.5^0$ and the morphology is given in Groth[35]. Since the susceptibility experiments indicated

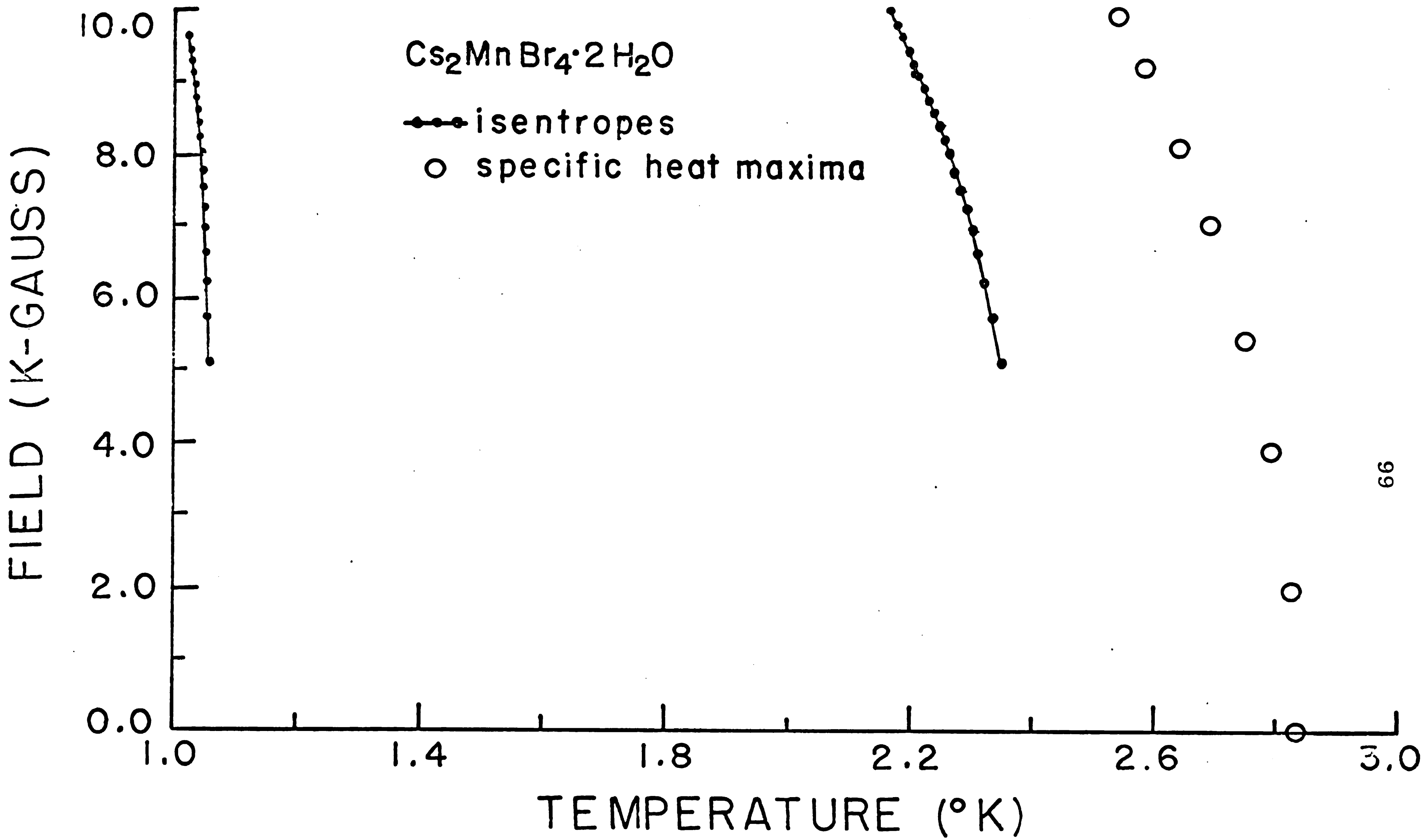

Fig. 33. $Cs_2MnBr_4 \cdot 2H_2O$ phase boundary and isentropes.

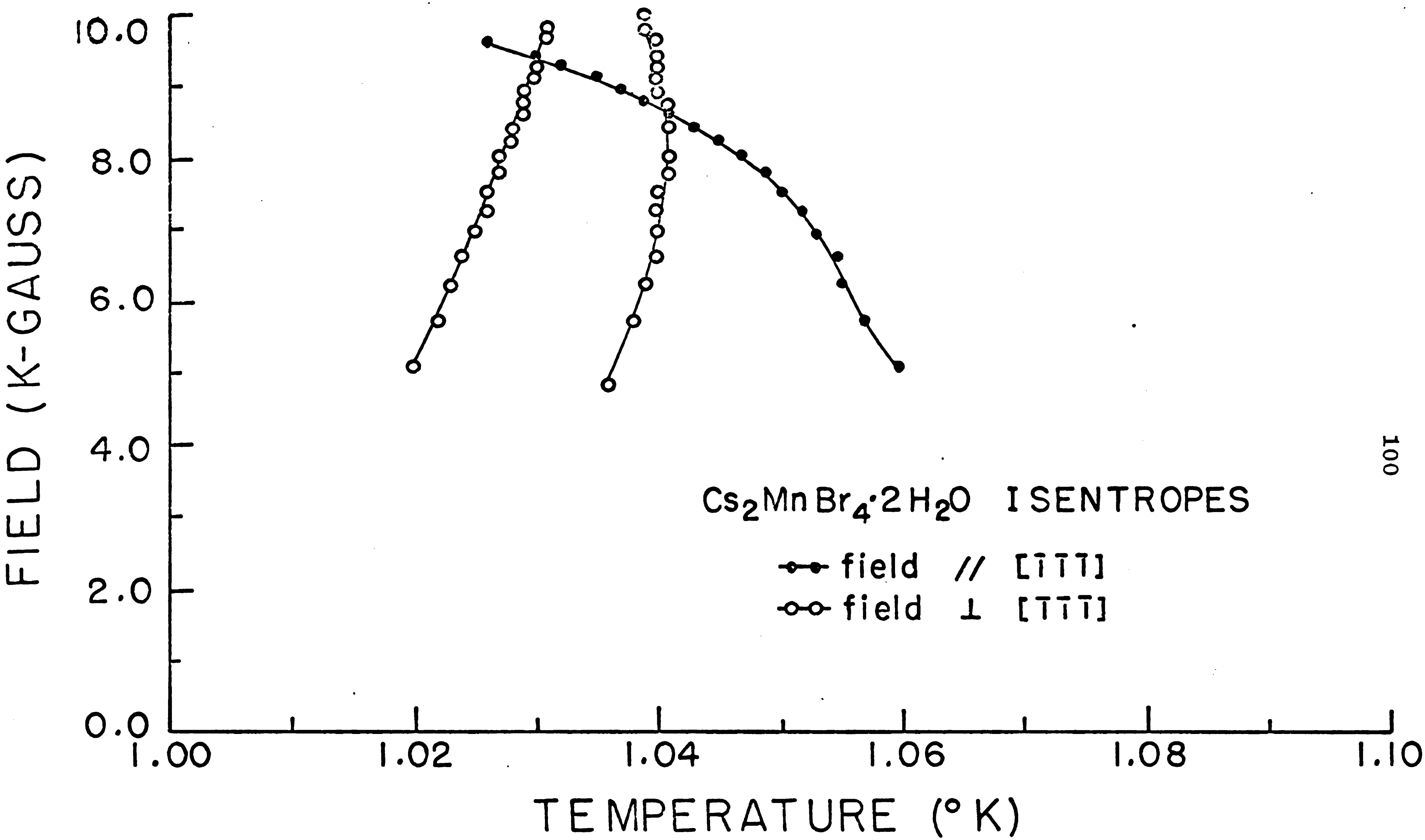

Fig. 34. $Cs_2MnBr_4 \cdot 2H_2O$ isentropes (expanded scale).

the A' axis to be the preferred axis, the crystal was oriented so that its AC plane was in the plane of rotation of the field.

The field was aligned along the A' axis by observation of the temperature in an isentropic rotation and isentropic magnetizations were then done at different temperature regions. Nothing remarkable was seen in the isentropic rotations done, other than a rather small temperature variation. The results of the only one which was recorded are shown in Fig. 35 and are given in Table 21 of Appendix III. The results of the isentropic magnetizations are shown in Fig. 36 and are listed in Table 22 of Appendix III. These results certainly are not similar to the previous results in the other crystals studied.

The nearly constant temperature isentropes would normally indicate a perpendicular spin state. However, since the field had been aligned along the axis of the isentropic rotation temperature minimum, the spins should have been expected to be in the parallel state. At present, the best explanation seems to be that the sample was not actually isolated, so that there would be a constant temperature in a magnetization. The lack of isolation can be explained by noting that the sample's specific heat is very small in the temperature region in which observations were made. Since, as noted in Chapter 2, the degree of apparent isolation depends on the specific heat of the sample being used, the $NiCl_2 \cdot 6H_2O$ sample may have been

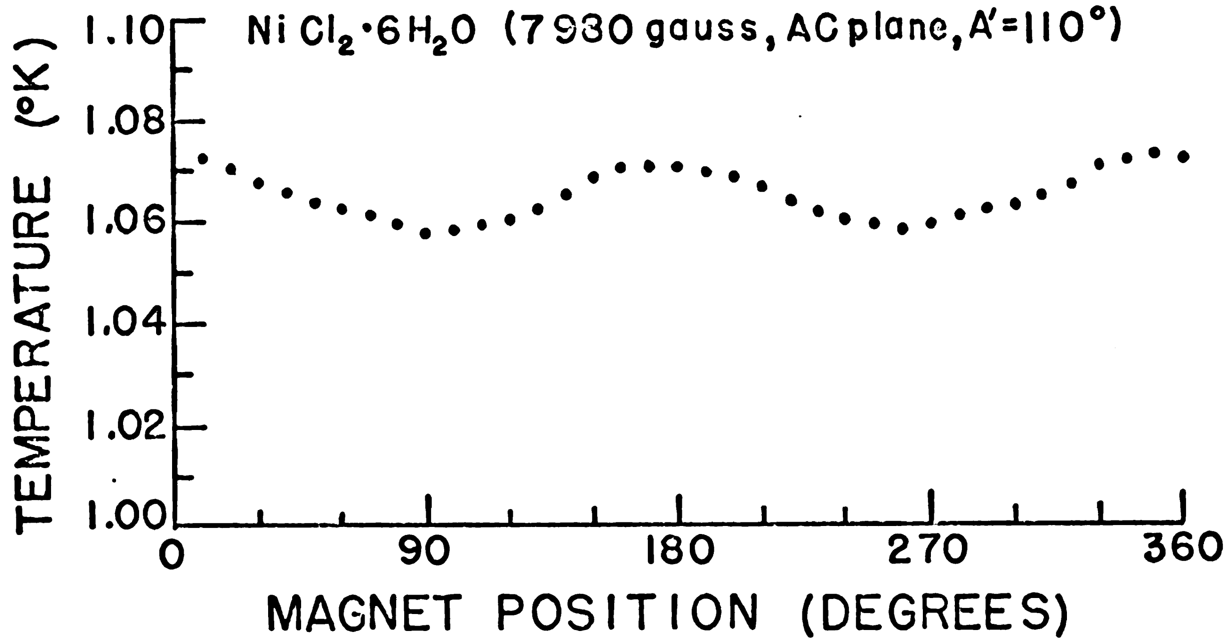

Fig. 35. $NiCl_2 \cdot 6H_2O$ AC plane isentropic rotation.

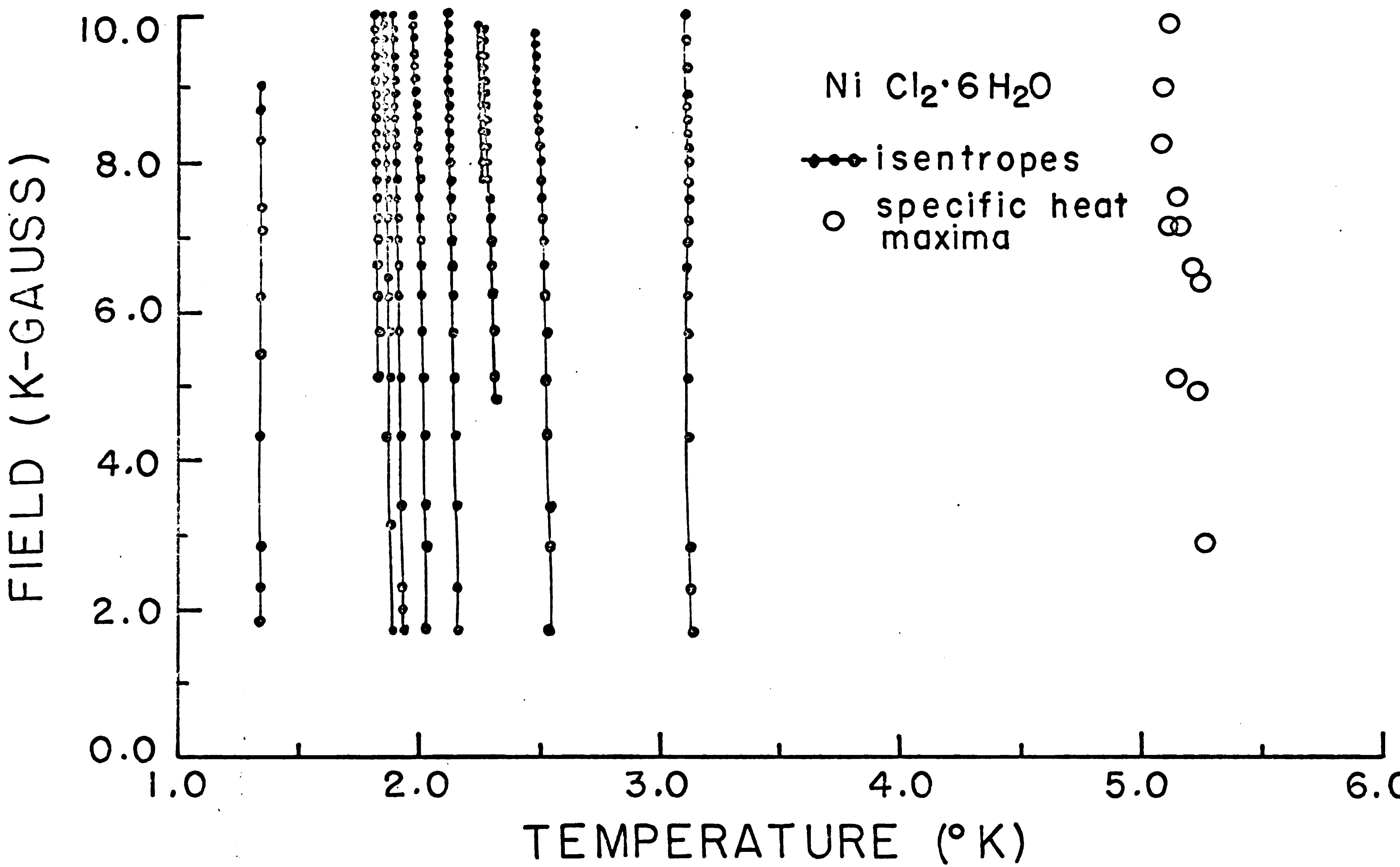

Fig. 36. $NiCl_2 \cdot 6H_2O$ phase boundary and isentropes.

relatively unisolated.

In addition to the isentropic magnetizations and rotations done, constant field specific heat measurements were used in an attempt to determine the paramagnetic phase boundary in $NiCl_2 \cdot 6H_2O$.

The results of these measurements are also shown in Fig. 36 and are given in Table 23 or Appendix III. As can be seen, there is a large amount of scatter in the points. Careful observation of the raw data shows the scatter to be independent of the calibration curves connected with determining temperatures. Thus the scatter is real, or more probably, there are hysterisis effects in crossing the $NiCl_2 \cdot 6H_2O$ paramagnetic boundary. In any case, all the $NiCl_2 \cdot 6H_2O$ measurements should be considered as preliminary results and further observations on this salt are needed.

II. Conclusions

In conclusion, this study has shown that adiabatic methods for observing the spin flop state of an antiferromagnet are practical, although there is yet room for their refinement. There are some drawbacks with the present method of mounting the crystal. Better adiabatic conditions would be desirable. Also, so that any crystalline axis might be easily aligned parallel to the field, a method to rotate the sample about an axis in the plane of rotation of the field, while it is in the calorimeter during the experiment, would be highly desirable. It would also be desirable if there were less metal in the calorimeter, to reduce eddy current heating which exists when the field is being rotated.

With the discovery of spin flopping properties of $CoBr_2 \cdot 6H_2O$ and $FeCl_2 \cdot 4H_2O$, new areas of research into some of the basic properties of these substances are possible. Also, it would be interesting to do a complete set of magnetic field specific heat experiments, magnetic susceptibility experiments and adiabatic magnetization experiments so that the theoretical relationship between the measured quantities might be tested for antiferromagnets.

Finally, from the theory, a new method to predict the critical field for spin flopping has been proposed. It would be interesting to do some susceptibility measurements to test the predictions of the simple molecular field theory regarding the critical field value. Such measurements on $MnBr_2 \cdot 4H_2O$ would be especially interesting.

REFERENCES

1. L. Néel, Ann. Physique 18, 5 (1932).
2. T. Nagamiya, K. Yosida and R. Kubo, Advances in Physics 4, 1 (1955).
3. W. Heisenberg, Phys. Z. 49, 619 (1928).
4. P. A. M. Dirac, Proc. Roy. Soc. 123, 714 (1929).
5. E. Ising, Z. Phys. 31, 253 (1925).
6. P. Weiss, J. Phys. 4, 661 (1907); J. Phys. 6, 667 (1907); Ann. Phys. 17, 97 (1932).
7. F. Bitter, Phys. Rev. 54, 79 (1937).
8. J. H. Van Vleck, J. Chem. Phys. 9, 85 (1941).
9. C. G. B. Garrett, J. Chem. Phys. 19, 1154 (1951).
10. P. W. Anderson, Phys. Rev. 79, 705 (1950).
11. T. Nagamiya, Prog. Theor. Phys. 6, 342 (1951).
12. K. Yosida, Prog. Theor. Phys. 7, 25 (1952).
13. C. J. Gorter and J. Haantjes, Physica 18, 285 (1952).
14. K. Yosida, Prog. Theor. Phys. 6, 691 (1951).
15. L. Néel, Ann. Physique 5, 232 (1936).
16. C. J. Gorter and Tineke Van Peski-Tinbergen, Physica 22, 273 (1956).
17. J. H. Van Vleck, The Theory of Electric and Magnetic Susceptibilities (Oxford, 1932), p. 257.
18. K. Yosida, Prog. Theor. Phys. 7, 425 (1952).
19. J. M. Ziman, Proc. Phys. Soc. 64, 1108 (1951).
20. N. J. Poulis, J. van den Handel, J. Ubbink, J. A. Poulis, and C. J. Gorter, Phys. Rev. 82, 552 (1951).
21. T. Nagamiya, Prog. Theor. Phys. 11, 309 (1954).
22. N. D. Love, Ph.D. Dissertation, Michigan State University (1967).

23. W. R. Eisenberg, M.S. Dissertation, Michigan State University (1963).

24. W. R. Roads and J. C. Wheatley, Rev. Sci. Instr. 35, 634 (1964).

25. W. F. Giauque, R. A. Fisher, E. W. Hornung, and G. E. Brodale, J. Chem. Phys. 43, 4387 (1965).

26. J. Butterworth (private communication).

27. A. C. Anderson, W. Reese, and J. C. Wheatley, Rev. Sci. Instr. 34, 1386 (1963).

28. F. G. Brickwedde, H. van Dyk, M. Durieux, J. R. Clement, and J. K. Logan, J. Res. Nat. Bur. Stand. 64A, 1 (1960).

29. G. T. Armstrong, J. Res. Nat. Bur. Stand. 53, 263 (1954).

30. J. R. Clement and E. H. Quinnel, Rev. Sci. Instr. 23, 213 (1952).

31. W. van der Lugt and N. J. Poulis, Physica 26, 917 (1960).

32. V. A. Schmidt and S. A. Friedberg, J. Appl. Phys., 38, 5319 (1967).

33. H. M. Gijsman, N. J. Poulis, and J. van den Handel, Physica 25, 954 (1959).

34. John E. Rives, Phys. Rev. 162, 491 (1967).

35. P. Groth, Chemische Kristallographie (Wilhelm Englemann, Leipzig, 1908), Vol. 1.

36. T. Haseda and E. Kanda, J. Phys. Soc. Japan 12, 1051 (1957).

37. S. A. Friedberg and J. H. Schelleng, Proceedings of the International Conference on Magnetism, Nottingham (1964), p. 90.

38. H. Forstat, G. Taylor and R. D. Spence, Phys. Rev. 116, 897 (1959).

39. M. Garber, J. Phys. Soc. Japan 15, 734 (1960).

40. S. A. Friedberg, A. F. Cohen, and J. H. Schelleng, J. Phys. Soc. Japan 17, Suppl. B-1, 515 (1962).

41. S. A. Friedberg and C. A. Raquet, International Congress on Magnetism, Boston Mass. (Sept. 11-15, 1967).

42. J. T. Schriempf and S. A. Friedberg, Phys. Rev. 136, A 518 (1964).

43. R. D. Spence, R. Au, and P. A. Van Dalen, Physica 30, 1612 (1964).

44. R. D. Spence (private communication)

45. J. N. McElearney, P. T. Bailey and H. Forstat, Bull. Am. Phys. Soc. 12, 1148 (1967).

46. Norikiyo Uryû, Phys. Rev. 136, A527 (1964).

47. D. G. Kapadnis and R. Hartmans, Physica 22, 181 (1956).

48. J. H. Schelleng and S. A. Friedberg, J. Appl. Phys. 34, 1017 (1963).

49. I. Tsujikawa and J. Kanda, J. Phys. Radium 20, 352 (1959).

50. B. Bolger, Communications Conference de Physique des Basses Temperatures, Paris (1955), p 244.

51. R. D. Spence, (private communication).

52. W. K. Robinson and S. A. Friedberg, Phys. Rev. 117, 402 (1960).

53. R. B. Flippen and S. A. Friedberg, J. Appl. Phys. 31S, 338S (1960).

APPENDIX I

COMPUTER PROGRAMS

PART A

FORTRAN Subroutines for Theory

```
      FUNCTION RBRIL(S,XP)
C     THE REDUCED BRILLOUIN FUNCTION
C     (FOR SPIN S, EVALUATED AT XP)
         SGN=1.0
         IF(XP.LT.0.0) SGN=-1.0
         IF(ABSF(XP).NE.0.0) GO TO 1
            RBRIL=0.0
            RETURN
  1      IF(ABSF(XP).LT.354.0) GO TO 2
            RBRIL=1.0
            RETURN
  2      X=3.0*S*ABSF(XP)/(S+1.0)
         A=2.0*S
         B=(A+1.0)/A
         C=1.0/A
 21      X1=B*X
         IF(X1.LT.354.0) GO TO 3
            X=353.9/B
            GO TO 21
  3      E2X1=EXPF(2.0*X1)
         COTH1=(E2X1+1.0)/(E2X1-1.0)
         X2=C*X
         E2X2=EXPF(2.0*X2)
         COTH2=(E2X2+1.0)/(E2X2-1.0)
         RBRIL=SGN*(B*COTH1-C*COTH2)
         RETURN
      END
```

```
      FUNCTION RBRILI(S,Y0,EPS)
C     INVERSE OF THE REDUCED BRILLOUIN FUNCTION
C     (FOR SPIN S, EVALUATED AT Y0 WITH AN ERROR NO GREATER THAN EPS)
        SGN=1.0
        IF(Y0.LT.0.0) SGN=-1.0
        Y1S=EPS/10.0
        X=EPS/10.0
 10     X=X*10.0
        Y1S=10.0*Y1S
        A=2.0*S
        B=(A+1.0)/A
        BSQ=B*B
        C=1.0/A
        CSQ=C*C
  1     X1=B*X
        IF(X1.LT.354.0) GO TO 2
           X=353.9/B
           GO TO 1
  2     E2X1=EXPF(2.0*X1)
        COTH1=(E2X1+1.0)/(E2X1-1.0)
        CSCHSQ1=COTH1*COTH1-1.0
        X2=C*X
        E2X2=EXPF(2.0*X2)
        COTH2=(E2X2+1.0)/(E2X2-1.0)
        CSCHSQ2=COTH2*COTH2-1.0
        Y1=B*COTH1-C*COTH2
        IF(Y1.LT.0.0) GO TO 10
        IF(Y1.GT.Y1S) GO TO 10
           Y1S=1.0
        SLP=-BSQ*CSCHSQ1+CSQ*CSCHSQ2
        DY=SGN*Y0-Y1
        IF(DY.LT.0.0) GO TO 3
        X=X+DY/SLP
        IF(ABSF(DY).GT.EPS) GO TO 1
  3     RBRILI=SGN*X*(S+1.0)/(3.0*S)
        RETURN
      END
```

```
      FUNCTION RBRILP(S,XP)
C     THE FIRST DERIVATIVE OF THE REDUCED BRILLOUIN FUNCTION
C     (FOR SPIN S, EVALUATED AT XP)
         SGN=1.0
         IF(XP.LT.0.0) SGN=-1.0
         X=3.0*S*ABSF(XP)/(S+1.0)
         A=2.0*S
         B=(A+1.0)/A
         C=1.0/A
         IF(X.NE.0.0) GO TO 1
            RBRILP=1.0
            RETURN
  1      IF(X.LT.354.0) GO TO 2
            RBRILP=1.0
            RETURN
  2      X1=B*X
         IF(X1.LT.354.0) GO TO 3
            X=353.9/B
            GO TO 2
  3      E2X1=EXPF(2.0*X1)
         COTH1=(E2X1+1.0)/(E2X1-1.0)
         CSCHSQ1=COTH1*COTH1-1.0
         X2=C*X
         E2X2=EXPF(2.0*X2)
         COTH2=(E2X2+1.0)/(E2X2-1.0)
         CSCHSQ2=COTH2*COTH2-1.0
         RBRILP=SGN*(-B*B*CSCHSQ1+C*C*CSCHSQ2)*3.0*S/(S+1.0)
         RETURN
      END
```

```
      FUNCTION RBRILPI(S,Y0,EPS)
C     THE INVERSE OF THE FIRST DERIVATIVE OF THE REDUCED BRILLOUIN FUNCTION
C     (FOR SPIN S, EVALUATED AT Y0 WITH AN ERROR NO GREATER THAN EPS)
         D=(S+1.0)/(3.0*S)
         Y0R=Y0*D
         SGN=1.0
         IF(Y0R.LT.0.0) SGN=-1.0
         Y0R=ABSF(Y0R)
         I=0
         DX=X=0.5
         A=2.0*S
         B=(A+1.0)/A
         BSQ=B*B
         BCB=B*BSQ
         C=1.0/A
         CSQ=C*C
         CCB=C*CSQ
 1       X1=B*X
         IF(X1.LT.354.0) GO TO 2
            X=353.9/B
            GO TO 1
 2       E2X1=EXPF(2.0*X1)
         COTH1=(E2X1+1.0)/(E2X1-1.0)
         CSCHSQ1=COTH1*COTH1-1.0
         X2=C*X
         E2X2=EXPF(2.0*X2)
         COTH2=(E2X2+1.0)/(E2X2-1.0)
         CSCHSQ2=COTH2*COTH2-1.0
         Y1=-BSQ*CSCHSQ1+CSQ*CSCHSQ2
         IF((Y1.GT.1.0).OR.(Y1.LT.0.0)) GO TO 3
         DY=Y0R-Y1
         IF(ABSF(DY).LT.EPS) GO TO 3
         IF(DY)22,3,21
 21      I=1
         DX=0.5*DX
         IF(DX.LE.EPS) GO TO 3
```

```
      X=X-DX
      GO TO 1
22    IF(I.EQ.1) GO TO 23
      X=2.0*X
      DX=X
      GO TO 1
23    DX=0.5*DX
      IF(DX.LE.EPS) GO TO 3
      X=X+DX
      GO TO 1
3     RBRILPI=X*D*SGN
      RETURN
      END
```

```
      FUNCTION RS0(S,T,EPS)
C     S-ZERO, THE REDUCED MAGNETIZATION BASED ON THE MOLECULAR FIELD THEORY
C     (FOR SPIN S, EVALUATED AT TEMPERATURE T WITH AN ERROR NO GREATER THAN EPS)
         X=0.0
         IF(T.GE.1.0) GO TO 5
         IF(T.NE.0.0) GO TO 1
            RS0=1.0
            RETURN
  1      DX=1.0/(2.0*T)
  2      X=X+DX
         GO TO 4
  3      X=X-DX
  4      D=T*X-RBRIL(S,X)
         IF(ABSF(D).LE.EPS) GO TO 5
         DX=DX/2.0
         IF(D) 2,5,3
  5      RS0=T*X
         RETURN
      END
```

PART B

FORTRAN Subroutines for Data Reduction

```
      SUBROUTINE ESPHALT(NDP,CP,T,C)
C                (EXPERIMENTAL SPECIFIC HEATS AT LOW TEMPERATURES)
C     PROGRAMMED BY J. N. MC ELEARNEY, 8-19-65
      DIMENSION C(10),CP(300),T(300),CLN(8,9),ZROPT(9),NAME(10),
     1          CCCOEF(5),XT(11),XTD(11),CMC(20)
      COMMON/CLN/CLN/NOPRNTTC/NOPRNTTC/NOPRNTVC/NOPRNTVC/TCF/TCF
      DATA (SP1=8H SPECIFI),(SP2=8HC HEAT  ),(SP3=8H (CAL/MO),
     1     (SP4=8HLE-DEG) ),(HC1=8H HEAT CA),(HC2=8HPACITY  ),
     1     (HC3=8H (ML-JLS),(HC4=8H/DEG-K) )
      DATA (XTD=8H   C,    ,8H  C/T,   ,8HC/T**1.5,8H C*T**2,,
     1      8H LOG(C),,8H LOG(T),,8H    T,    ,8H  T**2, ,8H  T**3, ,
     2      8H  T**5, ,8H T**1.5,)
1010  FORMAT (10A8)
1020  FORMAT (3I5,2F10.3,9F5.1/9I5,2F10.5,2I5)
1030  FORMAT (5E16.8)
1040  FORMAT (1H1/29X,10A8/48X,4H(WT=,F7.3,20H GMS   GRAM-MOLE-WT=,
     1          F8.3,1H)//15H POINT   TEMP  ,2A8,12HDELTA TEMP  ,
     1         46HR-START   R-END   R-ZERO    DS    DE   TIME   ,
     1         47H CURRENT   VOLTAGE    ENERGY      POWER    CODE/
     1         7X,8H (DEG-K),2A8,30H (DEG-K)     (OHMS)    (OHMS)  ,
     1         6H(OHMS),15X,38H(SEC)  (MLE-AMPS) (VOLTS)   (MLE-JLS) ,
     1         11H(MLE-WATTS)/)
1050  FORMAT (F10.1,F10.1,F8.1,F8.1,I2,I1,F9.5,F10.6)
1060  FORMAT (I5,F9.3,F11.3,F15.6,F10.2,2F9.2,3F6.1,F11.5,F11.6,
     1         F10.5,F11.5,I5,I1)
1070  FORMAT (I5,F9.3,F11.3,6A8,1X,A6)
1080  FORMAT (1H1/29X,10A8//
     1          10X,45HCP          CP/T     CP/(T**3/2)  CP*(T**2)    ,
     2          45H LOG(CP)     LOG(T)          T           T**2   ,
     3          36H      T**3          T**5        T**3/2  /)
1090  FORMAT (I4,11E12.4)
1100  FORMAT (3X,F6.3,F7.3,F8.3,6A8,A6)
1110  FORMAT (/23X,44HFOR THE FOLLOWING POINTS A THERMOMETER LEAD ,
     1          13HRESISTANCE OF,F6.1,27H OHMS WAS TAKEN ACCOUNT OF./
     1          9X,19HQUANTITIES EQUAL TO,F8.5,12H MLE-JLS AND,F8.5,
     1          48H TIMES THE MEASURED HEATER CURRENT WERE ADDED TO,
```

```
     1            23H THE CALCULATED ENERGY,/)
1120      FORMAT (2E12.4,6A8,A6)
1130      FORMAT (I5,F8.0,F11.4,F9.1,F12.2,F13.2,I4,I1)
1140      FORMAT (1H1/1X,10A8//37H POINT   FIELD    TEMP    MAG ANGLE  ,
     1            27HMAG CURRENT   R=ZERO   CODE/8X,9H(GAUSS)  ,
     1            30H(DEG-K)  (DEGREES)   (AMPERES)/)
          ID=IDRUN(2)
 10       CCCOEF(1)=CCCOEF(2)=CCCOEF(3)=CCCOEF(4)=CCCOEF(5)=NZ=RL=EE=EI=0
          EPS=0
C                              READ A TITLE AND INITIAL DATA
          READ 1010,(NAME(I),I=1,10)
          READ 1020,NVCP,NTCP,NDP,WT,GMOLWT,(ZROPT(I),I=1,9),NVCC,NTCC,
     1            NOPRNTVC,NOPRNTTC,NOPRNTD,NOPRNTXT,IFCAN,IFPUNCH,
     1            LISTPUN,TCU,ATC,NMCP,NDMC
C                  IF A POLYNOMIAL IN TEMPERATURE TO BE SUBTRACTED FROM DATA..
          IF(IFCAN) READ 1030,(CCCOEF(I),I=1,5)
          TCF=1.0
C                  IF ACTUAL THERMOMETER CURRENT DIFFERENT FROM THERMOMETER
C                  CURRENT USED, ADJUST..
          IF(TCU) TCF=TCU/ATC
C                  ANALYIZE MAGNET CALIBRATION CURVE
          IF(NMCP) CALL CALBMAG(NMCP,NDMC,CMC)
C                              ANALYIZE VOLTAGE CALIBRATION CURVE
          CALL CALBLNR(NVCP,CP,T,CLN,ZROPT,NVCC)
C                              ANALYIZE TEMPERATURE CALIBRATION CURVE
          CALL TEMPCALB(NTCP,CP,T,C,NTCC)
          IF(NDP)400,20,30
 20          NDP=NVCP+NTCP
             RETURN
C                  CALCULATE SPECIFIC HEATS, TEMPERATURES, FIELDS
 30       READ 1010,J
          DO 290 J=1,NDP
             JZ=J-NZ
100          LLP1=LP1
             LLP2=LP2
C                 FOR LP1=          THE TYPE OF DATA IS..
```

```
C                   1                        CP  (LP2=AMPLIFIER SCALE CODE)
C                   2                        MAGNET EXPT,  LP2=1..ROT, =2..H-T
C                   4                        CP, START NEW SERIES-FOR LAST HALF OF PT
C                   5                        CP, NEW VPD AND/OR NEW SERIES-(≠≠)
          READ 1050,R0,DS,DE,TM,LP2,LP1,HC,HV
          IF(J.GT.1) GO TO 110
          LLP1=LP1
          LLP2=LP2
          GO TO 120
110       IF(LP1.EQ.LLP1) GO TO 160
120       GO TO (130,150,130,130,130),LP1
130       IF(WT) GO TO 140
          GMOL=1.0
          IF(NOPRNTD) GO TO 160
          PRINT 1040,(NAME(I),I=1,10),WT,GMOLWT,HC1,HC2,HC3,HC4
          GO TO 160
140       GMOL=GMOLWT/(WT*4186.0)
          IF(NOPRNTD) GO TO 160
          PRINT 1040,(NAME(I),I=1,10),WT,GMOLWT,SP1,SP2,SP3,SP4
          GO TO 160
150       IF(NOPRNTD) GO TO 160
          PRINT 1140,(NAME(I),I=1,10)
160       IF(LP1) GO TO 170
             RL=R0
             EE=TM
             EI=HC
             PRINT 1110,RL,EE,EI
             GO TO 100
170       R0=R0*TCF
          IF(XSIGNF(1,LP2).GE.0) GO TO (180,250,180,190,190),LP1
             CP(JZ)=T(JZ)=0
             NZ=NZ+1
             GO TO 240
180       LNCLBST=LP2+1
          EN=DS-ZROPT(LNCLBST)
          RS=CALCOR(R0,EN,LNCLBST,CLN)
```

```
      GO TO 200
190   LNCLBST=LP2+1
      EN=DS-ZROPT(LNCST1M)
      RS=CALCOR(ROJ1M,EN,LNCST1M,CLN)
200   EN=DE-ZROPT(LNCLBST)
      RE=CALCOR(RO,EN,LNCLBST,CLN)
210   TS=TEMP(RS-RL,C,NTCC)
      TE=TEMP(RE-RL,C,NTCC)
      DELTAT=TE-TS
      IF(HV.EQ.0) HV=HC*RH
      IF(HC.EQ.0) HC=HV/RH
      PWR=HC*HV-HC*HC*0.001*RL
      EN=PWR*TM+EE+EI*HC
      T(JZ)=TS+0.5*DELTAT
      CP(JZ)=EN/DELTAT
      IF(IFCAN.EQ.0) GO TO 230
      ROJ1M=CCCOEF(5)
      DO 220 I=1,4
220      ROJ1M=ROJ1M*T(JZ)+CCCOEF(5-I)
      IF(IFCAN.GT.0) CP(JZ)=CP(JZ)-ROJ1M
230   IF(IFCAN.GE.0) ROJ1M=0
      CP(JZ)=GMOL*CP(JZ)*ROJ1M
      ROJ1M=RO
      IF((CP(JZ).EQ.0).OR.NOPRNTD) GO TO 240
      PRINT 1060,J,T(JZ),CP(JZ),DELTAT,RS,RE,RO,DS,DE,TM,HC,HV,EN,
     1     PWR,LP2,LP1
240   IF((IFPUNCH.EQ.1).AND.(CP(JZ).GT.0))
     1   PUNCH 1070,J,T(JZ),CP(JZ),(NAME(I),I=3,8),ID
      IF((LISTPUN.EQ.1).AND.(CP(JZ).GT.0))
     1   PUNCH 1100,CP(JZ),DELTAT,T(JZ),(NAME(I),I=3,8),ID
      LNCST1M=LNCLBST
      IF((HC.NE.0).AND.(HV.NE.0)) RH=HV/HC
      GO TO 290
250   IF(LLP2.EQ.LP2) GO TO 260
         LLP2=LP2
         GO TO 150
```

```
260       GO TO (270,280),LP2
C            ADIABATIC CHANGE OF MAGNETIC FIELD CALCULATION
270       CP(JZ)=FIELDMAG(DS,NDMC,CMC)
          T(JZ)=TEMP(R0-RL,C,NTCC)
          IF(NOPRNTD) GO TO 240
          PRINT 1130,J,CP(JZ),T(JZ),DE,DS,R0,LP2,LP1
          GO TO 240
C               ADIABATIC ROTATION OF MAGNETIC FIELD CALCULATION
280       CP(JZ)=TEMP(R0-RL,C,NTCC)
          T(JZ)=DE
          HV=FIELDMAG(DS,NDMC,CMC)
          IF(NOPRNTD) GO TO 240
          PRINT 1130,J,HV,CP(JZ),T(JZ),DS,R0,LP2,LP1
          GO TO 240
290       CONTINUE
       NDP=NDP-NZ
       IF(NOPRNTXT) RETURN
400    NZ=NDP
       NDP=XABSF(NDP)
       JZ=1
       IF(NZ.LT.0) JZ=0
C                          CALCULATE CROSS TERMS
       DO 610 J=1,NDP
          I=J-1
          IF((((I/56)*56-I).EQ.0).AND.(NOPRNTXT.EQ.0))
     1       PRINT 1080,(NAME(I),I=1,10)
          XT(8)=DS=T(J)*T(J)
          XT(9)=DE=DS*T(J)
          T2=SQRTF(T(J))
          XT(11)=RS=T(J)*T2
          XT(10)=RE=DS*DE
          XT(4)=TS=CP(J)*DS
          XT(3)=TE=CP(J)/RS
          XT(5)=DELTAT=LOGF(ABSF(CP(J)))
          XT(6)=PWR=LOGF(ABSF(T(J)))
          XT(2)=EN=CP(J)/T(J)
```

```
            XT(1)=CP(J)
            XT(7)=T(J)
            IF(JZ) GO TO 600
               IF(LISTPUN+IFPUNCH)
     1            PUNCH 1120,XT(NVCC),XT(NTCC),XTD(NVCC),XTD(NTCC),
     2                    (NAME(I),I=3,6),ID
600         IF(NOPRNTXT) GO TO 610
            PRINT 1090,J,CP(J),EN,TE,TS,DELTAT,PWR,T(J),DS,DE,RE,RS
610         CONTINUE
700      RETURN
      END
```

```
      SUBROUTINE CALBMAG(NPF,NDMC,CMC)
C     MAGNET CALIBRATION
      DIMENSION W(130),Z(18,130),R(2,130),CMC(16),NAME(10),H(130),
     1          RMC(130)
      COMMON/ETS/W,Z,R
101   FORMAT (A4,9A8)
102   FORMAT (3E20.11/3E20.11)
103   FORMAT (F5.2,F5.0)
104   FORMAT (1H1/32X,A4,9A8/)
105   FORMAT (47X,41HEQUATION USED..H=SUM(C(I)*CURRENT**(I-1)),
     1          //14X,4HC 1=,E18.11,7X,4HC 2=,E18.11,7X,4HC 3=,E18.11,
     1          7X,4HC 4=,E18.11/14X,4HC 5=,E18.11,7X,4HC 6=,E18.11,
     1          7X,4HC 7=,F18.11,7X,4HC 8=,E18.11/14X,4HC 9=,E18.11,
     1          7X,4HC10=,E18.11,7X,4HC11=,E18.11,7X,4HC12=,E18.11/
     1          14X,4HC13=,E18.11,7X,4HC14=,E18.11,7X,4HC15=,E18.11,
     1          7X,4HC16=,F18.11)
106   FORMAT (/60X,15HANALYSIS OF FIT//11X,7HCURRENT,16X,9HMEASURED ,
     1          5HFIELD,12X,16HCALCULATED FIELD,14X,10HDIFFERENCE,11X,
     1          21HPERCENTAGE DIFFERENCE/11X,6H(AMPS),21X,7H(GAUSS),
     1          20X,7H(GAUSS)/(I4,1X,0PE16.8,6X,3(5X,0PE16.8,6X),5X,
     1          2PF12.4,10X))
      NP=NPF
      IF(NP.EQ.0) RETURN
      NS=NDMC
      NDMC=XABSF(NDMC)
      IF(NDMC)2,1,2
  1      NDMC=13
  2   IF(NP-1)60,3,4
  3      READ 101,(NAME(I),I=1,10)
         READ 102,(CMC(I),I=1,16)
         GO TO 30
  4   READ 101,(NAME(I),I=1,10)
      DO 7 I=1,NP
         W(I)=1.0
         READ 103,RMC(I),H(I)
  7      CONTINUE
```

```
 8    CALL PALS(NP,NDMC,0,W,RMC,H,Z,R,CMC,I)
      DO 10 I=1,NP
 10      Z(1,I)=H(I)-R(1,I)
 15   K=NDMC+2
      DO 20 I=K,16
 20      CMC(I)=0
 30   PRINT 104,(NAME(I),I=1,10)
      PRINT 105,(CMC(I),I=1,16)
      IF(NP-1) PRINT 106,(I,RMC(I),H(I),Z(1,I),R(1,I),R(2,I),
     1                    I=1,NP)
 50   RETURN
 60   RMC(1)=0
      DO 62 I=1,100
         ZP=CMC(16)
         FCTR=RMC(I)
         DO 61 J=2,16
 61         ZP=ZP*FCTR+CMC(17-J)
         H(I)=ZP
 62      RMC(I+1)=RMC(I)+0.5
      NPF=100
      RETURN
     END
```

```
      SUBROUTINE CALBLNR(NVCPF,DRDD,R0,CLN,ZROPT,NFIT)
C                           (CALIBRATE L AND N RECORDER)
C     PROGRAMMED BY J. N, MC ELEARNEY, 8-19-65
         DIMENSION W(130),Z(10,130),R(2,130),C(10),
     1             NAME(10),CLN(8,9),ZROPT(9),RNG(9),DRDD(130),R0(130)
         COMMON/ETS/W,Z,R
         COMMON/NOPRNTVC/NOPRNTVC/IC/IC/TCF/TCF
         DATA (RNG(1)=1.0),(RNG(2)=2.0),(RNG(3)=4.0),(RNG(4)=10.0),
     1        (RNG(5)=20.0),(RNG(6)=40.0),(RNG(7)=50.0),(RNG(8)=100.0),
     1        (RNG(9)=200.0)
101      FORMAT (A4,9A8)
102      FORMAT (3E20.11/3E20.11)
103      FORMAT (4F10.2,I4)
104      FORMAT (1H1/32X,A4,9A8/)
105      FORMAT (22X,41HTHE EQUATION IS..DR/DD=(C1+C2*R+C3*(R**2),
     1             51H+C4*(R**3)+C5*(R**4)+C6*(R**5)+C7*(R**6)+C8*(R**7))
     1             //14X,3HC1=,E18.11,8X,3HC2=,E18.11,8X,3HC3=,E18.11,8X,
     1             3HC4=,E18.11/14X,3HC5=,E18.11,8X,3HC6=,E18.11,8X,
     1             3HC7=,E18.11,8X,3HC8=,E18.11)
106      FORMAT (/60X,15HANALYSIS OF FIT//13X,2HR0,19X,14HMEASURED DR/DD
     1             ,12X,16HCALCULATED DR/DD,14X,10HDIFFERENCE,11X,
     2             21HPERCENTAGE DIFFERENCE/11X,6H(OHMS),19X,
     3             10H(OHMS/DIV),17X,10H(OHMS/DIV)/(I4,1X,0PE16.8,6X,
     4             3(5X,0PE16.8,6X),5X,2PF12.4,10X))
107      FORMAT (//34X,32HTHE FOLLOWING POINTS FROM ABOVE ,
     1             36HARE BEING DELETED FOR A BETTER FIT..//(66X,F4.0))
108      FORMAT (//37X,31HTHE DEGREE OF THE FIT IS BEING ,
     1                    13HINCREASED TO ,I1,17H FOR A BETTER FIT)
         NVCP=NVCPF
         IF(NVCP.EQ.0) RETURN
         NS=NFIT
         NFIT=XABSF(NFIT)
         IF(NFIT)2,1,2
  1         NFIT=1
  2      IF(NVCP-1)60,3,4
  3         READ 101,(NAME(I),I=1,10)
```

```
      READ 102,(C(I),I=1,8)
      IC=2
      GO TO 30
4     READ 101,(NAME(I),I=1,10)
      EPS=0.10
      DO 7 I=1,NVCP
        W(I)=1.0
        READ 103,RL,DRL,RR,DRR,IC
        RL=RL*TCF
        RR=RR*TCF
        IF(RR)6,5,6
5         RR=RL1M
6       ZP=ZROPT(IC+1)
        DRDD(I)=(RR-RL)/(DRR-DRL)
        FCTR=0.5*DRDD(I)
        R0(I)=((ZP-DRR)+(ZP-DRL))*FCTR+(RR+RL)*0.5
        DRDD(I)=DRDD(I)/RNG(IC+1)
        RL1M=RL
7       CONTINUE
      IC=0
8     CALL PALS(NVCP,NFIT,0,W,R0,DRDD,Z,R,C,I)
9     J=0
      IF(NS.LT.0) GO TO 15
      DO 10 I=1,NVCP
        IF(ABSF(R(2,I)).LE.EPS) GO TO 10
          IF(IC.GT.0) GO TO 401
          J=J+1
          Z(2,J)=I
10      Z(1,I)=DRDD(I)-R(1,I)
      IC=IC+1
      IF(IC.EQ.2) GO TO 42
15    K=NFIT+2
      DO 20 I=K,8
20      C(I)=0
30    IF(NOPRNTVC) GO TO 40
      IF((NS.NE.NFIT).AND.(NS.GT.0)) PRINT 108,NFIT
```

```
      PRINT 104,(NAME(I),I=1,10)
      PRINT 105,(C(I),I=1,8)
      IF(NVCP-1) PRINT 106,(I,RO(I),DRDD(I),Z(1,I),R(1,I),R(2,I),
     1                          I=1,NVCP)
 40   IF(IC.GE.2) GO TO 42
      EPS=0.075
      IF(J.NE.0) GO TO 402
      IF(IC.EQ.1) GO TO 9
 401  IC=IC+1
         IF(NFIT.EQ.7) GO TO 30
         NFIT=NFIT+1
         GO TO 8
 402  DO 41 I=1,J
         IC=Z(2,I)-I+1
         NVCP=NVCP-1
         DO 41 K=IC,NVCP
            K1=K+1
            RO(K)=RO(K1)
 41         DRDD(K)=DRDD(K1)
      IC=IC+1
      IF(NOPRNTVC) GO TO 8
      PRINT 107,(Z(2,I),I=1,J)
      GO TO 8
 42   DO 43 I=1,9
      DO 43 J=1,8
 43      CLN(J,I)=C(J)*RNG(I)
 50   RETURN
 60   RO(1)=0
      DO 62 I=1,100
         ZP=C(8)
         FCTR=RO(I)
         DO 61 J=3,9
 61         ZP=ZP*FCTR+C(10-J)
         DRDD(I)=ZP
 62      RO(I+1)=RO(I)+250.0
      NVCPF=100
      RETURN
     END
```

```
      SUBROUTINE TEMPCALB(M,Y,X,C,N)
C     THERMOMETER CALIBRATION
C     PROGRAMMED BY J. N. MC ELEARNEY, 8-19-65
      DIMENSION R(50),T(50),W(130),X(50),Y(50),Z(10,130),ER(2,130),
     1          C(10),NAME(10)
      COMMON/ETS/W,Z,ER
      COMMON/NOPRNTTC/NOPRNTTC
100   FORMAT (1H2,51X,32HANALYSIS OF CALIBRATION CURVE OF/32X,10A8//)
101   FORMAT (22X,48HTHE EQUATION IS..1/T=C1+C2*LOG(R)+C3*(LOG(R)**2)
     1          ,45H+C4*(LOG(R)**3)+C5*(LOG(R)**4)+C6*(LOG(R)**5))
102   FORMAT (13X,48HTHE EQUATION IS.. SQRT(LOG(R)/T)=(C1+C2*LOG(R))/
     1          ,46H(1-(C3+C4*LOG(R)+C5*(LOG(R)**2)+C6*(LOG(R)**3),
     1          17H+C7*(LOG(R)**4))))
103   FORMAT (/14X,3HC1=,E18.11,8X,3HC2=,E18.11,8X,3HC3=,E18.11,
     1          8X,3HC4=,E18.11/14X,3HC5=,E18.11,8X,3HC6=,E18.11,
     1          8X,3HC7=,E18.11,8X,3HC8=,E18.11)
104   FORMAT (/4X,
     1          19HMEASURED RESISTANCE,8X,20HMEASURED TEMPERATURE,6X,
     2          22HCALCULATED TEMPERATURE,11X,10HDIFFERENCE,11X,
     3          21HPERCENTAGE DIFFERENCE/11X,6H(OHMS),21X,7H(DEG-K),
     4          20X,7H(DEG-K),18X,11H(MLE-DEG-K)/
     5          (8X,0PF9.2,10X,2(7X,0PF12.8,8X),9X,3PF8.2,15X,2PF12.4,
     6          10X))
105   FORMAT (3E20.11)
106   FORMAT (////52X,30HINTERPOLATED CALIBRATION CURVE//)
201   FORMAT (10A8)
202   FORMAT (F9.1,F9.4)
      IF(M.EQ.0) RETURN
      IF(N.EQ.0) N=1
      IF(M;EQ.-1) GO TO 60
      IF(M.GT.0) READ 201,(NAME(J),J=1,10)
      IF(M.GT.0) MT=M
      IF(M.GT.1) READ 202,(R(J),T(J),J=1,M)
      M=XABSF(M)
      M1=M+1
      LPON=0
```

```
      IF(N,LT,0) LPON=1
      N=XABSF(N)
      DO 59 NLP=1,6
         IF(((LPON.EQ.0).AND.(NLP.NE.N))
     1      .OR.((LPON.EQ.1).AND.(NLP.EQ.N))) GO TO 59
         I=NLP
 1       IF(.NOT.NOPRNTTC) PRINT 100,(NAMF(J),J=1,10)
         C(1)=C(2)=C(3)=C(4)=C(5)=C(6)=C(7)=C(8)=C(9)=C(10)=0
         GO TO (2,3,4,5,6),I
 2       L=5$   GO TO 10
 3       L=4$   GO TO 10
 4       L=5$   GO TO 20
 5       L=3$   GO TO 10
 6       L=4$   GO TO 20
10       DO 11 J=1,M
            W(J)=T(J)*T(J)
            X(J)=LOGF(R(J))
11          Y(J)=1.0/T(J)
         CALL PALS(M,L,0,W,X,Y,Z,ER,C,J)
         DO 12 J=1,M
            W(J)=TEMP(R(J),C,I)
            ER(1,J)=T(J)-W(J)
12          ER(2,J)=ER(1,J)/T(J)
         GO TO 30
20       DO 21 J=1,M
            W(J)=1.0
            X(J)=LOGF(R(J))
21          Y(J)=SQRTF(X(J)/T(J))
         CALL PALS(M,1,0,W,X,Y,Z,ER,C,J)
         IF(I,GT.5) GO TO 24
         C1=C(1)
         C2=C(2)
         DO 22 J=1,M
22          Y(J)=ER(2,J)
         CALL PALS(M,L-1,0,W,X,Y,Z,ER,C,J)
         DO 23 J=1,L
```

```
              K=L-J
23            C(K+3)=C(K+1)
           C(1)=C1
           C(2)=C2
24         DO 25 J=1,M
              Y(J)=SQRTF(X(J)/T(J))
              W(J)=TEMP(R(J),C,I)
              ER(1,J)=T(J)*W(J)
25            ER(2,J)=ER(1,J)/T(J)
30         GO TO (31,31,32,31,32),I
31         IF(.NOT.NOPRNTTC) PRINT 101
           GO TO 40
32         IF(.NOT.NOPRNTTC) PRINT 102
40         IF(M.NE.1) GO TO 50
              READ 105,(C(J),J=1,8)
              IF(.NOT.NOPRNTTC) PRINT 103,(C(J),J=1,8)
              RETURN
50         IF(NOPRNTTC) RETURN
           PRINT 103,(C(J),J=1,8)
           PRINT 104,(R(J),T(J),W(J),ER(1,J),ER(2,J),J=1,M)
           IF(M1.GT.MT) GO TO 52
           DO 51 J=M1,MT
              W(J)=TEMP(R(J),C,I)
              ER(1,J)=T(J)*W(J)
51            ER(2,J)=ER(1,J)/T(J)
           PRINT 106,(NAME(J),J=1,10)
           PRINT 104,(R(J),T(J),W(J),ER(1,J),ER(2,J),J=M1,MT)
52         IF((NLP.LT.6).OR.(LPON.EQ.0)) GO TO 59
              LPON=0
              I=N
              GO TO 1
59         CONTINUE
        RETURN
60      IF(N.GE.0) GO TO 62
        DO 61 I=1,MT
           X(I)=LOGF(R(I))
```

```
61          Y(I)=ER(-N,I)
        M=MT
        RETURN
62      X(1)=0.0001
        DO 63 I=1,100
            Y(I)=1.0/TEMP(EXPF(X(I)),C,N)
            IF((N.EQ.3).OR.(N.GE.5)) Y(I)=SQRTF(X(I)*Y(I))
63          X(I+1)=X(I)+0.11
        M=100
        RETURN
      END
```

```
      FUNCTION CALCOR(R0,DIV,ICF,C)
C     CALCULATE CORRECTED RESISTANCE (FOR NON-NULL RECORDER READING)
         DIMENSION C(8,9)
         IC=ICF
         R=R0
 1       SUM=6.0*C(8,IC)
         DO 2 I=1,5
            RI=I
 2          SUM=SUM*R+(6.0-RI)*C(8-I,IC)
         C1P=C(1,IC)-SUM*R*R
         SUM=7.0*C(8,IC)
         DO 3 I=1,5
            RI=I
 3          SUM=SUM*R+(7.0-RI)*C(8-I,IC)
         C2P=C(2,IC)+SUM*R
         RI=R
         R=(R0-C1P*DIV)/(1.0+C2P*DIV)
         IF(((ABSF(RI-R))/R).GT.0.001) GO TO 1
         CALCOR=R
         RETURN
      END
```

```
      FUNCTION TEMP(R,C,N)
C     CONVERT RESISTANCE TO TEMPERATURE
C     PROGRAMMED BY J. N. MC ELEARNEY, 8-19-65
         DIMENSION C(10)
         GO TO (1,2,3,4,5),N
  1      I=5$    GO TO 10
  2      I=4$    GO TO 10
  3      I=5$    GO TO 20
  4      I=3$    GO TO 10
  5      I=4$    GO TO 20
 10      RLOG=LOGF(R)
         I1=I+1
         SUM=C(I1)
         DO 11 K=1,I
            SUM=RLOG*SUM+C(I1-K)
 11
         TEMP=1.0/SUM
         RETURN
 20      RLOG=LOGF(R)
         I2=I+2
         SUM=C(I2)
         I1=I-1
         DO 21 K=1,I1
 21         SUM=RLOG*SUM+C(I2-K)
         SUM=(C(1)+C(2)*RLOG)/(1.0-SUM)
         SUM=SUM*SUM
         TEMP=RLOG/SUM
         RETURN
      END
```

```
      SUBROUTINE PALS(M,NN,EPS,W,X,Y,Z,R,C,N)
C     POLYNOMIAL APPROXIMATION BY LEAST SQUARES
         DIMENSION W(M),X(M),Y(M),Z(10,M),R(2,M),C(20),A(9)
         N=NN
         IF(M-N-1)940,942,942
940         N=M-1
942      N3=N+3
         N2=N+2
         N1=N+1
C        THIS IS A TRANSLATION OF A STANFORD SUBALGOL PROCEDURE
         GO TO 93
C        START SUM
99          BOX=0
            DO 98 I=1,M
               ZN3=Z(N3,I)
98             BOX=BOX+ZN3*ZN3
            IF(TGL)97,95,97
97          IF(BOX-TOT)95,96,96
96             K=K-1
               GO TO 82
95          DO 94 I=1,M
               IF(EPS-ABSF(Z(N3,I)))941,94,94
94             CONTINUE
            GO TO 82
941         TOT=BOX
            TGL=1.0
            GO TO 89
C        END SUM
93       K=0
         TGL=0
         DO 92 J=1,M
92          Z(2,J)=W(J)
         DO 91 I=1,N
            I2=I+2
            I1=I+1
            DO 91 J=1,M
```

```
91            Z(I2,J)=X(J)*Z(I1,J)
        DO 90 J=1,M
90         Z(N3,J)=Y(J)*W(J)
89      K=K+1
        K1=K+1
        DO 88 I=K,N2
           A(I)=0
           I1=I+1
           DO 88 J=1,M
88            A(I)=Z(K1,J)*Z(I1,J)+A(I)
        DO 86 I=K,N1
86         Z(K,I)=A(I+1)/A(K)
        DO 85 I=K,N1
           I2=I+2
           DO 85 J=1,M
85            Z(I2,J)=Z(I2,J)-Z(K,I)*Z(K1,J)
        IF(K-1)84,99,84
84      K1=K-1
        DO 83 I=1,K1
           DO 83 J=K,N1
83            Z(I,J)=Z(I,J)-Z(I,K1)*Z(K,J)
        IF(K-N1)99,82,99
82      DO 81 I=1,K
81         C(I)=Z(I,N1)
        DO 80 I=1,M
           R(1,I)=Z(N3,I)
80         R(2,I)=R(1,I)/Y(I)
        N=K-1
        RETURN
     END
```

PART C

Typical Data Deck Input

```
                          01/26/68 RJN 4 SAMPLE 1 CO=BR2.6H2O
   6   13  111                           50.0 50.0 50.0 50.0 50.0 50.0 50.0 50.0 50.0
   1    3                                     1                            51    8
                          03/30/68 MAGNET CALIBRATION
00.0 0060
03.2 1810
04.7 2680
04.2 2360
05.0 2800
06.0 3330
07.0 3870
08.0 4300
09.0 4760
10.0 5100
11.0 5410
12.0 5700
13.0 5950
```

14.0	6200
15.0	6390
16.0	6600
17.0	6780
18.0	6920
19.0	7090
20.0	7250
21.0	7390
22.0	7510
23.0	7610
24.0	7750
25.0	7850
26.0	7980
27.0	8090
28.0	8180
29.0	8280
30.0	8390
31.0	8470
32.0	8570
33.0	8660
34.0	8740
35.0	8820
36.0	8900
37.0	9000
38.0	9100
39.0	9170
40.0	9240
41.0	9320
42.0	9400
43.0	9480
44.0	9550
45.0	9620
46.0	9690
47.0	9750
48.0	9810
49.0	9900

```
50.0 9990
51.010050
                          01/26/68 1 MV VOLTAGE CALIBRATION
  1480.0       10.3     1535.0       92.6     11
  1430.0       13.5     0000.0       87.8     11
  1320.0       13.0     0000.0       96.0     21
  1215.0       07.3     0000.0       85.6     21
  1125.0       11.9     0000.0       82.4     21
  1032.0       13.0     0000.0       83.4     21
                          01/26/68 THERMOMETER CALIBRATION
 0060.6   77.1570
 0551.0    4.1990
 0572.2    4.0933
 0599.0    3.9902
 0626.5    3.8874
 0657.0    3.7866
 0695.0    3.6740
 0738.0    3.5585
 0798.0    3.4191
 0890.6    3.2408
 0997.9    3.0713
 1187.6    2.8402
 1415.0    2.6365
                          01/26/68 RJN DATA
  1415.5       03.0    060.0              12
  1421.0       04.0    060.0              12
  1425.0       04.8    060.0              12
  1432.0       06.0    060.0              12
  1441.5       07.0    060.0              12
  1450.5       08.0    060.0              12
  1459.0       09.0    060.0              12
  1468.0       10.0    060.0              12
  1474.5       11.0    060.0              12
  1483.0       12.0    060.0              12
  1489.5       13.0    060.0              12
  1497.0       14.0    060.0              12
```

1502.0	15.0	060.0		12		
1507.0	16.0	060.0		12		
1512.5	17.0	060.0		12		
1517.5	18.0	060.0		12		
1522.5	19.0	060.0		12		
1527.0	20.0	060.0		12		
1531.0	21.0	060.0		12		
1533.5	22.0	060.0		12		
1537.0	23.0	060.0		12		
1541.0	24.0	060.0		12		
1545.5	25.0	060.0		12		
1547.5	26.0	060.0		12		
1552.5	27.0	060.0		12		
1555.5	28.0	060.0		12		
1559.5	29.0	060.0		12		
1562.5	30.0	060.0		12		
1566.0	31.0	060.0		12		
1568.5	32.0	060.0		12		
1570.5	33.0	060.0		12		
1574.0	34.0	060.0		12		
1576.0	35.0	060.0		12		
1577.0	36.0	060.0		12		
1576.0	37.0	060.0		12		
1571.0	38.0	060.0		12		
1568.0	39.0	060.0		12		
1566.5	40.0	060.0		12		
1565.5	41.0	060.0		12		
1564.5	43.0	060.0		12		
1564.5	45.0	060.0		12		
1564.2	47.0	060.0		12		
1563.6	50.0	060.0		12		
1535.0	07.8	23.6	30.0	11	0.09800	0.039200
1535.0	23.8	38.6	30.0	11	0.09800	0.039200
1535.0	37.6	53.1	30.0	11	0.09800	0.039200
1535.0	51.7	66.3	30.0	11	0.09800	0.039200
1535.0	65.4	80.6	30.0	11	0.09800	0.039200

1535.0	77.5	92.8	30.0	11	0.09800	0.039200
1480.0	10.2	22.8	30.0	11	0.09800	0.039200
1480.0	21.8	35.0	30.0	11	0.09800	0.039200
1480.0	33.2	47.2	30.0	11	0.09800	0.039200
1480.0	43.8	59.9	30.0	11	0.09800	0.039200
1480.0	56.3	68.6	30.0	11	0.09800	0.039200
1480.0	65.0	74.8	30.0	11	0.09800	0.039200
1480.0	77.6	88.3	30.0	11	0.09800	0.039200
1430.0	12.4	25.3	30.0	11	0.09800	0.039200
1430.0	24.1	34.3	30.0	11	0.09800	0.039200
1430.0	32.8	64.3	20.2	11	0.19800	0.079200
1430.0	55.0	76.2	30.0	21	0.19800	0.079200
1430.0	76.2	98.0	30.0	21	0.19800	0.079200
1320.0	09.3	29.6	30.0	21	0.19800	0.079200
1320.0	26.6	44.7	30.0	21	0.19800	0.079200
1320.0	43.6	59.9	30.0	21	0.19800	0.079200
1320.0	58.7	76.4	30.0	21	0.19800	0.079200
1320.0	71.7	88.3	30.0	21	0.19800	0.079200
1215.0	02.9	20.2	30.0	21	0.19800	0.079200
1215.0	17.0	30.5	30.0	21	0.19800	0.079200
1215.0	30.3	43.5	30.0	21	0.19800	0.079200
1215.0	42.0	53.5	30.0	21	0.19800	0.079200
1215.0	53.4	65.2	30.0	21	0.19800	0.079200
1215.0	63.6	77.1	30.0	21	0.19800	0.079200
1215.0	73.2	84.8	30.0	21	0.19800	0.079200
1125.0	11.2	20.1	30.0	21	0.19800	0.079200
1125.0	20.4	29.5	30.0	21	0.19800	0.079200
1125.0	28.2	37.6	30.0	21	0.19800	0.079200
1125.0	37.3	45.6	30.0	21	0.19800	0.079200
1125.0	44.8	54.0	30.0	21	0.19800	0.079200
1125.0	52.1	60.0	30.0	21	0.19800	0.079200
1125.0	57.7	65.5	30.0	21	0.19800	0.079200
1125.0	64.3	72.1	30.0	21	0.19800	0.079200
1125.0	70.5	82.0	30.0	21	0.19800	0.079200
1125.0	76.3	89.8	30.0	21	0.19800	0.079200
1032.0	07.7	16.9	30.0	21	0.19800	0.079200

1032.0	14.3	20.0	23.0	21	0.19800	0.079200
1032.0	18.4	23.3	21.0	21	0.19800	0.079200
1032.0	22.2	30.1	31.9	21	0.19800	0.079200
1032.0	28.1	34.7	19.0	21	0.19800	0.079200
1032.0	32.4	45.8	31.0	21	0.19800	0.079200
0932.0	04.6	11.0	32.0	21	0.19800	0.079200
0932.0	08.9	14.8	32.9	21	0.19800	0.079200
0932.0	13.9	18.7	30.0	21	0.19800	0.079200
0932.0	17.8	24.7	30.0	21	0.19800	0.079200
0932.0	23.0	34.5	30.0	21	0.19800	0.079200
0932.0	07.6	13.3	30.0	21	0.19800	0.079200
0932.0	12.5	18.4	30.0	21	0.19800	0.079200
0932.0	16.6	21.5	30.0	21	0.19800	0.079200
0932.0	20.9	25.6	30.0	21	0.19800	0.079200
0932.0	25.4	32.2	30.0	21	0.19800	0.079200
0932.0	30.3	40.6	30.0	21	0.19800	0.079200
0932.0	13.2	19.2	30.0	21	0.19800	0.079200
0932.0	18.2	24.0	30.0	21	0.19800	0.079200
0932.0	23.1	28.6	30.0	21	0.19800	0.079200
0932.0	27.7	32.5	30.0	21	0.19800	0.079200
0932.0	31.9	36.3	30.0	21	0.19800	0.079200
0932.0	35.3	42.0	30.0	21	0.19800	0.079200
0932.0	40.6	51.2	30.0	21	0.19800	0.079200
0932.0	32.3	36.5	30.0	21	0.19800	0.079200
0932.0	36.2	40.7	30.0	21	0.19800	0.079200
0932.0	39.5	47.5	30.0	21	0.19800	0.079200
0932.0	45.5	55.9	30.0	21	0.19800	0.079200

APPENDIX II

RESISTANCE CALCULATION WITH AN UNBALANCED POTENTIOMETER SETTING

APPENDIX II

RESISTANCE CALCULATION WITH AN UNBALANCED POTENTIOMETER SETTING

When Kirchoff's Circuit Law is applied to the potentiometer circuit shown in Fig. 37, the result is

$$(I_E - I_P)R_P + I_E R + (I_E + I_T)R_T = 0. \qquad (1)$$

I_P is the potentiometer current; R_P is the potentiometer resistance; R_T is the thermometer resistance; I_T is the thermometer current; R is the lead resistance; and I_E is the unbalance current. When $I_E = 0$ (1) becomes $I_P R_P = I_T R_T$. If V_0 is the potentiometer voltage reading, then $V_0 = I_P R_P$, so (1) becomes

$$(1 - I_E/I_P)V_0 = I_E R + (1 + I_E/I_T)I_T R_T. \qquad (2)$$

In the actual experimental apparatus, the galvanometer consisted of a microvolt amplifier used with a chart recorder. Experiments have shown that I_E is proportional to the pen deflection from the null position, and that it is less than, at most, 0.1 microampere. For the K-3 potentiometer I_P is never less than 200 microamperes. Thus I_E/I_P is negligible compared to 1. Then, if the recorder deflection is D, and $I_E = aD$, (2) becomes

$$V_0 = aDR + (1 + aD/I_T)I_T R_T. \qquad (3)$$

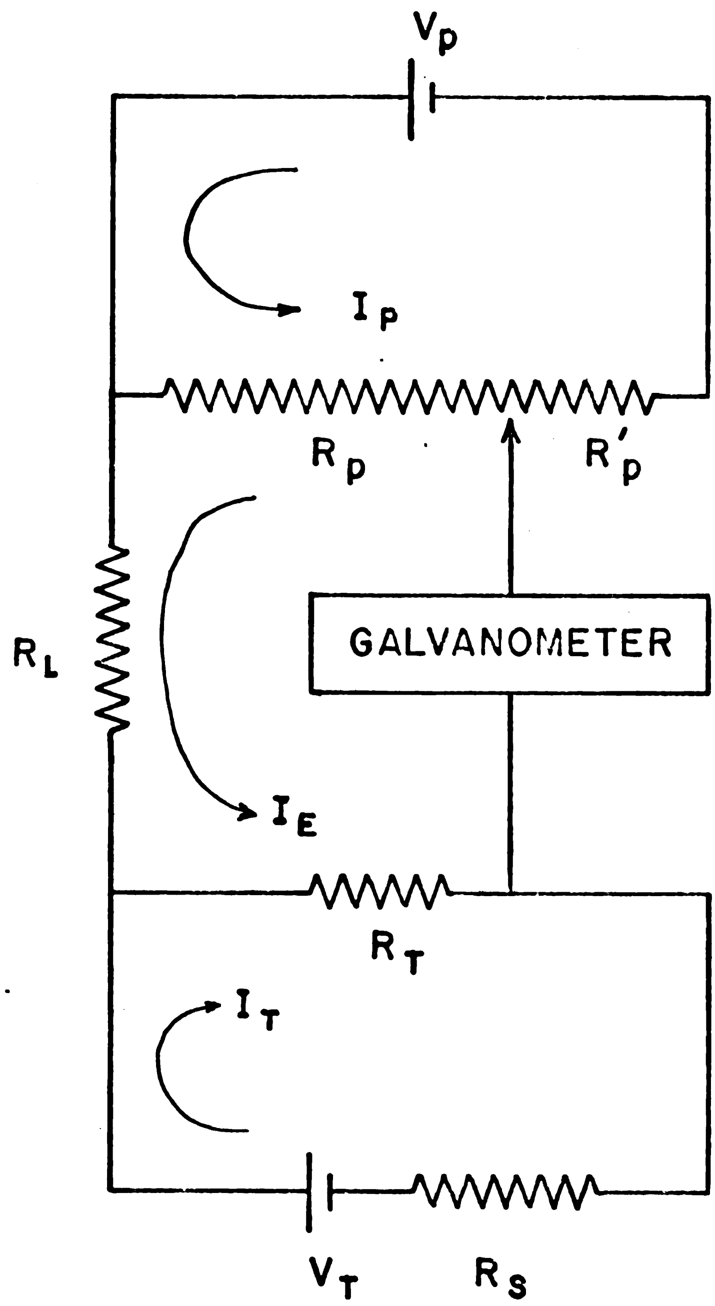

Fig. 37. Circuit diagram of a simple potentiometer.

Since the thermometer current is constant, (3) becomes, setting $R_0 = V_0/I_T$,

$$R_0 = (a/I_T)RD + [1 + (a/I_T)D]R_T \tag{4}$$

If the potentiometer setting is changed, while R_T and R are constant, then, denoting the new values of R_0 and D by primes:

$$R_0' = (a/I_T)RD' + [1 + (a/I_T)D']R_T. \tag{5}$$

If (5) is subtracted from (4), then

$$R_0 - R_0' = (a/I_T)(R + R_T)(D - D') \tag{6}$$

or, $$\Delta R_0/\Delta D = C_1 + C_2 R_T, \tag{7}$$

where $C_1 = (a/I_T)R$ and $C_2 = a/I_T$. This is the voltage calibration curve, in theory.

To calculate R_T using (7), (4) is solved for R_T:

$$R_T = [R_0 - (a/I_T)RD]/[1 + (a/I_T)D] \tag{8}$$

or,

$$R_T = \frac{R_0 - C_1 D}{1 + C_2 D} \quad . \tag{9}$$

In practice (7) turns out to be non-linear, so a modified form of (9) was used:

$$R_T = \frac{R_0 - [C_1 - C_2 R - 2C_3 R^2 - 3C_4 R^3]D}{1 + [C_2 + 2C_3 R + 3C_4 R^2]D} \quad . \tag{10}$$

This equation was arrived at empirically.

APPENDIX III

EXPERIMENTAL DATA

Table 1. $CoCl_2 \cdot 6H_2O$ BC plane isentropic rotations ($C = 55^0$)

θ	$T(^0K)$	θ	$T(^0K)$	θ	$T(^0K)$
		1/5/68, 6350 Gauss			
70	1.287	175	1.278	305	1.336
73	1.294	180	1.270	310	1.336
77	1.301	185	1.262	315	1.330
80	1.306	190	1.253	320	1.324
85	1.315	195	1.243	325	1.321
88	1.318	200	1.233	330	1.316
90	1.319	205	1.223	335	1.311
93	1.320	210	1.214	340	1.316
95	1.321	215	1.204	345	1.298
98	1.323	220	1.215	350	1.291
100	1.323	225	1.201	355	1.284
103	1.324	230	1.186	0	1.276
105	1.324	235	1.184	5	1.266
108	1.324	240	1.203	10	1.256
115	1.322	245	1.222	15	1.245
120	1.322	250	1.243	20	1.234
125	1.322	255	1.260	25	1.222
130	1.321	260	1.274	30	1.210
135	1.320	265	1.287	35	1.193
140	1.313	270	1.299	40	1.178
145	1.309	275	1.309	45	1.162
150	1.305	280	1.317	50	1.149
155	1.300	285	1.324	55	1.145
160	1.295	290	1.329	60	1.162
165	1.291	295	1.332	65	1.185
170	1.285	300	1.334	70	1.206
		1/5/68, 7860 Gauss			
35	1.303	265	1.293	135	1.367
25	1.333	255	1.262	125	1.358
15	1.357	245	1.227	115	1.345
5	1.376	235	1.202	107	1.329
355	1.389	225	1.225	95	1.302
345	1.397	215	1.261	85	1.271
335	1.400	205	1.294	75	1.237
325	1.398	195	1.320	65	1.199
315	1.392	185	1.342	60	1.185
305	1.381	175	1.358	55	1.179
295	1.368	165	1.368	50	1.189
285	1.347	155	1.371	45	1.207
275	1.322	145	1.371		

Table 2. $CoCl_2 \cdot 6H_2O$ AB plane isentropic rotations ($B = 0^0$)

θ	$T(^oK)$	θ	$T(^oK)$	θ	$T(^oK)$
		1/11/68, 6410 Gauss			
70	1.224	200	1.259	320	1.266
80	1.223	210	1.256	330	1.268
90	1.228	217	1.253	340	1.267
100	1.238	220	1.252	350	1.265
110	1.246	230	1.245	0	1.265
120	1.255	240	1.240	0	1.262
130	1.260	250	1.237	10	1.259
140	1.262	260	1.237	20	1.257
150	1.263	270	1.241	30	1.253
160	1.265	280	1.248	40	1.247
170	1.265	290	1.256	50	1.242
180	1.263	300	1.263	60	1.236
190	1.262	310	1.269	70	1.232
		1/11/68, 9700 Gauss			
270	1.197	160	1.293	40	1.286
260	1.297	150	1.289	30	1.294
250	1.218	140	1.284	20	1.301
240	1.240	130	1.276	10	1.304
230	1.257	120	1.265	0	1.306
225	1.262	110	1.250	350	1.305
220	1.272	100	1.233	340	1.303
210	1.281	90	1.215	330	1.299
200	1.287	80	1.210	320	1.292
190	1.291	70	1.236	310	1.283
180	1.294	60	1.257	300	1.272
170	1.294	50	1.273	290	1.256

Table 3. $CoCl_2 \cdot 6H_2O$ AC plane isentropic rotations ($C = 70^0$)

θ	$T(^0K)$	θ	$T(^0K)$	θ	$T(^0K)$
		1/9/68, 6410 Gauss			
335	1.315	215	1.225	95	1.182
325	1.300	205	1.255	85	1.167
315	1.279	195	1.284	75	1.164
305	1.250	185	1.308	65	1.171
295	1.221	175	1.321	55	1.184
285	1.194	165	1.328	45	1.205
275	1.172	155	1.327	35	1.234
265	1.161	145	1.314	25	1.265
255	1.157	135	1.292	15	1.291
245	1.160	125	1.264	5	1.315
235	1.175	115	1.233	355	1.329
225	1.198	105	1.203	345	1.334
		1/9/68, 9620 Gauss			
350	1.359	230	1.221	110	1.182
340	1.365	220	1.216	100	1.208
330	1.349	210	1.200	90	1.219
320	1.313	200	1.223	80	1.227
310	1.263	190	1.283	70	1.230
300	1.206	180	1.331	60	1.230
290	1.175	170	1.363	50	1.225
280	1.203	160	1.372	40	1.217
270	1.215	150	1.357	30	1.197
260	1.222	140	1.326	20	1.232
250	1.225	130	1.278	10	1.296
240	1.224	120	1.220	0	1.341

Table 4. $CoCl_2 \cdot 6H_2O$ C-axis isentropic magnetizations

T(^oK)	H(Gauss)	T(^oK)	H(Gauss)	T(^oK)	H(Gauss)
		1/9/68			
1.207	6450	1.226	8290	1.238	9480
1.195	6780	1.229	8480	1.239	9620
1.196	7090	1.231	8660	1.240	9760
1.203	7370	1.234	8830	1.241	9890
1.212	7620	1.235	9000	1.241	9970
1.219	7860	1.236	9160		
1.223	8080	1.237	9320		
		1/6/68			
1.244	8570	1.221	7230	1.335	4310
1.242	8380	1.222	6940	1.358	3360
1.240	8190	1.236	6600	1.372	2260
1.237	7970	1.256	6200	1.372	1850
1.232	7740	1.279	5700		
1.225	7500	1.303	5080		

Table 5. $CoCl_2 \cdot 6H_2O$ antiferromagnetic-spin flop boundary points (H // C-axis)

T(^oK)	H(Gauss)
1/5/68	
1.219	7140
1.273	7110
1.365	7260
1.502	7420
1.679	7440
1/6/68	
1.186	7060
1.218	7100
1.279	7120
1.353	7190
1.445	7310
1.513	7420
1.579	7540
1.664	7680
1/9/68	
1.491	7290
1.532	7380
1.588	7450
1.674	7610

Table 6. $CoCl_2 \cdot 6H_2O$ BC plane paramagnetic isentropic rotation ($C = 55^0$)

θ	T(^{0}K)	θ	T(^{0}K)	θ	T(^{0}K)
		1/6/68			
55	2.459	285	2.467	5	3.209
65	2.459	295	2.472	355	3.215
75	2.463	305	2.476	345	3.219
85	2.468	315	2.478	335	3.221
95	2.474	325	2.478	325	3.222
105	2.479	335	2.475	315	3.223
115	2.484	345	2.471	305	3.223
125	2.487	355	2.464	295	3.222
135	2.489	5	2.457	285	3.222
145	2.489	15	2.448	275	3.221
155	2.486	25	2.442	265	3.224
165	2.482	35	2.436	255	3.227
175	2.476	45	2.431	245	3.228
185	2.469	55	2.430	235	3.231
195	2.461	65	2.432	225	3.233
205	2.456	75	2.435	215	3.238
215	2.450	85	2.441	205	3.242
225	2.447	95	2.447	195	3.246
235	2.446	55	3.192	185	3.252
245	2.447	45	3.194	175	3.257
255	2.451	35	3.195	165	3.262
265	2.455			155	3.267
275	2.461				

Table 7. $MnCl_2 \cdot 4H_2O$ AC plane isentropic rotations ($C = 45^0$)

θ	$T(^0K)$	θ	$T(^0K)$	θ	$T(^0K)$
		2/6/68, 6410 Gauss			
10	1.079	260	1.080	110	1.122
360	1.097	250	1.063	100	1.111
355	1.107	240	1.043	90	1.096
350	1.115	230	1.037	80	1.079
345	1.122	220	1.037	70	1.060
340	1.126	210	1.040	60	1.041
335	1.130	200	1.050	50	1.036
330	1.133	190	1.070	45	1.035
320	1.135	180	1.091	40	1.035
315	1.135	170	1.110	35	1.036
310	1.134	160	1.123	30	1.039
300	1.129	150	1.131	25	1.042
290	1.122	140	1.135	20	1.049
280	1.110	130	1.134	15	1.058
270	1.096	120	1.130		
		2/6/68			
75	1.054	200	1.018	320	1.135
80	1.066	205	1.015	325	1.133
85	1.078	210	1.013	330	1.130
90	1.088	215	1.016	335	1.124
95	1.097	220	1.016	340	1.116
100	1.107	225	1.016	345	1.107
105	1.115	230	1.017	350	1.066
110	1.121	235	1.018	355	1.081
115	1.127	240	1.022	360	1.096
120	1.131	245	1.026	355	1.081
125	1.133	250	1.042	360	1.096
130	1.135	255	1.054	5	1.051
135	1.135	260	1.066	10	1.034
140	1.134	265	1.077	25	1.016
145	1.132	270	1.088	30	1.016
150	1.129	275	1.098	35	1.014
155	1.123	280	1.107	40	1.015
165	1.104	285	1.114	45	1.015
170	1.093	290	1.120	50	1.016
175	1.078	295	1.126	55	1.018
180	1.063	300	1.130	60	1.022
185	1.048	305	1.133	65	1.026
190	1.031	310	1.135	70	1.040
195	1.017	315	1.135		

Table 8. $MnCl_2 \cdot 4H_2O$ BC plane isentropic rotations ($C = 55^0$)

θ	$T(^0K)$	θ	$T(^0K)$	θ	$T(^0K)$
		8/21/67, 6690 Gauss			
65	0.899	185	0.987	305	1.038
70	0.909	190	0.971	310	1.045
75	0.919	195	0.954	315	1.057
80	0.933	200	0.939	320	1.052
85	0.948	205	0.924	325	1.052
90	0.963	210	0.910	330	1.050
95	0.977	215	0.897	335	1.046
100	0.991	220	0.886	340	1.041
105	1.005	225	0.878	345	1.033
110	1.017	230	0.873	350	1.022
115	1.028	235	0.872	355	1.011
120	1.038	240	0.876	360	0.999
125	1.047	245	0.882	5	0.984
130	1.053	250	0.891	10	0.968
135	1.057	255	0.904	15	0.952
140	1.058	260	0.919	20	0.936
145	1.058	265	0.934	25	0.921
150	1.056	270	0.950	30	0.905
155	1.052	275	0.966	35	0.892
160	1.045	280	0.981	40	0.882
165	1.037	285	0.994	45	0.874
170	1.027	290	1.007	50	0.869
175	1.015	295	1.020	55	0.868
180	1.001	300	1.029	60	0.870

Table 8. (Cont.)

θ	T(°K)	θ	T(°K)	θ	T(°K)
		8/21/67, 9970 Gauss			
55	0.858	180	0.973	305	1.050
65	0.858	185	0.943	310	1.063
65	0.857	190	0.912	315	1.072
70	0.857	195	0.883	320	1.076
75	0.856	200	0.865	325	1.077
80	0.854	205	0.858	330	1.075
85	0.852	210	0.857	335	1.068
90	0.864	215	0.858	340	1.058
95	0.899	220	0.859	345	1.044
100	0.933	225	0.860	350	1.025
105	0.959	230	0.860	355	1.005
110	0.986	235	0.861	360	0.981
115	1.009	240	0.861	5	0.953
120	1.029	245	0.861	10	0.926
125	1.045	250	0.860	15	0.899
130	1.058	255	0.859	20	0.878
135	1.067	260	0.857	25	0.872
140	1.072	265	0.853	30	0.871
145	1.073	270	0.870	35	0.872
150	1.070	275	0.904	40	0.873
155	1.063	280	0.937	45	0.875
160	1.052	285	0.965	50	0.878
165	1.037	290	0.992	55	0.879
170	1.019	295	1.014		
175	0.997	300	1.034		

Table 9. $MnCl_2 \cdot 4H_2O$ C-axis isentropic magnetizations

T(^oK)	H(Gauss)	T(^oK)	H(Gauss)	T(^oK)	H(Gauss)
		8/21/67			
0.875	6640	0.839	7690	0.847	8430
0.867	6780	0.839	7740	0.848	8480
0.862	6860	0.839	7800	0.848	8520
0.858	6940	0.839	7860	0.849	8570
0.856	7010	0.840	7920	0.849	8660
0.852	7090	0.841	7970	0.849	8740
0.850	7160	0.842	8030	0.850	8830
0.847	7230	0.843	8080	0.850	8910
0.843	7300	0.843	8130	0.851	9000
0.841	7370	0.844	8190	0.851	9080
0.841	7430	0.845	8240	0.851	9160
0.840	7500	0.845	8290	0.852	9240
0.840	7560	0.846	8340	0.854	9620
0.839	7620	0.845	8390	0.855	9970
		3/1/68			
1.007	6410	0.965	8080	0.963	9160
0.991	6780	0.964	8290	0.963	9400
0.980	7090	0.963	8480	0.965	9620
0.972	7370	0.962	8660	0.965	9760
0.969	7620	0.962	8830	0.967	9970
0.967	7860	0.963	9000		
		3/1/68			
1.123	4910	1.011	7620	1.003	9000
1.101	5410	1.007	7860	1.003	9160
1.078	5970	1.005	8080	1.003	9400
1.056	6410	1.004	8290	1.003	9620
1.039	6780	1.003	8480	1.003	9760
1.025	7090	1.003	8660	1.003	9890
1.014	7370	1.003	8830		
		3/1/68			
1.171	4980	1.049	7620	1.039	9000
1.154	5410	1.045	7860	1.039	9160
1.126	5970	1.043	8080	1.039	9400
1.106	6410	1.041	8290	1.039	9620
1.086	6780	1.040	8480	1.039	9760
1.068	7090	1.040	8660	1.038	9970
1.056	7370	1.039	8830		

Table 9. (Cont.)

T(°K)	H(Gauss)	T(°K)	H(Gauss)	T(°K)	H(Gauss)
		2/20/68			
1.129	9970	1.131	8570	1.157	7230
1.129	9620	1.131	8380	1.169	6940
1.130	9240	1.132	8190	1.185	6600
1.130	9080	1.134	7970	1.201	6200
1.130	8910	1.137	7740	1.220	5700
1.130	8740	1.144	7500	1.232	5320
		3/2/68			
1.235	5080	1.113	7740	1.106	9080
1.207	5700	1.110	7970	1.106	9240
1.186	6200	1.107	8190	1.106	9480
1.167	6600	1.106	8380	1.106	9690
1.149	6940	1.106	8570	1.106	9970
1.134	7230	1.106	8740		
1.121	7500	1.106	8910		
		2/20/68			
1.218	5700	1.134	7740	1.130	8910
1.199	6200	1.132	7970	1.130	9080
1.182	6600	1.130	8190	1.130	9240
1.166	6940	1.130	8380	1.129	9620
1.152	7230	1.129	8570	1.129	9970
1.142	7500	1.130	8740		
		2/20/68			
1.164	9400	1.165	8380	1.213	6940
1.164	9240	1.166	8190	1.228	6600
1.164	9080	1.169	7970	1.246	6200
1.165	8910	1.174	7740	1.266	5700
1.165	8740	1.184	7500	1.282	5320
1.165	8570	1.198	7230		
		2/20/68			
1.336	5250	1.231	7500	1.203	8910
1.320	5700	1.219	7740	1.203	9080
1.298	6200	1.207	8190	1.202	9240
1.278	6600	1.205	8380	1.201	9620
1.262	6940	1.204	8570	1.199	9970
1.246	7230	1.204	8740		

Table 9. (Cont.)

T(°K)	H(Gauss)	T(°K)	H(Gauss)	T(°K)	H(Gauss)
		2/20/68			
1.392	5700	1.285	7740	1.260	8910
1.372	6200	1.273	7970	1.261	9080
1.347	6600	1.266	8190	1.262	9240
1.328	6940	1.262	8380	1.266	9620
1.312	7230	1.261	8570	1.274	9970
1.298	7500	1.260	8740		
		2/20/68			
1.293	9400	1.278	8380	1.335	6940
1.289	9240	1.279	8190	1.353	6600
1.286	9080	1.283	7970	1.371	6200
1.283	8910	1.293	7740	1.393	5700
1.280	8740	1.304	7500	1.417	5080
1.279	8570	1.317	7230		
		2/20/68			
1.449	5410	1.402	7500	1.426	8740
1.435	5700	1.404	7740	1.433	8910
1.418	6200	1.407	7970	1.439	9080
1.406	6600	1.411	8190	1.445	9240
1.402	6940	1.416	8380	1.465	9620
1.402	7230	1.421	8570	1.486	9970

Table 10. $MnCl_2 \cdot 4H_2O$ specific heat maxima (H // C-axis)

$T(^oK)$	H(Gauss)
2/20/68	
1.458	5410
3/1/68	
1.210	9970
3/2/68	
1.220	9320
1.225	8480
1.238	7980
1.303	7230

Table 11a. $CoBr_2 \cdot 6H_2O$ BC plane isentropic rotations (C = 60°)

θ	T(°K)	θ	T(°K)	θ	T(°K)
		1/22/68, 6410 Gauss			
90	1.281	220	1.214	350	1.307
100	1.301	230	1.197	0	1.291
110	1.311	240	1.198	10	1.275
120	1.317	250	1.231	20	1.256
130	1.320	260	1.262	30	1.238
140	1.317	270	1.288	40	1.216
150	1.313	280	1.304	50	1.196
160	1.305	290	1.318	60	1.195
170	1.294	300	1.326	70	1.224
180	1.280	310	1.327	80	1.258
190	1.266	320	1.327	90	1.287
200	1.250	330	1.325		
210	1.233	340	1.318		
		1/22/68, 8830 Gauss			
350	1.373	230	1.230	110	1.320
340	1.375	220	1.259	100	1.300
330	1.372	210	1.294	90	1.275
320	1.365	200	1.319	80	1.251
310	1.352	190	1.340	70	1.224
300	1.337	180	1.353	60	1.223
290	1.318	170	1.362	50	1.234
280	1.295	160	1.367	40	1.266
270	1.270	150	1.366	30	1.297
260	1.246	140	1.360	20	1.321
250	1.221	130	1.351	10	1.344
240	1.219	120	1.338	0	1.358

Table 11b. $CoBr_2 \cdot 6H_2O$ AC plane isentropic rotations (C = 22°)

θ	T(°K)	θ	T(°K)	θ	T(°K)
		1/17/16, 6410 Gauss			
210	1.259	330	1.304	90	1.359
220	1.274	340	1.285	100	1.365
230	1.292	350	1.266	110	1.365
240	1.310	0	1.253	120	1.358
250	1.329	10	1.246	130	1.344
260	1.344	20	1.247	140	1.324
270	1.355	30	1.254	150	1.303
280	1.362	40	1.268	160	1.281
290	1.363	50	1.285	170	1.263
300	1.357	60	1.307	180	1.250
310	1.344	70	1.327	190	1.242
320	1.325	80	1.345	200	1.242
		1/17/68, 8830 Gauss			
70	1.314	200	1.296	330	1.310
80	1.351	210	1.293	340	1.271
90	1.382	220	1.281	350	1.239
100	1.401	230	1.234	360	1.276
110	1.405	240	1.271	10	1.294
120	1.396	250	1.312	20	1.296
130	1.374	260	1.350	30	1.294
140	1.341	270	1.381	40	1.282
150	1.305	280	1.399	50	1.235
160	1.264	290	1.405	60	1.272
170	1.233	300	1.397	70	1.313
180	1.281	310	1.378		
190	1.293	320	1.347		

Table 12. $CoBr_2 \cdot 6H_2O$ C-axis isentropic magnetizations.

T(^oK)	H(Gauss)	T(^oK)	H(Gauss)	T(^oK)	H(Gauss)
		1/22/68			
1.254	6410	1.249	8080	1.288	9160
1.243	6780	1.268	8290	1.288	9320
1.238	7090	1.279	8480	1.291	9620
1.232	7370	1.285	8660	1.296	9970
1.231	7620	1.285	8830		
1.233	7860	1.288	9000		
		1/22/68			
1.258	4910	1.210	7500	1.285	9080
1.255	5080	1.209	7620	1.288	9240
1.249	5410	1.208	7860	1.289	9400
1.245	5700	1.228	8080	1.293	9550
1.236	6200	1.265	8380	1.293	9620
1.222	6780	1.273	8570	1.295	9760
1.216	7090	1.278	8740	1.297	9890
1.211	7370	1.282	8910	1.298	9970
		1/17/68			
1.291	6410	1.269	7860	1.327	8830
1.280	6780	1.302	8080	1.328	9000
1.273	7090	1.309	8290	1.328	9160
1.267	7370	1.324	8480	1.334	9620
1.265	7620	1.325	8660	1.333	9720
		1/22/68			
1.864	5080	1.793	7090	1.798	8660
1.852	5410	1.783	7370	1.802	8830
1.843	5700	1.773	7690	1.806	9240
1.832	5970	1.768	7860	1.809	9620
1.826	6200	1.765	8080	1.811	9970
1.818	6410	1.771	8290		
1.804	6810	1.788	8480		
		1/22/68			
2.549	5080	2.492	7500	2.464	8740
2.537	5700	2.486	7740	2.465	8910
2.526	6200	2.480	7970	2.470	9080
2.516	6600	2.475	8190	2.474	9240
2.506	6940	2.469	8380	2.476	9620
2.499	7230	2.466	8570	2.477	9970
		1/24/68			
2.267	5080	2.205	7500	2.193	8740
2.254	5700	2.199	7740	2.201	8910
2.240	6200	2.194	7970	2.204	9080
2.230	6600	2.188	8190	2.206	9240
2.221	6940	2.184	8380	2.208	9620
2.213	7230	2.183	8570	2.209	9970

Table 12. (Cont.)

T(^{0}K)	H(Gauss)	T(^{0}K)	H(Gauss)	T(^{0}K)	H(Gauss)
		1/24/68			
3.107	5350	3.055	7860	3.022	9240
3.087	5970	3.047	8190	3.012	9620
3.082	6600	3.040	8480	3.004	9970
3.071	7090	3.034	8740	3.004	9970
3.062	7500	3.027	9000		
		1/26/68			
2.636	1680	2.559	6940	2.522	8660
2.631	2260	2.555	7090	2.520	8740
2.628	2710	2.552	7230	2.518	8830
2.623	3360	2.549	7370	2.518	8910
2.615	3860	2.548	7500	2.518	9000
2.608	4310	2.545	7620	2.522	9080
2.602	4720	2.542	7740	2.524	9160
2.595	5080	2.539	7860	2.525	9240
2.590	5410	2.538	7970	2.525	9320
2.584	5700	2.534	8080	2.526	9480
2.579	5970	2.532	8190	2.526	9620
2.574	6200	2.530	8290	2.526	9760
2.570	6410	2.527	8380	2.527	9970
2.567	6600	2.525	8480		
2.563	6780	2.523	8570		

Table 13. $CoBr_2 \cdot 6H_2O$ antiferromagnetic-spin flop boundary points (H // C-axis).

T(°K)	H(Gauss)	T(°K)	H(Gauss)
	1/17/68		
1.180	7670	1.906	8150
1.211	7680	1.962	8200
1.270	7690	2.030	8270
1.331	7740	2.098	8320
1.417	7790	2.224	8470
1.506	7830	2.337	8590
1.564	7870	2.506	8790
1.651	7930	2.739	9070
1.755	8010		
	1/22/68		
1.260	7860	1.850	8180
1.296	7890	1.970	8290
1.351	7900	2.062	8380
1.425	7940	2.195	8530
1.485	7970	2.383	8740
1.539	8000	2.485	8870
1.610	8040	2.607	9030
1.705	8050	2.730	9240
1.777	8100	2.771	9260

Table 14. Specific heat maxima (H // C-axis, $CoBr_2 \cdot 6H_2O$)

H(Gauss)	T(°K)
1/24/68	
2.981	8380
3.030	7090
3.087	5350
1/26/68	
2.938	9970
2.989	8290
3.109	4310
3.125	3090
3.143	1970
3.152	0
1/27/68	
2.941	9100
2.923	9420
2.930	9550
2.916	9360

Table 15. $FeCl_2 \cdot 4H_2O$ isentropic rotations

θ	T(^{0}K)	θ	T(^{0}K)	θ	T(^{0}K)
		4/25/68, AB Plane, B = 22^0			
330	1.078	210	0.973	90	1.097
320	1.092	200	0.968	80	1.096
310	1.085	190	0.977	70	1.078
300	1.039	180	0.995	60	1.051
290	0.989	170	1.023	50	1.021
280	1.061	160	1.054	40	0.997
270	1.095	150	1.083	30	0.983
260	1.090	140	1.097	20	0.979
250	1.072	130	1.088	10	0.988
240	1.045	120	1.043	0	1.008
230	1.014	110	0.996	350	1.036
220	0.991	100	1.061	340	1.066
		5/1/68, BC Plane, B = 2^0			
70	1.045	190	1.022	310	0.990
80	1.096	200	1.013	320	0.991
90	1.130	210	1.002	330	1.004
100	1.109	220	0.991	340	1.020
110	1.055	230	0.991	350	1.030
120	1.006	240	1.013	360	1.036
130	0.982	250	1.056	10	1.034
140	0.982	260	1.106	20	1.024
150	0.995	270	1.138	30	1.011
160	1.011	280	1.117	40	0.998
170	1.020	290	1.065	50	0.995
180	1.025	300	1.016	60	1.015

Table 16. $FeCl_2 \cdot 4H_2O$ B-axis isentropic magnetizations.

T(°K)	H(Gauss)	T(°K)	H(Gauss)	T(°K)	H(Gauss)
		5/2/68			
0.693	6600	0.678	8190	0.679	9240
0.686	6940	0.678	8380	0.680	9400
0.680	7230	0.678	8570	0.684	9620
0.679	7500	0.679	8740	0.692	9820
0.679	7740	0.679	8910		
0.678	7970	0.679	9080		
		5/1/68			
0.991	1910	0.683	6940	0.677	8570
0.955	3360	0.679	7230	0.677	8740
0.919	4310	0.678	7500	0.678	8910
0.878	5080	0.677	7740	0.679	9080
0.740	5700	0.677	7970	0.681	9240
0.709	6200	0.677	8190		
0.692	6600	0.677	8380		
		4/26/68			
1.111	1560	0.912	6940	0.918	8740
1.102	1910	0.906	7230	0.925	8910
1.056	3360	0.903	7500	0.934	9080
1.014	4310	0.901	7740	0.943	9240
0.977	5080	0.902	7970	0.953	9400
0.952	5700	0.904	8190	0.970	9620
0.933	6200	0.907	8380	0.988	9820
0.920	6600	0.912	8570	1.008	10060
		4/25/68			
1.030	2820	0.780	7500	0.826	9080
0.956	4310	0.776	7740	0.839	9240
0.901	5080	0.779	7970	0.853	9400
0.863	5700	0.782	8190	0.876	9620
0.833	6200	0.792	8380	0.900	9820
0.812	6600	0,798	8570	0.925	10060
0.795	6940	0.806	8740		
0.786	7230	0.815	8910		
		4/25/68			
1.189	3040	1.102	7230	1.173	8910
1.169	3710	1.107	7500	1.185	9080
1.148	4310	1.113	7740	1.197	9240
1.126	5080	1.121	7970	1.208	9400
1.113	5700	1.130	8190	1.228	9620
1.104	6200	1.140	8380	1.248	9820
1.100	6600	1.150	8570	1.267	10060
1.100	6940	1.161	8740		

Table 17. Specific heat maxima ($H \parallel$ B-axis, $FeCl_2 \cdot 4H_2O$)

T(^oK)	H(Gauss)
4/26/68	
1.121	0
1.056	2820
1.055	2820
1.020	3860
4/29/68	
0.972	4310
0.941	4640
0.912	4830
5/1/68	
0.769	8070
5/2/68	
0.752	9570
0.766	10010
0.755	8760
0.748	9230
0.740	9820
0.761	7500
0.759	6620
0.759	5990
0.755	10000
0.759	9240
0.756	10060
5/6/68	
0.762	9620
0.756	9000
0.765	8080
0.756	8740
0.758	7500
0.759	6600
0.760	5970
0.763	5970
0.765	5500

Table 18. $MnBr_2 \cdot 4H_2O$ C-axis isentropic magnetizations.

T(^oK)	H(Gauss)	T(^oK)	H(gauss)	T(^oK)	H(Gauss)
		3/6/68			
1.022	1620	0.952	6600	0.913	8570
1.018	2030	0.945	6940	0.909	8740
1.015	2540	0.938	7230	0.905	8910
1.006	3360	0.933	7500	0.902	9080
0.990	4310	0.929	7740	0.899	9240
0.978	5080	0.924	7970	0.895	9480
0.966	5700	0.920	8190	0.892	9690
0.958	6200	0.916	8380	0.888	9970
		3/6/68			
0.907	9810	0.952	8570	1.030	6600
0.910	9690	0.959	8380	1.045	6200
0.915	9550	0.967	8190	1.062	5700
0.920	9400	0.976	7970	1.079	5080
0.926	9240	0.985	7740	1.109	4090
0.932	9080	0.995	7500	1.149	1210
0.938	8910	1.005	7230		
0.945	8740	1.017	6940		
		3/6/68			
1.185	1850	1.025	7230	0.946	9080
1.174	2660	1.014	7500	0.939	9240
1.165	3200	1.003	7740	0.934	9400
1.135	4310	0.994	7970	0.928	9550
1.108	5080	0.984	8190	0.922	9690
1.087	5700	0.975	8380	0.918	9820
1.068	6200	0.968	8570	0.913	9970
1.052	6600	0.960	8740		
1.037	6940	0.953	8910		
		3/6/68			
0.914	9970	0.964	8740	1.044	6940
0.919	9820	0.972	8570	1.058	6600
0.924	9690	0.980	8380	1.075	6200
0.930	9550	0.990	8190	1.093	5700
0.936	9400	0.999	7970	1.111	5150
0.942	9240	1.009	7740	1.145	4180
0.949	9080	1.020	7500	1.190	1910
0.956	8910	1.031	7230		

Table 18. (Cont.)

T(°K)	H(Gauss)	T(°K)	H(Gauss)	T(°K)	H(Gauss)
		3/6/68			
1.249	1910	1.073	7230	0.979	9080
1.236	2710	1.059	7500	0.972	9240
1.225	3260	1.048	7740	0.964	9400
1.192	4310	1.037	7970	0.957	9550
1.166	5080	1.026	8190	0.950	9690
1.141	5700	1.014	8380	0.944	9820
1.120	6200	1.006	8570	0.937	9970
1.104	6600	0.996	8740		
1.088	6940	0.988	8910		
		3/6/68			
0.938	9970	1.000	8740	1.091	6940
0.945	9820	1.010	8570	1.107	6600
0.952	9690	1.020	8380	1.124	6200
0.959	9550	1.030	8190	1.145	5700
0.966	9400	1.041	7970	1.165	5080
0.974	9240	1.052	7740	1.199	4220
0.982	9080	1.063	7500	1.248	1970
0.991	8910	1.077	7230		
		3/6/68			
1.342	1850	1.151	7230	1.042	9080
1.329	2660	1.138	7500	1.033	9240
1.319	3100	1.124	7740	1.024	9400
1.282	4310	1.110	7970	1.014	9550
1.252	5080	1.098	8190	1.005	9690
1.226	5700	1.085	8380	0.996	9820
1.204	6200	1.074	8570	0.988	9970
1.185	6600	1.064	8740		
1.167	6940	1.053	8910		
		3/6/68			
0.990	9970	1.066	8740	1.169	6940
0.998	9820	1.078	8570	1.186	6600
1.006	9690	1.088	8380	1.205	6200
1.015	9550	1.100	8190	1.226	5700
1.026	9400	1.112	7970	1.248	5080
1.035	9240	1.125	7740	1.285	4180
1.045	9080	1.140	7500	1.334	1910
1.055	8910	1.154	7230		

Table 18. (Cont.)

T(^{0}K)	H(Gauss)	T(^{0}K)	H(Gauss)	T(^{0}K)	H(Gauss)
		3/6/68			
1.511	1850	1.308	7230	1.189	9080
1.499	2660	1.292	7500	1.177	9240
1.442	4310	1.280	7740	1.167	9400
1.409	5080	1.264	8190	1.155	9550
1.384	5700	1.238	8380	1.144	9690
1.363	6200	1.226	8570	1.134	9820
1.344	6600	1.212	8740	1.123	9970
1.325	6940	1.201	8910		
		3/6/68			
1.298	9890	1.377	8740	1.485	6940
1.302	9820	1.390	8570	1.501	6600
1.312	9690	1.401	8380	1.519	6200
1.323	9550	1.414	8190	1.541	5700
1.334	9400	1.427	7970	1.565	5080
1.344	9240	1.440	7740	1.603	4040
1.355	9080	1.453	7500	1.650	1850
1.366	8910	1.468	7230		
		3/6/68			
1.974	1850	1.795	7230	1.679	9080
1.963	2710	1.781	7500	1.668	9240
1.953	3100	1.768	7740	1.656	9400
1.921	4310	1.755	7970	1.645	9550
1.891	5080	1.740	8190	1.633	9690
1.868	5700	1.728	8380	1.622	9820
1.846	6200	1.715	8570	1.607	9970
1.829	6600	1.704	8740		
1.802	7090	1.691	8910		

Table 19. $Cs_2MnBr_4 \cdot 2H_2O$ Isentropic magnetizations

T(^oK)	H(Gauss)	T(^oK)	H(Gauss)	T(^oK)	H(Gauss)
		3/20/68, $H \parallel [\bar{1}\ \bar{1}\ \bar{1}]$			
1.026	9600	1.041	8570	1.052	7230
1.030	9400	1.043	8380	1.053	6940
1.032	9240	1.045	8190	1.055	6600
1.035	9080	1.047	7970	1.055	6200
1.037	8910	1.049	7740	1.057	5700
1.039	8740	1.050	7500	1.060	5080
		3/21/68, $H \parallel [\bar{1}\ \bar{1}\ \bar{1}]$			
2.210	9120	2.208	9240	2.284	7500
2.204	9240	2.216	9080	2.293	7230
2.197	9400	2.225	8910	2.304	6940
2.185	9620	2.232	8740	2.313	6600
2.179	9760	2.241	8570	2.326	6200
2.168	9970	2.250	8380	2.338	5700
2.181	9760	2.258	8190	2.353	5080
2.189	9620	2.267	7970		
2.201	9400	2.275	7740		
		3/20/68, $H \perp [\bar{1}\ \bar{1}\ \bar{1}]$			
1.031	9780	1.029	8570	1.025	6940
1.031	9620	1.028	8380	1.024	6600
1.030	9400	1.028	8190	1.023	6200
1.030	9240	1.027	7970	1.022	5700
1.030	9080	1.027	7740	1.020	5080
1.029	8910	1.026	7500		
1.029	8740	1.026	7230		
		3|20|68, $H \perp [\bar{1}\ \bar{1}\ \bar{1}]$			
1.036	4800	1.041	7740	1.040	9080
1.038	5700	1.041	7970	1.040	9240
1.039	6200	1.045	8190	1.040	9400
1.040	6600	1.041	8380	1.040	9620
1.040	6940	1.041	8570	1.039	9760
1.040	7230	1.041	8740	1.039	9970
1.040	7500	1.040	8910		

Table 20. $Cs_2MnBr_4 \cdot 2H_2O$ specific heat maxima (H // $[\bar{1}\ \bar{1}\ \bar{1}]$)

T(^{o}K)	H(Gauss)
3/21/68	
2.584	9200
2.542	9920
2.642	8080
2.692	7010
2.751	5420
2.795	3860
2.828	1970
2.834	0000

Table 21. $NiCl_2 \cdot 6H_2O$ AC plane isentropic rotation (A' = 110^{o})

θ	T(^{o}K)	θ	T(^{o}K)	θ	T(^{o}K)
		4/9/68			
80	1.059	200	1.068	320	1.067
90	1.057	210	1.066	330	1.071
100	1.058	220	1.063	340	1.072
110	1.059	230	1.061	350	1.073
120	1.060	240	1.060	360	1.072
130	1.062	250	1.059	10	1.072
140	1.065	260	1.058	20	1.070
150	1.068	270	1.059	30	1.067
160	1.070	280	1.061	40	1.065
170	1.070	290	1.062	50	1.063
180	1.070	300	1.063	60	1.062
190	1.069	310	1.065	70	1.061

Table 22. $NiCl_2 \cdot 6H_2O$ A'-axis isentropic magnetizations.

T(^oK)	H(Gauss)	T(^oK)	H(Gauss)	T(^oK)	H(Gauss)
		4|9|68			
1.344	1790	1.345	5410	1.345	8290
1.343	2260	1.344	6200	1.345	8660
1.344	2820	1.344	7090	1.347	9000
1.345	4310	1.344	7370		
		4|11|68			
1.839	5080	1.826	7740	1.827	9080
1.836	5700	1.826	7970	1.827	9240
1.832	6200	1.826	8190	1.826	9400
1.823	6600	1.828	8380	1.825	9620
1.829	6940	1.827	8570	1.824	9760
1.828	7230	1.827	8740	1.824	9970
1.827	7500	1.827	8910		
		4|11|68			
1.846	9970	1.859	8570	1.874	6410
1.848	9820	1.860	8380	1.874	6200
1.850	9620	1.862	8190	1.877	5700
1.852	9400	1.864	7970	1.880	5080
1.854	9240	1.866	7740	1.883	4310
1.854	9080	1.867	7500	1.887	3100
1.856	8910	1.869	7230	1.888	1680
1.858	8740	1.871	6940		
		4|11|68			
1.929	1680	1.904	6940	1.894	8910
1.928	1970	1.903	7230	1.893	9080
1.928	2260	1.901	7500	1.893	9240
1.924	3360	1.899	7740	1.892	9400
1.920	4310	1.899	7970	1.890	9620
1.916	5080	1.897	8190	1.890	9760
1.912	5700	1.896	8380	1.888	9970
1.909	6200	1.895	8570		
1.907	6600	1.894	8740		

Table 22. (cont.)

T(^{0}K)	H(Gauss)	T(^{0}K)	H(Gauss)	T(^{0}K)	H(Gauss)
		4|11|68			
1.972	9970	1.988	8570	2.003	6600
1.974	9820	1.989	8380	2.006	6200
1.977	9620	1.991	8190	2.009	5700
1.979	9400	1.993	7970	2.012	5080
1.981	9240	1.995	7740	2.016	4310
1.982	9080	1.997	7500	2.021	3360
1.985	8910	1.999	7230	2.021	2820
1.986	8740	2.001	6940	2.011	1680
		4|11|68			
2.156	1680	2.134	6940	2.123	8740
2.155	2260	2.132	7230	2.123	8910
2.152	3360	2.130	7500	2.122	9080
2.148	4310	2.129	7740	2.122	9240
2.144	5080	2.127	7970	2.121	9400
2.140	5700	2.126	8190	2.119	9620
2.138	6200	2.125	8380	2.118	9820
2.136	6600	2.124	8570	2.118	9970
		4|18|68			
2.264	7730	2.257	8740	2.252	9620
2.263	7970	2.256	8910	2.250	9820
2.262	8190	2.255	9080	2.249	10060
2.260	8380	2.254	9240		
2.259	8570	2.253	9400		
		4|18|68			
2.268	9760	2.281	8570	2.295	6940
2.270	9620	2.283	8380	2.297	6600
2.272	9400	2.285	8190	2.300	6200
2.274	9240	2.287	7970	2.303	5700
2.276	9080	2.288	7740	2.305	5080
2.277	8910	2.290	7500	2.307	4800
2.279	8740	2.292	7230		

Table 22. (Cont.)

T(^{0}K)	H(Gauss)	T(^{0}K)	H(Gauss)	T(^{0}K)	H(Gauss)
		4|11|68			
2.477	9690	2.494	8380	2.514	6200
2.479	9550	2.496	8190	2.519	5700
2.481	9400	2.498	7970	2.522	5080
2.483	9240	2.501	7740	2.528	4310
2.485	9080	2.503	7500	2.533	3360
2.488	8910	2.505	7230	2.535	2820
2.489	8740	2.508	6940	2.538	1680
2.492	8570	2.511	6600		
		4|11|68			
3.134	1680	3.118	6600	3.114	8380
3.134	2260	3.117	6940	3.116	8570
3.133	2820	3.116	7230	3.116	8740
3.128	4310	3.116	7500	3.116	8910
3.124	5080	3.116	7740	3.115	9240
3.121	5700	3.115	7970	3.112	9620
3.119	6200	3.115	8190	3.111	9970

Table 23. $NiCl_2 \cdot 6H_2O$ specific heat maxima (H // A').

T(^{0}K)	H(Gauss)
4/18/68	
5.229	4940
5.241	6410
5.112	9840
5.087	8950
5.088	8270
5.139	7550
5.112	7230
5.149	7230
5.159	7150
5.212	6600
5.212	6600
5.151	5120
5.154	5120
5.263	2880